ISSN 2782-2192 (Print)
ISSN 2782-2206 (Online)

Journal of Advanced Materials and Technologies

J·A·M·T

Vol.9, No.4.
2024

TSTU Publishing

ISSN 2782-2192 (Print)
ISSN 2782-2206 (Online)
DOI: 10.17277/issn.2782-2192

Journal of Advanced Materials and Technologies

**Vol. 9, No. 4.
2024**

**Том 9, № 4.
2024**

16+

Journal of Advanced Materials and Technologies

Scientific Journal

“Journal of Advanced Materials and Technologies” is a peer-reviewed scientific journal of research in materials science and related issues in materials physics and mechanics.

“Journal of Advanced Materials and Technologies” publishes original articles, reviews, short reports written by both renowned scientists and young researchers that contribute to the development of modern materials science.

The journal promotes research and exchange of information in the field of theoretical and practical research into materials science, modeling of processes involved in the creation of new materials, including nanomaterials, their properties and application.

The journal papers and metadata abstracted and indexed in Chemical Abstracts, RSCI, CAS (American Chemical Society), Google Scholar, WorldCat, ROAR (Registry of Open Access Repositories), OpenAIRE (OpenAIRE – Open Access Infrastructure for Research in Europe), BASE (Bielefeld Academic Search Engine), RePEc: Research Papers in Economics, EBSCO.

ISSN 2782-2192 (Print), ISSN 2782-2206 (Online)

Rename information	Advanced materials & technologies (2016-2021) Print ISSN 2414-4606, Online ISSN 2541-8513
The journal was founded	2016
Publication frequency	Quarterly
Founders	Tambov State Technical University (TSTU), Merzhanov Institute of Structural Macrokinetics and Materials Sciences of Russian Academy of Sciences (ISMAN)
Postal address	TSTU: Bld. 2, 106/5, Sovetskaya St., Tambov, 392000 ISMAN: 8, Academician Osipyan St., Moscow region, Chernogolovka, 142432
Editorial office address	Bld. 2, 106/5, Sovetskaya St., Tambov, 392000
Contacts	Phone + 7 4752 63 03 91; amt.journal@yandex.ru
Printing House	TSTU Publishing, 112A, Michurinskaya St., Tambov, 392032 Phone + 7 4752 63 03 91; + 7 4752 63 07 46
Website	http://amt.tstu.ru/
E-mail	amt.journal@yandex.ru
Phone	+7 4752 63 92 93
Subscription	The electronic version of the Journal is freely available on the journal’s website, as well as in open access databases. The subscription index for the Journal printed version in the unified catalog “Press of Russia” is 80453
Editor-in-Chief	Mikhail I. Alymov, D. Sc. (Engineering), Professor, Corresponding Member of the Russian Academy of Sciences

Journal of Advanced Materials and Technologies

Научный журнал

«Journal of Advanced Materials and Technologies» – научный рецензируемый журнал, посвященный исследованиям в области материаловедения и примыкающих вопросов физики и механики материалов.

Журнал «Journal of Advanced Materials and Technologies» публикует оригинальные статьи, обзоры, краткие сообщения, содействующие развитию современной науки о материалах, подготовленные как известными учеными, так и молодыми специалистами.

Миссия журнала – обмен актуальной научной информацией в области теоретических и практических исследований и моделирования процессов, связанных с получением, определением свойств новых материалов, в том числе наноразмерных, и их применения.

Средство массовой информации периодическое печатное издание, журнал «Journal of Advanced Materials and Technologies» зарегистрировано Федеральной службой по надзору в сфере связи, информационных технологий и массовых коммуникаций. Регистрационный номер СМИ ПИ № ФС 77-74804 от 25.01.2019.

Журнал входит в перечень рецензируемых научных изданий (перечень ВАК Минобрнауки РФ) от 16 декабря 2021 г. по научным специальностям: 1.4.15 – Химия твердого тела; 2.6.6 – Нанотехнологии и наноматериалы; 2.6.13 – Процессы и аппараты химических технологий; 2.6.17 – Материаловедение.

Журнал индексируется в РИНЦ, RSCI, Chemical Abstracts, CAS (American Chemical Society), Академия Google (Google Scholar), WorldCat, СОЦИОНЕТ, ROAR (Registry of Open Access Repositories), OpenAIRE (OpenAIRE – Open Access Infrastructure for Research in Europe), BASE (Bielefeld Academic Search Engine), RePEc: Research Papers in Economics, EBSCO.

ISSN 2782-2192 (Print), ISSN 2782-2206 (Online)

Сведения о переименовании	«Advanced materials & technologies» (2016–2021) Print ISSN 2414-4606, Online ISSN 2541-8513
Журнал основан	2016 г.
Периодичность	4 раза в год
Учредители	Федеральное государственное бюджетное образовательное учреждение высшего образования «Тамбовский государственный технический университет» (ФГБОУ ВО «ТГТУ»), Федеральное государственное бюджетное учреждение науки Институт структурной макрокинетики и проблем материаловедения им. А. Г. Мержанова Российской академии наук (ИСМАН)
Адреса учредителей	ФГБОУ ВО «ТГТУ»: 392000, Тамбовская область, г.о. город Тамбов, г. Тамбов, ул. Советская, д. 106/5, помещ. 2, ИСМАН: 142432, Московская область, г. Черноголовка, ул. Академика Осипьяна, д. 8
Адрес издателя	ФГБОУ ВО «ТГТУ»: 392000, Тамбовская область, г.о. город Тамбов, г. Тамбов, ул. Советская, д. 106/5, помещ. 2
Адрес редакции	392000, Тамбовская область, г.о. город Тамбов, г. Тамбов, ул. Советская, д. 106/5, помещ. 2
Контакты	Тел.: + 7 4752 63 03 91; amt.journal@yandex.ru
Адрес типографии	392032, Тамбовская обл., г. Тамбов, ул. Мичуринская, д. 112А Тел.: + 7 4752 63 03 91; + 7 4752 63 07 46
Сайт	http://amt.tstu.ru/
E-mail	amt.journal@yandex.ru
Телефон	+7 4752 63 92 93
Подписка	Подписку на печатную версию журнала можно оформить по объединенному каталогу «Пресса России». Подписной индекс – 80453
Главный редактор	Алымов Михаил Иванович, д. т. н., профессор, член-корреспондент РАН

EDITORS

Mikhail I. Alymov, D. Sc. (Eng.), Professor, Corresponding Member of the Russian Academy of Sciences (RAS), Director of Merzhanov Institute of Structural Macrokinetics and Materials Sciences RAS (ISMAN), Chernogolovka, Moscow Region, Russian Federation

Mikhail N. Krasnyansky, D. Sc. (Eng.), Professor, Rector of Tambov State Technical University (TSTU), Tambov, Russian Federation

Alexey G. Tkachev, D. Sc. (Eng.), Professor, Head of Department of Technologies and Methods of Nanoproducts Manufacturing, TSTU, Tambov, Russian Federation

Irina V. Burakova, Ph.D., Associate Professor of Department of Technologies and Methods of Nanoproducts Manufacturing, TSTU, Tambov, Russian Federation

Imran Ali, Ph.D., FRSC, Professor, Department of Chemistry, Jamia Millia Islamia (Central University), New Delhi, India

Vyacheslav M. Buznik, D. Sc. (Chem.), Professor, RAS Academician, All-Russian Scientific Research Institute of Aviation Materials, Moscow, Russian Federation

Stepan N. Kalmykov, D. Sc. (Chem.), Professor, RAS Academician, Dean of the Faculty of Chemistry at the Lomonosov Moscow State University, Moscow, Russian Federation

Valeriy P. Meshalkin, D. Sc. (Eng.), Professor, RAS Academician, Head of Department of Logistics and Economic Informatics, Mendeleev University of Chemical Technology of Russia, Moscow, Russian Federation

Tatyana P. Dyachkova, D. Sc. (Chem.), Professor, Director of Center for Collective Use of Scientific Equipment “Production and Application of Multifunctional Nanomaterials”, TSTU, Tambov, Russian Federation

Jesus Iniesta Valcarcel, Ph.D., Associate Professor, Department of Physical Chemistry, University of Alicante, Alicante, Spain

Rami J. Sldozian, PhD, Lecturer at the Department of Applied Science, University of Technology, Baghdad, Iraq

Ruslan Kh. Khamizov, D. Sc. (Chem.), Professor, Director of Vernadsky Institute of Geochemistry and Analytical Chemistry of RAS, Moscow, Russian Federation

Mikhail L. Kheifetz, D. Sc. (Eng.), Professor, Director of Institute of Applied Physics of National Academy of Science of Belarus, Minsk, Belarus

Roman B. Morgunov, D. Sc. (Phys. and Math.), Professor, Leading Researcher, Institute of Problems of Chemical Physics RAS, Chernogolovka, Moscow Region, Russian Federation

Fadei F. Komarov, D. Sc. (Phys. and Math.), Professor, Academician of the National Academy of Sciences of Belarus, Head of Elionics Laboratory at A. N. Sevchenko Institute of Applied Physical Problems of Belarusian State University, Minsk, Belarus

Stephane Mangin, Ph.D., Professor, Physics of Matter and Materials Department, Institute Jean Lamour, University of Lorraine, Nancy, France

Dimiter Stavrev, D. Sc. (Eng.), Professor, Professor of Department of Materials Science at the Technical University of Varna, Varna, Bulgaria

Alexander M. Stolin, D. Sc. (Phys. and Math.), Professor, Head of Laboratory, ISMAN RAS, Chernogolovka, Moscow Region, Russian Federation

Yoshifumi Tanimoto, Ph.D., Professor, Hiroshima University, Japan

Vener A. Valitov, D. Sc. (Eng.), Leading Researcher, Institute for Metals Superplasticity Problems of the Russian Academy of Sciences, Ufa, Russian Federation

Sergey M. Arakelian, D. Sc. (Phys. and Math.), Professor, Head of the Department of Physics and Applied Mathematics, Vladimir State University, Vladimir, Russian Federation

Arif A. Babaev, D. Sc. (Phys. and Math.), Professor, Head of the Laboratory of Optical Phenomena in Condensed Matter, Institute of Physics of Dagestan Scientific Center of Russian Academy of Sciences, Makhachkala, Republic of Dagestan, Russian Federation

Evgeniy I. Terukov, D. Sc. (Eng.), Professor, Deputy Director for Science of R&D Center of Thin-Film Technology for Energetics under Ioffe Institute, St. Petersburg, Russian Federation

Valeriy Yu. Dolmatov, D. Sc. (Eng.), Head of Research Laboratory at the “Special Construction and Technology Bureau “Technolog”, St. Petersburg, Russian Federation

Valeriy V. Savin, D. Sc. (Phys. and Math.), Leading Researcher, Head of the Laboratory of Physical Materials Science, International Research Center “X-ray Coherent Optics”, Immanuel Kant Baltic Federal University, Kaliningrad, Russian Federation

Gennady E. Selyutin, Ph.D., Associate Professor, Senior Researcher, Federal Research Center “Krasnoyarsk Science Center” of Siberian Branch of the Russian Academy of Sciences, Krasnoyarsk, Russian Federation

Vladimir V. Petrov, D. Sc. (Phys. and Math.), Professor, Saratov State University, Saratov, Russian Federation

Yury E. Kalinin, D. Sc. (Phys. and Math.), Professor, Voronezh State Technical University, Voronezh, Russian Federation

Vladimir S. Sevostyanov, D. Sc. (Eng.), Professor, Head of the Department “Technological Complexes, Machines and Mechanisms”, V. G. Shukhov Belgorod State Technological University, Belgorod, Russian Federation

Victor M. Mukhin, D. Sc. (Eng.), Professor, D. Mendeleev University of Chemical Technology of Russia, Moscow, Russian Federation

Vladimir D. Vermel, D. Sc. (Eng.), Professor, Head of the Scientific and Technical Center of the Scientific and Production Complex, Central Aerohydrodynamic Institute, Zhukovsky, Moscow Region, Russian Federation

Nadezhda V. Usoltseva, D. Sc. (Chem.), Professor, Director of the Research Institute of Nanomaterials, Ivanovo State University, Ivanovo, Russian Federation

Lyaylya A. Abdrakhmanova, D. Sc. (Eng.), Professor, Kazan State University of Architecture and Engineering, Kazan, Russian Federation

Vyacheslav A. Sergeev, D. Sc. (Eng.), Professor, Director of the Ulyanovsk branch of Kotelniкov Institute of Radioengineering and Electronics of Russian Academy of Science, Ulyanovsk, Russian Federation

Irina V. Zaporotskova, D. Sc. (Phys. and Math.), Professor, Director of the Institute of Priority Technologies, Volgograd State University, Volgograd, Russian Federation

Vladimir E. Guterman, Ph.D., Professor, Leading Researcher, Southern Federal University, Rostov-on-Don, Russian Federation

Valeria S. Tafintseva, Ph.D., Researcher, Department of Physics, Faculty of Science and Engineering, Norwegian University of Life Sciences, Norway

Vyacheslav M. Tyutyunik, D. Sc. (Eng.), Professor, Director General of International Nobel Information Centre (INIC), Ltd., TSTU, Tambov, Russian Federation

Translator: Natalia A. Gunina, Ph.D., Associate Professor, Head of Department of International Professional and Scientific Communication, TSTU, Tambov, Russian Federation

СОВЕТ РЕДАКТОРОВ

Алымов Михаил Иванович, д.т.н., профессор, член-корреспондент РАН, директор Института структурной макрокинетики и материаловедения им. А.Г. Мержанова РАН (ИСМАН), Черноголовка, Московская область, Россия

Краснянский Михаил Николаевич, д.т.н., профессор, ректор, Тамбовский государственный технический университет (ТГТУ), Тамбов, Россия

Ткачев Алексей Григорьевич, д.т.н., профессор, заведующий кафедрой «Техника и технологии производства нанопродуктов», ТГТУ, Тамбов, Россия

Буракова Ирина Владимировна, к.т.н., доцент, доцент кафедры «Техника и технологии производства нанопродуктов», ТГТУ, Тамбов, Россия

Али Имран, PhD, FRSC, профессор кафедры химии, Джамия Миллия Исламия (Центральный университет), Нью-Дели, Индия

Бузник Вячеслав Михайлович, д.х.н., профессор, академик РАН, Всероссийский научно-исследовательский институт авиационных материалов, Москва, Россия

Калмыков Степан Николаевич, д.х.н., профессор, академик РАН, декан химического факультета Московского государственного университета им. М. В. Ломоносова, Москва, Россия

Мешалкин Валерий Павлович, д.т.н., профессор, академик РАН, заведующий кафедрой «Логистики и экономической информатики» Российского химико-технологического университета им. Д. И. Менделеева, Москва, Россия

Дьячкова Татьяна Петровна, д.х.н., профессор, директор центра коллективного пользования научным оборудованием «Получение и применение полифункциональных наноматериалов», ТГТУ, Тамбов, Россия

Иньеста Хесус Валькарсель, Ph.D., доцент кафедры физической химии Университета Аликанте, Аликанте, Испания

Слдозьян Рами Джозеф, к.т.н., преподаватель кафедры прикладных наук, Технологический университет, Багдад, Ирак

Хамизов Руслан Хажсетович, д.х.н., профессор, директор, Институт геохимии и аналитической химии им. В. И. Вернадского РАН, Москва, Россия

Хейфец Михаил Львович, д.т.н., профессор, директор института, Институт прикладной физики НАН Беларуси, Минск, Беларусь

Моргунов Роман Борисович, д.ф.-м.н., профессор, главный научный сотрудник, Институт проблем химической физики РАН, г. Черноголовка, Московская область, Россия

Комаров Фадей Фадеевич, д.ф.-м.н., профессор, академик Национальной академии наук Республики Беларусь, заведующий лабораторией элионики, Институт прикладных физических проблем им. А. Н. Севченко Белорусского государственного университета, Минск, Беларусь

Мангин Стефан, Ph.D., профессор кафедры физики материи и материалов Института Жана Ламура, Университет Лотарингии, Нанси, Франция

Ставрев Димитр, д.т.н., профессор, профессор кафедры «Материаловедения», Варненский технический университет, Варна, Болгария

Столин Александр Моисеевич, д.ф.-м.н., профессор, заведующий лабораторией, ИСМАН РАН, Черноголовка, Московская область, Россия

Танимото Есифуми, Ph.D., профессор, Хиросимский университет, Япония

Валитов Венер Анварович, д.т.н., ведущий научный сотрудник, Институт проблем сверхпластичности металлов РАН, Уфа, Республика Башкортостан, Россия

Аракелян Сергей Мартиросович, д.ф.-м.н., профессор, заведующий кафедрой физики и прикладной математики, Владимирский государственный университет им. А. Г. и Н. Г. Столетовых, Владимир, Россия

Бабаев Ариф Азимович, д.ф.-м.н., профессор, заведующий лабораторией оптических явлений в конденсированных средах Института физики им. Х. И. Амирханова ДНЦ РАН, Махачкала, Республика Дагестан, Россия

Теруков Евгений Иванович, д.т.н., профессор, заместитель генерального директора по научной работе ООО «НТЦ тонкопленочных технологий в энергетике при ФТИ им. А.Ф. Иоффе», Санкт-Петербург, Россия

Долматов Валерий Юрьевич, д.т.н., начальник научно-исследовательской лаборатории, «Специальное конструкторско-технологическое бюро «Технолог», Санкт-Петербург, Россия

Савин Валерий Васильевич, д.ф.-м.н., ведущий научный сотрудник, заведующий лабораторией физического материаловедения МНИЦ «Когерентная рентгеновская оптика для установок «Мегасайенс», Балтийский федеральный университет им. Иммануила Канта, Калининград, Россия

Селютин Геннадий Егорович, к.ф-м.н., доцент, старший научный сотрудник, Институт химии и химической технологии Сибирского отделения Российской академии наук ФИЦ КНЦ СО РАН, Красноярск, Россия

Петров Владимир Владимирович, д.ф.-м.н., профессор, Саратовский национальный исследовательский университет им. Н. Г. Чернышевского, Саратов, Россия

Калинин Юрий Егорович, д.ф.-м.н., профессор, Воронежский государственный технический университет, Воронеж, Россия

Севостьянов Владимир Семенович, д.т.н., профессор, заведующий кафедрой «Технологические комплексы, машины и механизмы», Белгородский государственный технологический университет им. В. Г. Шухова, Белгород, Россия

Мухин Виктор Михайлович, д.т.н., профессор, Российский химико-технологический университет им. Д. И. Менделеева», Москва, Россия

Вермель Владимир Дмитриевич, д.т.н., профессор, начальник Научно-технического центра научно-производственного комплекса, Центральный аэрогидродинамический институт им. профессора Н. Е. Жуковского, Московская область, Жуковский, Россия

Усольцева Надежда Васильевна, д.х.н., профессор, директор НИИ наноматериалов, Ивановский государственный университет, Иваново, Россия

Абдрахманова Ляйля Абдулловна, д.т.н., профессор, Казанский государственный архитектурно-строительный университет, Казань, Россия

Сергеев Вячеслав Андреевич, д.т.н., профессор, директор Ульяновского филиала ФГБУН «Институт радиотехники и электроники им. В. А. Котельникова» РАН, Ульяновск, Россия

Запороцкова Ирина Владимировна, д.ф.-м.н., профессор, директор института приоритетных технологий, Волгоградский государственный университет, Волгоград, Россия

Гутерман Владимир Ефимович, д.х.н., профессор, главный научный сотрудник, Южный федеральный университет, Ростов-на-Дону, Россия

Тафинцева Валерия Сергеевна, Ph.D., научный сотрудник, кафедра физики, факультет науки и технологий, Норвежский университет естественных наук, Норвегия

Тютюнник Вячеслав Михайлович, д.т.н., профессор, генеральный директор ООО «Международный информационный Нобелевский центр» (МИНЦ), ТГТУ, Тамбов, Россия

Переводчик: Гунина Наталия Александровна, к.ф.н., заведующий кафедрой «Международная научная и профессиональная коммуникация», ТГТУ, Тамбов, Россия

CONTENTS

Original papers

Nanostructured, nanoscale materials and nanodevices

Advanced structural materials, materials for extreme conditions

Biological materials;
nanomedicine, and novel technologies for clinical and medical applications

Manufacturing processes and systems

Reviews

Advanced structural materials, materials for extreme conditions

СОДЕРЖАНИЕ

Оригинальные статьи

Наноструктурированные, наноразмерные материалы и наноустройства

Современные конструкционные материалы, материалы для экстремальных условий

Биологические материалы;
наномедицина и новые технологии для клинического и медицинского применения

Производственные процессы и системы

Обзор

Современные конструкционные материалы, материалы для экстремальных условий

Journal of Advanced Materials and Technologies. Vol. 9, No. 4. 2024

Original papers
Nanostructured, nanoscale materials and nanodevices

УДК 662.215 DOI: 10.17277/jamt.2024.04.pp.244-256

Predictive estimation of detonation nanodiamond yield based on the characteristics of carbon-containing explosives

© Valerii Yu. Dolmatov [a]✉, Dmitry V. Rudenko [a], Evgeny D. Eidelman[b], Maria A. Blinova[a, c]

[a] *Special Design and Technological Bureau "Technolog", 33-a, Sovetskiy Av., St. Petersburg, 192076, Russian Federation,*
[b] *Saint Petersburg State Chemical and Pharmaceutical University of the Ministry of Healthcare of the Russian Federation, 14A, Professor Popov St., St. Petersburg, 197022, Russian Federation,*
[c] *St. Petersburg State Technological Institute (Technical University), 24-26/49A, Moskovskiy Av., St. Petersburg, 190013, Russian Federation*

✉ diamondcentre@mail.ru

Abstract: The paper gives a predictive estimate of detonation nanodiamond (DND) yield depending on the value of oxygen balance, zone length, and chemical reaction time of explosives. The dependences of the main characteristics of explosives on each other are determined. It is shown that practically any characteristic of explosives (e.g., detonation velocity) can be used to calculate other characteristics of explosives, as well as the DND yield during their synthesis. The DND yield from hydrogen-free benzotrifuroxane (1.88 wt. %) was determined for the first time. According to the data of the Institute of Hydrodynamics named after M.A. Lavrentiev (Russia, Novosibirsk), such nanodiamonds have a spherical shape (diameter ~100 nm) due to a very high temperature (4300 K) and pressure of 36 GPa. Moreover, the thermal effect of combustion and the thermal effect of the explosion can be accurately calculated based on the elemental composition of explosives. From there, the specific power of the explosives and all other characteristics, including the DND yield, can be determined. Predictive evaluation does not exclude the need for experimental work, but determines its feasibility.

Keywords: detonation nanodiamonds; yield; explosives; oxygen balance; detonation velocity; pressure; reaction time; chemical reaction zone length.

For citation: Dolmatov VYu, Rudenko DV, Eidelman ED, Blinova MA. Predictive estimation of detonation nanodiamond yield based on the characteristics of carbon-containing explosives. *Journal of Advanced Materials and Technologies*. 2024;9(4):244-256. DOI: 10.17277/jamt.2024.04.pp.244-256

Прогнозная оценка выхода детонационных наноалмазов на основе характеристик углеродсодержащих взрывчатых веществ

© В. Ю. Долматов[a]✉, Д. В. Руденко[a], Е. Д. Эйдельман [b], М. А. Блинова [a, c]

[a] *Специальное конструкторско-технологическое бюро «Технолог»,*
Советский пр., 33-а, Санкт-Петербург, 192076, Российская Федерация,
[b] *Санкт-Петербургский государственный химико-фармацевтический университет*
Министерства здравоохранения Российской Федерации,
ул. Профессора Попова, 14, лит. А, Санкт-Петербург, 197022, Российская Федерация,
[c] *Санкт-Петербургский государственный технологический институт (технический университет),*
Московский пр., 24-26/49, лит. А, Санкт-Петербург, 190013, Российская Федерация

✉ diamondcentre@mail.ru

Аннотация: Дана прогнозная оценка выхода детонационных наноалмазов (ДНА) в зависимости от значения кислородного баланса, длины зоны и времени химической реакции взрывчатых веществ (ВВ). Определены зависимости основных характеристик ВВ друг от друга. Показано, что практически любой параметр ВВ (например, скорость детонации) может быть использован для расчета других их характеристик, а также выхода

ДНА при их синтезе. Впервые определен выход ДНА из безводородного бензотрифуроксана (1,88 мас. %). Такие наноалмазы по данным Института гидродинамики им. М. А. Лаврентьева (Россия, Новосибирск) имеют сферическую форму (диаметр ~100 нм) из-за очень высокой температуры (4300 К) и давления 36 ГПа. По элементному составу ВВ рассчитаны тепловой эффект сгорания, тепловой эффект взрыва, удельная мощность ВВ и все остальные характеристики, включая выход ДНА. Прогнозная оценка не исключает необходимость проведения экспериментальных работ, но определяет их целесообразность.

Ключевые слова: детонационные наноалмазы; выход; взрывчатые вещества; кислородный баланс; скорость детонации; давление; время реакции; длина зоны химической реакции.

Для цитирования: Dolmatov VYu, Rudenko DV, Eidelman ED, Blinova MA. Predictive estimation of detonation nanodiamond yield based on the characteristics of carbon-containing explosives. *Journal of Advanced Materials and Technologies*. 2024;9(4):244-256. DOI: 10.17277/jamt.2024.04.pp.244-256

1. Introduction

Detonation nanodiamonds (DND) are currently one of the most sought-after allotropies of carbon, with attention being paid to the development of technologies for obtaining various types of DND, selection of initial explosives for their production, investigation of properties, and most importantly, their application in various fields of industry, medicine, and agriculture [1–16].

As a rule, explosive is a polynitro compound that contains in each molecule both a “fuel” (carbon, hydrogen) and an “oxidizer” (oxygen), with oxygen bonded to nitrogen. The exothermic reactions of oxidation of carbon to CO and CO_2; hydrogen to H_2O – represent the source of energy of the explosion. When there is a shortage of oxygen (negative oxygen balance (OB)), free carbon appears in detonation products (DP), which can be in the form of DND and non-diamond carbon of various allotropic forms.

The composition of DP depends largely on the equilibrium position of the two reactions:

$$2CO \leftrightarrow CO_2 + C;$$

$$H_2 + CO \leftrightarrow H_2O + C.$$

According to [7] the equilibrium of the second reaction is shifted to the right in all cases, while in the first reaction the equilibrium is shifted to the right only for high initial densities at $\rho_0 > 1.5\ g{\cdot}cm^{-3}$. Thus, hydrogen of explosive molecules oxidized to H_2O, and carbon can be oxidized to CO_2 almost completely only for high-density charges with $\rho_0 \rightarrow \rho_{max}$, or distributed between CO_2 and CO (for low-density charges). The decomposition of explosives is a complex multistage set of reactions in series and in parallel. The course of reactions and the composition of reaction products can change with the changes in temperature and pressure.

By now, the process of DND synthesis from charges of TNT and hexogen mixture is well enough studied, and the optimal empirical values of the main control parameters of synthesis are known [17]. Charge composition (~60 % TNT and ~40 % hexogen), charge density (1,6–1,7 $g{\cdot}cm^{-3}$), optimal oxygen balance (–35÷–60), presence of water or water-salt armor of the charge, non-oxidizing, or better, reducing medium of detonation. At the same time, the pressure in the chemical reaction zone (CRZ) should exceed 17 GPa, and the temperature should be at least 3000 K.

The output and quality of the DND depend on a variety of parameters:

1. Composition of the explosive charge and its specific power.
2. Oxygen balance of explosives.
3. Charge density.
4. Composition and heat capacity of the medium in the explosion chamber (EC).
5. Charge form.
6. The armor (shell) of the charge.
7. Charge mass to explosive chamber (EC) volume ratio.
8. Modification of the charge composition by doping elements or substances.
9. The magnitude of the pulse and the location of charge initiation.
10. EC design and its wall material.

Given the presence of such a large number of influencing factors, it is clear that reference in multiple works to only the same composition cannot guarantee the same yield of nanodiamonds in these studies. Moreover, the basic explosion parameters for the same explosives for charges of the same density do not guarantee the identity of the values of detonation velocity, pressure in the Chapman-Jouguet plane, time, length (width) of the chemical reaction zones (CRZ), and the DND yield. The value of the parameters is influenced not only by the skill of the performers, but also by the availability of hardware capabilities.

However, all of the above is not a hindrance to predictive and evaluative determination with all the above optimized parameters to determine the feasibility of working with a particular explosive, which was undertaken in this paper.

The paper aims to study the inter-relationship between the main characteristics of carbon-containing high explosives (oxygen balance, detonation velocity *D*, pressure *P* in the Chapman-Jouguet plane, residence time τ, and CRZ length *L* and their influence on the DND yield.

2. Materials and Methods

To carry out the charge explosion we used a steel explosion chamber "Alpha-2M" (Russia) with a capacity of 2.14 m^3. The explosion of charges was carried out in a water shell, the mass ratio of explosives: water – 1 : 10. The explosion medium was gaseous products of previous explosions. The mass of each charge was 0.5 kg, five charges were detonated in each experiment, the charges were made of pentaerythritetetranitrate, 2,4,6-trinitrotoluene, cyclotrimethylenetrinitramine, 2,4,6-trinitrophenol, 2,4,6-trinitro-N-methyl-N-nitroaniline and their mixtures in different ratios. The charges were manufactured and detonated by the same operator. The diamond blend resulting from the explosion was dried, then treated with dilute (Russian Standard 4461-77) nitric acid of concentration 40–50 % at temperature 220–230 °C and pressure 80–100 atm at the pilot plant. Further, the separated nanodiamonds were washed with distilled water in a cascade of countercurrent glass columns. Once the pH of the aqueous medium reached 6–7, the purified nanodiamonds were dried at a temperature of 115–120 °C, the temperature in the drying chamber was maintained by supplying superheated water vapor.

3. Results and Discussion

3.1. Interdependencies of characteristics

Since any use of explosives is a dangerous process and not all potentially suitable substances for producing DND are readily available, it is expedient to theoretically determine the possibility of using a particular explosive to produce DND. At present, only two methods of producing DND are known – from a mixture of TNT and hexogen and from tetryl, but due to the rising cost of raw materials of explosives and their scarcity, it has become necessary to search for new, more affordable types of explosives [18]. The best-known characteristics of explosives are detonation velocity and oxygen balance. In [17], it was found that for some aromatic polynitro compounds of explosives, the optimal oxygen balance for producing DND with an acceptable yield ≥ 5 % of the mass of explosives was –35÷–60 %. These data, with a significant degree of probability, can be used by relating this value to the velocity of detonation of explosives, since [19] showed the dependence of the DND yield on the detonation velocity of a number of aromatic polynitro compounds (mainly mixtures of TNT and hexogen) with an optimum of 7250–8000 $m \cdot s^{-1}$ (DND yield ≥ 5 % of the mass of explosives).

The explosion parameters and the achieved yield from a range of explosives are shown in Table 1.

However, tabular material is difficult to perceive without graphical representation. In Fig. 1, in the coordinates of detonation velocity to OB, the region bounded by oxygen balance –35÷–60 % and optimum *D* = 7250–8000 $m \cdot s^{-1}$ is highlighted.

Table 1. Detonation velocity, oxygen balance and DND yield depending on the type of explosives [3, 7, 17, 18]

No.	Explosives	D, $m \cdot s^{-1}$	Oxygen balance, %	DND yield, %
1	2	3	4	5
1	Aminotrinitrobenzene (trinitroaniline)	8100	–56.16	
2	BTF	8610	–38.08	1.88
3	Hexogen	8383 8850	–21.6	~1.0
4	Hexanitrodiphenyl	7100	–52.8	
5	Hexyl	7145	–52.8	
6	1,3-diamino-2,4,6-trinitrobenzene	7450	–55.97	
7	Octogen	9124	–21.6	~1.0
8	TEN	8142 8277 8590	–10.1	0.15
9	Tetranitroaniline	7630	–32.2	
10	Tetranitrobenzene	8000	–31	
11	Tetryl	7573	–47.4	7.6

Continuation of the Table 1

1	2	3	4	5
12	TATB	7606 7970	–55.8	4.1
13	Trinitroanisole	7640	–62.5	
14	Trinitrobenzene	7350	–56.3	
15	Trinitrophenol (picricacid)	7350	–45.4	~1.5
16	TNT	7000	–73.9	~1.0
17	EDNA	7570 7750	–32	
18	TH 70/30	7420	–58.3	4.7
19	TH 60/40	7510	–53	8.5
20	TH 50/50	7670	–47.8	6.0
21	TH 40/60	7850	–42.6	5.8
22	TH 36/64 (pres.)	8000	–40.5	5.4
23	TH 30/70	8052	–37.3	4.4
24	GNAB	7311	–49.6	6.63
25	Z-TACOT	7250	–74.2	3.34

BTF: Benzotrifuroxane;
Hexogen: cyclotrimethylenetrithramine;
Hexyl: hexanitrodiphenylamine, dipicrylamine;
Octogen: cyclotetramethylenetetranitramine, 1,3,5,7-tetranitro-1,3,5,7-tetrazacyclooctane;
TEN: pentaerythritetetranitrate, pentrithritol;
Tetryl: 2,4,6-trinitro-N-methyl-N-nitroaniline, methylpicrylnitramine, N-methyl-2,4,6-trinitrophenylnitramine;
TATB: 1,3,5-triamino-2,4,6-trinitrobenzene
EDNA: ethylene-N,N′-dinitramine, ethylenedinitramine, gallium;
GNAB: bis-(2,4,6-trinitrophenyl)-diazine;
Z-TACOT: 2,4,8,10-tetranitro-5H-benzotriazolo-[2,1-a]-benzotriazol-6-um;
TH: alloys or mixtures of TNT and hexogen.

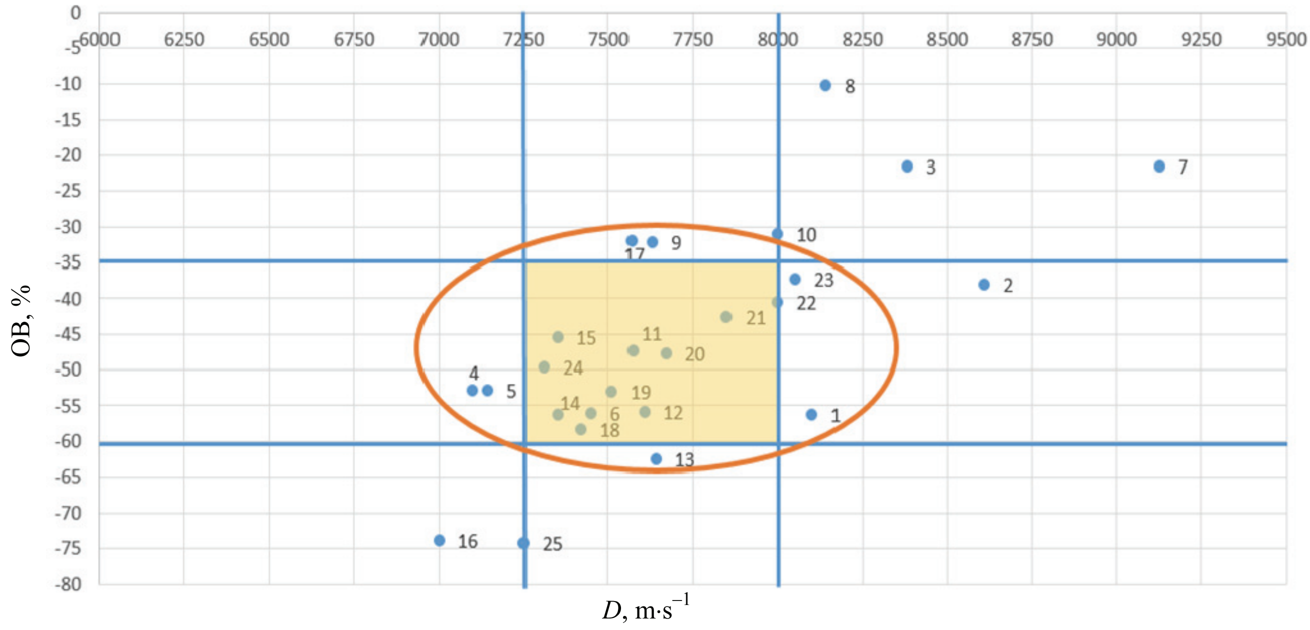

Fig. 1. Detonation velocity *D* and OB of explosives optimal for producing DND with yield ≥ 5 % of the mass of explosives

All explosives inside this region (as well as those lying immediately beyond it) are likely to provide an acceptable yield of DND (≥ 5 wt. %). These new initial explosives can include: hexyl (hexanitrodiphenylamine), hexanitrodiphenyl, tetranitroaniline, tetranitrobenzene, trinitroaniline, trinitroanisole, 1,3-diamino-2,4,6-trinitrobenzene, trinitrobenzene and their mixtures, i.e. polynitroaromatic compounds. The dependences obtained below with a high degree of probability can be extended only to powerful polyaromatic explosives. In addition, the value of DND yield obtained under different conditions for one and the same type of explosives can significantly differ from each other for different researchers.

In Fig. 1, the ellipse highlights the region with explosives that can theoretically provide an acceptable yield of DND (~5 wt. %).

It is equally important to trace the dependences of the DND yield on the other explosion parameters listed in Table 2.

Table 2 shows experimental and literature data reflecting the main parameters of the detonation process. Table 2 shows how much the specific explosive power differs – up to ~6 times, in contrast to the thermal effect – the maximum difference is only 1.35 times [17]. Part of the heat of explosion was calculated by additivity (by the proportional contribution of individual explosives constituting the mixture). It was preliminarily established by well-known thermal effects of mixed explosives that this technique gives an error of 1.4–1.8 %, which is insignificant.

Table 2. Explosion parameters and the DND yield depending on the type of explosives [7, 17, 19, 20]

No.	Explosive	Specific charge density ρ, g·cm^{-3}	Heat of explosion *Q*, kJ·kg^{-1}	Specific power *W*, kJ·(kg·μs)$^{-1}$	Detonation velocity *D*, m·s^{-1}	Pressure in flat. of Chapman-Jouget *P*, GPa	Chemical reaction time τ, μs	Length of the chemical reaction zone *L*, mm	DND yield *Y*, wt. %
1	TNT pres.	1.61	4190	22053	6611	**17.1 (7)**	0.19	1.25	**0.6–2.1** **1.4 (1)**
2	TH 80/20 molded	1.64	4440	**34154-55500 (8)**	7200	21.5	**0.13 (6)**	**0.65 (8)**	7.88
3	TH 70/30	1.64	4565	57063	7420	21.4	0.08	0.44	**7.61 (1)**
4	TH 60/40 molded 1	1.67	4690	33500	7510	24.4	0.14	0.72	**5.46 (1)**
5	TH 60/40 molded 2	1.64	4690	39083	7500	22.2	**0.12 (6)**	0.4	**7.92 (1)**
6	TH 50/50	1.68	4815	37003	7670	25.9	0.13	0.64	**6.07 (1)**
7	TH 40/60 pres.	1.61	4940	44909	7850	22.8	0.11	0.50	**7.15 (1)**
8	TH 30/70 pres.	1.60	5065	42208	8052	27.6	0.12	**0.5 (3)**	**5.0 (1)**
9	Z-TACOT	1.85	4103	32564	7250	26.3	**0.126 (6)**	**0.57 (3) – 0.60 (6)**	**3.44 (2) – 6.61 (1)**
10	Z-TACOT/Octogen80/20	1.58	4388	27425	8040	22.2	0.16	**0.71 (1)**	**6.38 (1)**
11	Hexogen	1.78	5440	77714	8670	34.5	0.07	0.36	1.1
12	TH 36/64	1.73	4990	49900	7920	28	0.10	0.60	**6.38 (1)**
13	TEN	1.76	6318	78975	8260	30.8	0.08	0.42	0.15
14	TATB	1.88	3473	14475	7350	29.7	0.24	1.18	**1.9 (1) – 4.43 (2)**
15	TATB/Octogen 70/30	1.85	3536	25257	**8129 (5)**	**23.8 (4)**	**0.14 (9)**	**0.71 (1)**	5.3
16	Octogen	1.91	5526	138150	8920	**34.4 (6)**	0.04	0.25	
17	Octogen/THT 90/10		5392	77028	8790	**33.4 (6)**	0.07	0.37	
18	TNT	1.73	4609	46090	7500	26.7	0.10	0.33	7.6

Bold indicate calculated data obtained using formulas (1) – (9), the number of the formula used for calculation is indicated in parentheses.

Table 2 presents the data of DND yield and such difficult-to-determine explosion parameters as the length of the chemical reaction zone (from the detonation wave front to the Chapman-Jouguet plane) and its time. By determining the time of the chemical reaction or the length of the chemical reaction zone, it is possible to predict the DND yield.

We are just discussing the DND yield here, and as previously stated, the found dependences of DND yield on different explosion parameters are only applicable to polynitroaromatic compounds and their combinations; they are not applicable for calculations for nitroolefins and nitroheterocycles. There is a correlation between the other characteristics of different explosives. For example, octogen is an analog of hexogen, and subsequently after detonation of octogen the DND yield of more than 1 % follows (exp. 16). Addition of 10 wt. % to TNT octogen cannot practically affect the DND yield (exp. 17).

In [19], it was postulated that in the process of DND synthesis, the chemical reaction time equal to the time of matter passage from the detonation wave front to the Chapman-Jouguet plane (i.e., from the beginning to the end of the chemical reaction zone) can be taken as the unit of time of energy release in an explosion. This time is tenths and hundredths of a microsecond. For many practical calculations, the exact time of existence of the CRZ is of critical importance, since it allows us to establish the real explosive power, which differs greatly for different types of explosives or their mixtures and affects the DND yield under other equal conditions. Therefore, it was proposed to determine the explosive power as the ratio of the heat of explosion of a unit mass to a unit time, i.e.

$$W = \frac{Q}{m\,\tau},$$

where W is the power of explosives, kJ·(kg·μs)$^{-1}$; Q is the heat of explosion, kJ·kg^{-1}; m is the mass of explosives, kg or g-mol; τ is the time of energy release from the detonation wave front to the Chapman-Jouguet plane, μs. The heat of explosion of individual types of explosives and their mixtures has been determined many times and depends slightly on the methodology of determination and specific performers [18]; the time of existence of CRZ is quite accurately determined in [20, 21]. However, the DND yield strongly depends on the conditions of the detonation synthesis process.

Table 2 also shows the specific power of explosives, then the graphical dependencies of the DND yield on various explosion parameters and their dependencies on each other, as well as the mathematical dependencies (formulas) describing the graphical material are presented.

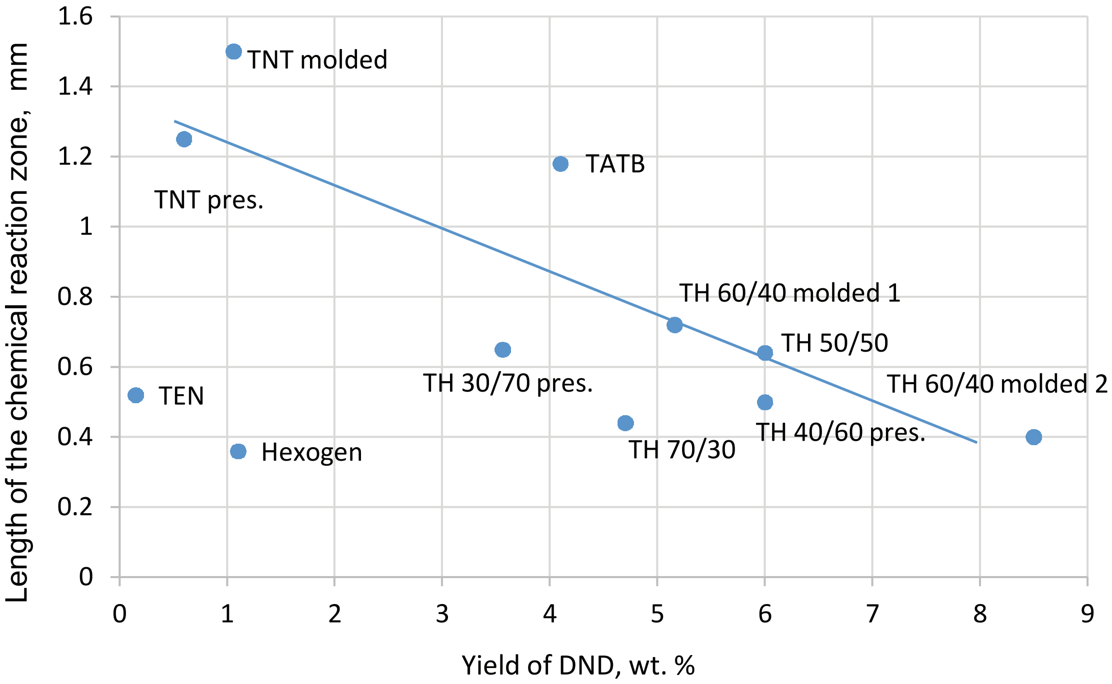

Fig. 2. Dependence of the DND yield on the length of the chemical reaction zone

The equation (Fig. 2) of the best linear approximation (without taking into account the points of the corresponding heating elements and hexogen) of the dependence DND yield, wt. %. (Y) from the length of chemical reaction zone, mm (L)

$$Y = -7.7L + 11. \quad (1)$$

The equation (Fig. 3) of the best approximation by a parabola (excluding the points of the corresponding TEN, hexogen, TNT pres. and TATB) of the dependence of yield of DND, wt. % (Y) on the chemical reaction time, μs (τ):

$$Y = 1.97(\tau - 0{,}15)^{0.5} + 4.25. \quad (2)$$

But the length of the CRZ of the recommended explosives can be determined very accurately by the dependence of the CRZ length on the pressure in the Chapman-Jouguet plane (a parameter that is known for many explosives).

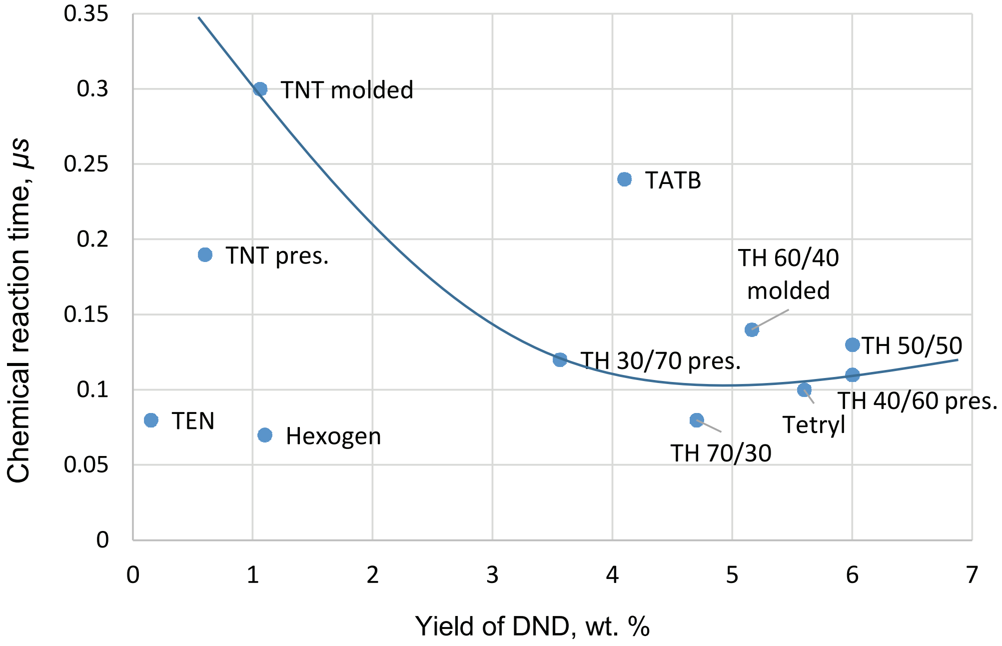

Fig. 3. Dependence of the DND yield on chemical reaction time

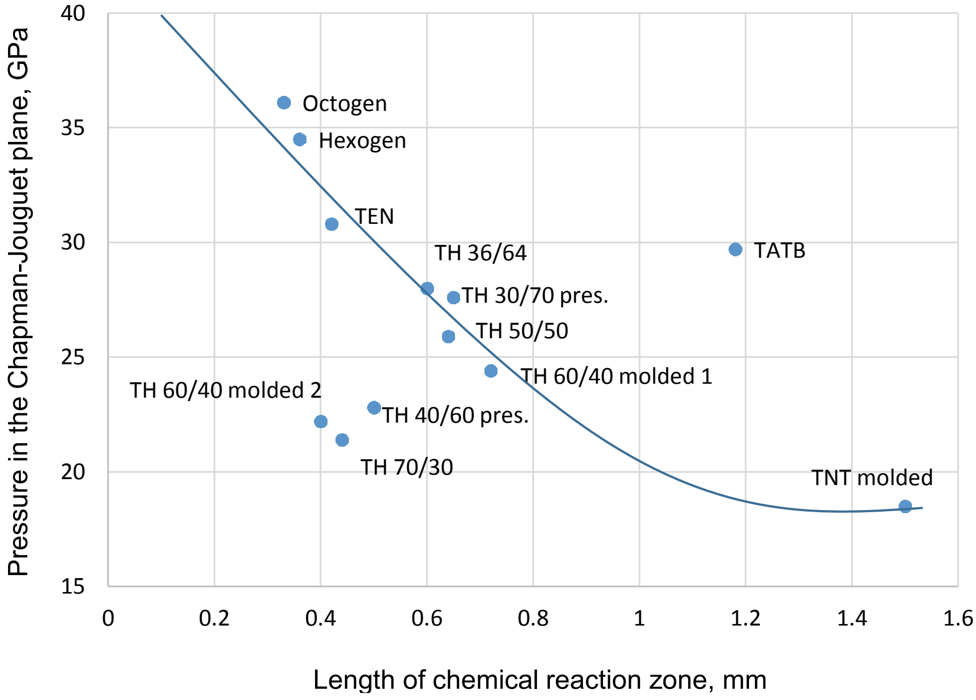

Fig. 4. Dependence of the CRZ length on pressure in the Chapman-Jouguet plane

The equation (Fig. 5) of the best approximation by hyperbola (excluding the points of the corresponding TH 70/30, TH 60/40 molded 2 and TATB) of the dependence CRZ length, mm (L) on P in the Chapman-Jouguet plane, GPa, (P):

$$L = -5.84 + 770/(P + 93.8). \qquad (3)$$

The equation (Fig. 5) of the best approximation by hyperbola (excluding the points corresponding TH 70/30, TH 60/40 molded 2 and TATB) of the dependence of P in the Chapman-Jouguet plane, GPa, (P) on the CRZ length, mm (L):

$$P = -93.8 + 770/(L + 5.84). \qquad (4)$$

It is more straightforward to determine the CRZ length from widely known values of the detonation velocity, which is first determined by the explosion parameters for new explosives and their mixtures according to Fig. 5. This dependence is expressed very clearly. The dropout of the TH 36/64 composition from the series, with high probability, indicates an incorrect determination: either of the detonation velocity, or of the CRZ length, or of the anomalously high (low) value of the specific density of the compacted charge.

The equation of the best approximation by a parabola (excluding the points corresponding to TH 60/40 molded 2, TH 70/30 and TATB) of the dependence of the detonation velocity, m/s (D) on the CRZ length, mm (L):

$$D = 1000L^2 - 2500L + 9400. \qquad (5)$$

The dependence of the chemical reaction time on the detonation velocity is also informative (Fig. 6). There is also a well-defined dependence here, which makes it easy (from the detonation velocity) to determine the time of the LCR. The dropout of TATB and TEN from this series may indicate "over compressed" detonation at too high a charge density.

The equation of the best approximation by hyperbola (excluding the points of the corresponding TH 70/30, TNT pres. and TATB) of the dependence of chemical reaction time, μs (τ) ondetonation velocity, m·s^{-1} (D) will be

$$\tau = 0.075 + 84/(D - 5600). \qquad (6)$$

The equation (Fig. 7) of the best linear approximation (excluding the points of the corresponding TATB, TH 70/30 pres., TH 40/60 pres.) of the dependence of pressure in the Chapman-Jouguet plane, GPa, (P) on detonation velocity, m·s^{-1} (D) will be

$$P = 0.0075D - 32.5. \qquad (7)$$

The equation of the best linear approximation (ignoring the point corresponding TNT pres.) of the dependence of CRZ length, mm (L) on chemical reaction time, μs (τ) will be

$$L = 5\tau. \qquad (8)$$

The equation of the best linear approximation (excluding the point of the corresponding TNT pres.) of the dependence of chemical reaction time, μs (τ) on CRZ length, mm (L) will be

$$\tau = 0.2L. \qquad (9)$$

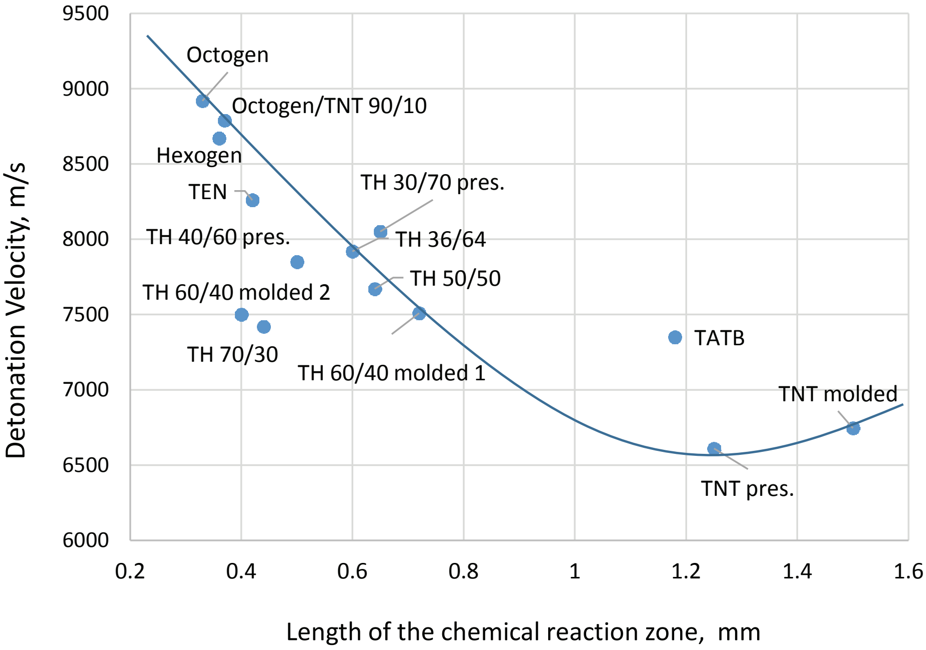

Fig. 5. Dependence of the CRZ length on the detonation velocity

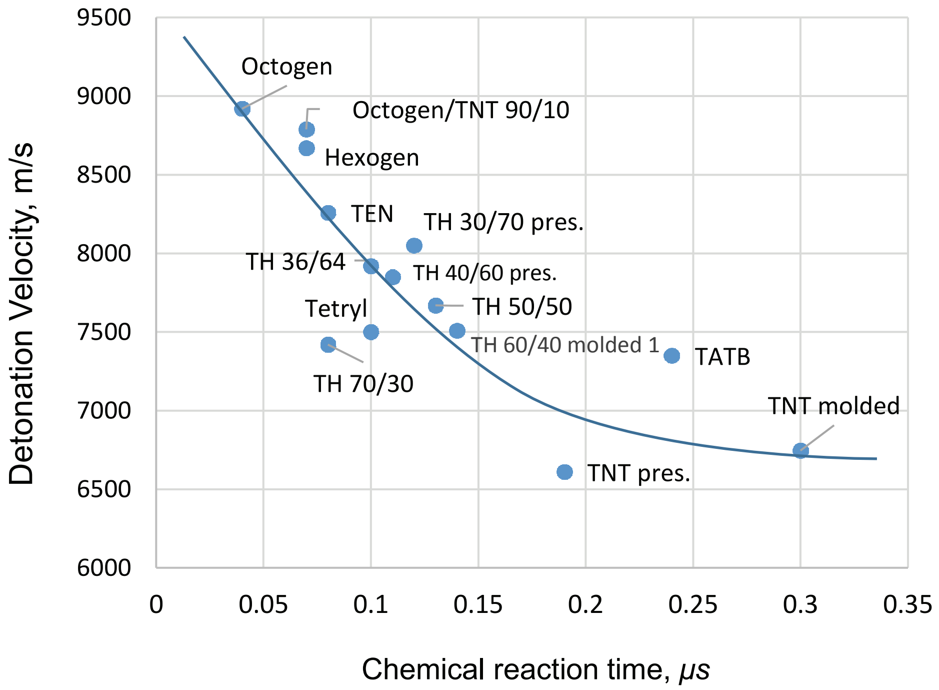

Fig. 6. Dependence of chemical reaction time on detonation velocity

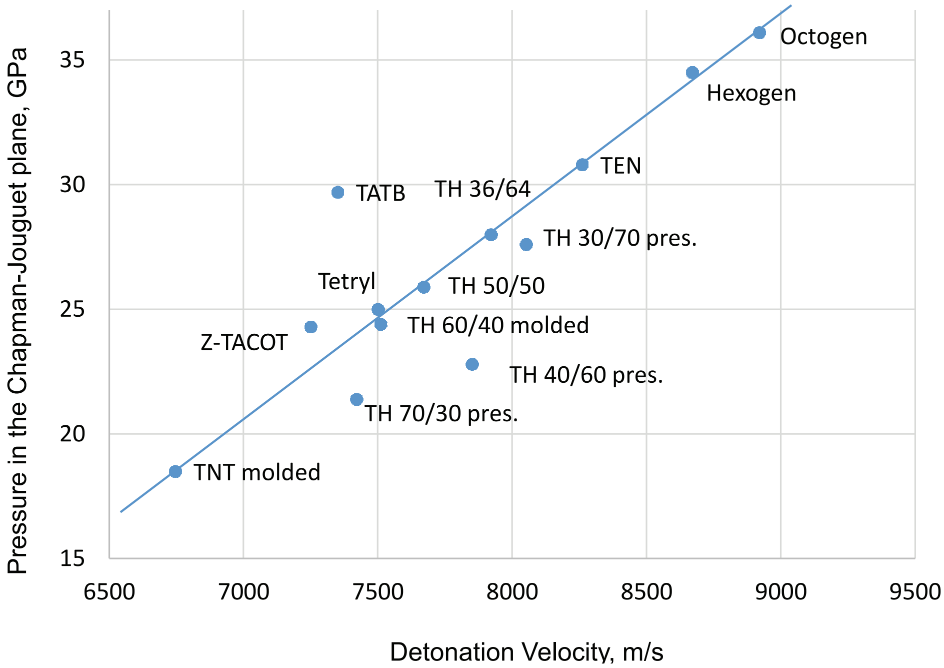

Fig. 7. Dependence of the pressure in the Chapman-Jouguet plane on the detonation velocity

The chemical reaction time, which is natural, correlates reasonably well with the CRZ length (Fig. 8), making it easy to determine one quantity by knowing the other.

Table 3 summarizes the calculated data based on the obtained dependencies for all eight recommended polynitroaromatic compounds: hexyl (hexanitrodiphenylamine), hexanitrodiphenyl, tetranitroaniline, tetranitrobenzene, trinitroaniline, trinitroanisole, 1,3-diamino-2,4,6-trinitrobenzene, and trinitrobenzene.

The expected DND yield, specific power of explosives, pressure in the Chapman-Jouguet plane, time, and CRZ length (width) were all calculated based on the known value, or detonation velocity.

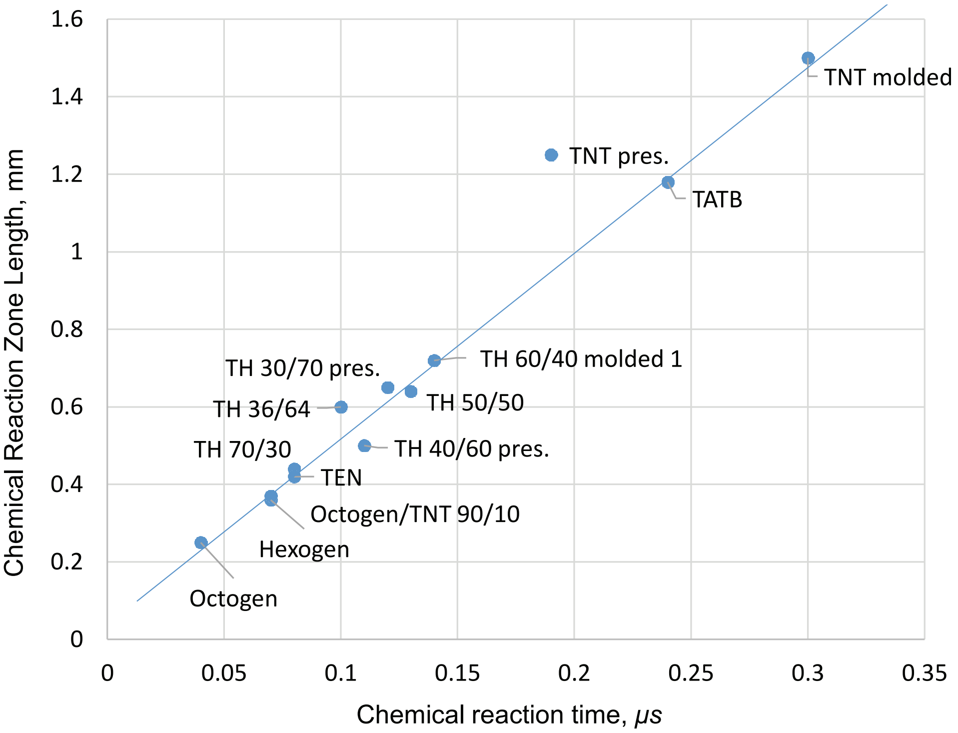

Fig. 8. Dependence of chemical reaction time on the CRZ length

Table 3. Explosion and DND yield parameters for polynitroaromatic compounds

No.	Explosive	Specific charge density ρ, g·cm^{-3}	Heat of explosion Q, kJ·kg^{-1}	Specific power W, kJ·(kg·μs)$^{-1}$	Detonation velocity D, m·s^{-1}	Pressure in flat. of Chapman-Jouget P, GPa	Chemical reaction time τ, μs	Length of the chemical reaction zone L, mm	Yield of DND Y, wt. %	Oxygen balance, %
1	Trinitroaniline	1.762	4148	37709	8100 **(ρ = 1.75)**	28.3 (7)	0.11 (6)	0.47 (3)	7.4 (1)	–56.16
2	Hexanitrodiphenyl	1.61			7100 **(ρ = 1.6)**	20.8 (7)	0.13 (6)	0.88 (3)	4.2 (1)	–52.8
3	Hexyl	1.653	4220	32462	7145 **(ρ = 1.6)**	21.1 (7)	0.13 (6)	0.86 (3)	4.4 (1)	–52.8
4	1,3-diamino-2,4,6-trinitrobenzene	1.8	4278	35650	7450 **(ρ = 1.79)**	23.4 (7)	0.12 (6)	0.73 (3)	5.4 (1)	–56.0
5	Tetranitroaniline	1.867	4261	35508	7630 **(ρ = 1.6)**	24.7 (7)	0.12 (6)	0.66 (3)	5.9 (1)	–32.2
6	Tetranitrobenzene	1.82			8000 **(ρ = 1.82)**	27.5 (7)	0.11 (6)	0.51 (3)	7.1 (1)	–31.0
7	Trinitroanisole	1.61			7640 **(ρ = 1.6)**	24.8 (7)	0.12 (6)	0.65 (3)	6.6 (1)	–62.6
8	Trinitrobenzene	1.688	4600	38333	7300 **(ρ = 1.65)**	22.3 (7)	0.12 (6)	0.79 (3)	4.9 (1)	–56.3

In [22] it was shown that the calculation of the value of heat of combustion (HC) (low calorific value Q_{low}, considering heat losses with water vapor) of elements, organic and inorganic substances with negative oxygen balance, including explosive, is carried out by a simple formula:

$$Q_{low} = 0.1387\ (OB).$$

From here, knowing the gross formula of the substance, it is easy to calculate the heat of combustion.

The calculation of OB is based on the assumption that the combustibles in a substance molecule (carbon and hydrogen) are oxidized during combustion or explosion by an oxidizer (oxygen in the molecule) to higher oxides – carbon to CO_2, and hydrogen to H_2O. In reality, some carbon is oxidized to carbon monoxide (CO), with less energy released. In addition, experimentally determined Q_{low} is not a constant, the accuracy of its determination is influenced by the method of determination, the peculiarities of the apparatus and the qualification of the experimenter, sometimes Q_{low} differs from each other (in different reference books) significantly. Considering the "ideality" of the Q_{low} calculation, it should be expected that the calculation and Q_{low}, as a rule, should give a higher value than the experimentally determined TC. It is to be expected that the smaller the difference between the calculated Q_{low} value (by OB) and the experimentally determined one, the more accurate the experimental data will be.

It is clear that at explosion due to incompleteness of redox reactions the heat of explosion (Q_{exp}) will be less than Q_{low}. Calculated and experimental data of explosions given in Table 3 [22] show that on average Q_{exp} Less, for dinitroaromatic compounds – by 5 times; for trinitroaromatic compounds – by 1.7 times. For tetranitroaromatic compounds by a factor of 1.05.

Thus, proceeding from the gross formula of explosive it is possible to determine with satisfactory accuracy Q_{low}, further – Q_{exp} (multiply reducing Q_{low}). Knowing the time of the CRZ existence, by the formula denoted earlier: $W = Q/m\,\tau$, we determine W. Then by the formula

$$Y = 0.36\cdot10^{-3}W^2 + + 3.24\cdot10^{-4}W - 1.31$$

– we determine the DND yield.

3.2. On deviations from approximation ratios and curves

Consider the deviations from the approximation relationships and curves for Z-TACOT/octogen 80/20 explosives (No. 10 in Table 2). The only known value that is included in the formulas and graphs, and even then without indication of the measurement error, is the DND yield, $Y = 6.28$ wt. %.

From the band of acceptable values, it can be found that the corresponding CRZ length, L, lies in the range from 0.4 to 1.0 mm (Fig. 2). This corresponds well to the value $L = 0.8$ mm found by the approximation relation (1) $Y = -7.7\,L + 11$, with a correlation of at least 50 %.

By the band of acceptable values, it can be found that the corresponding chemical reaction time lies in the range from 0.12 to 0.16 μs (Fig. 3). This corresponds well to the value of $\tau = 0.16$ μs found by the approximation relation (2) $Y = 1.97\,(\tau - - 0.15)^{0.5} + 4.25$, with a correlation of at least 75 %.

From the band of valid values for the calculated value of L = 0.8 mm, it can be found that the corresponding Chapman-Jouguet plane pressure P lies in the range of 22 to 26 GPa (Fig. 4). This corresponds well to the value $P = -93.8 + + 770 / (L + 5.84)$ found by the approximation relation (4) to be $P = 22.2$ GPa, with a correlation of at least 84 %. Note that for the values of L corresponding to the edges of its band of acceptable values from 0.4 to 1.0 mm the value of P lies in the range from 31 to 21 GPa, giving a correlation of about 50 %.

From the band of acceptable values for the calculated value of $L = 0.8$ mm, it can be found that the corresponding detonation velocity D, lies in the range of 7400 to 8000 $m\cdot s^{-1}$ (Fig. 5). This corresponds to the value $D = 8040$ $m\cdot s^{-1}$ found by the approximation relation (5) $D = 1000\,L^2 - - 2500\,L + 9400$, with a correlation of at least 90 %. Note that for the values of L corresponding to the edges of its band of admissible values from 0.4 to 1.0 mm the value of D lies in the range from 8700 to 6800 $m\cdot s^{-1}$, giving a correlation of about 85 %.

From the band of acceptable values for the calculated value of $\tau = 0.16$ μs, it can be found that the corresponding detonation velocity D, lies in the range of 6800 to 7200 $m\cdot s^{-1}$ (Fig. 6). This corresponds to the value $D = 8040$ $m\cdot s^{-1}$ found by the approximation relation (6) $\tau = 0.075 + 84 / (D - 5600)$, with a correlation of at least 85 %. Note that for values of τ corresponding to the edges of its bandwidth of 0.12 to 0.16 μs the value of D lies between 7200 and 7800 $m\cdot s^{-1}$, giving a correlation of about 85 %.

Calculating the correlation in Fig. 7 for P from D and the correlation in Fig. 8 for L from τ requires determining the band of acceptable values of the first parameter from the band of acceptable values of the second. Such calculations will contain a significant error.

4. Conclusion

Using widely known data on explosives (detonation velocity, oxygen balance), a predictive evaluation of the applicability of explosives for DND production was carried out, and using the found complex of dependencies, it became possible to determine various characteristics of explosives, including the DND yield, knowing at least one of the characteristics.

Thus, by the formula $Y = -\ 7.7L + 11$, where Y is the DNDyield and L is the CRZ length (mm), we determine the nanodiamond yield.

Using the formula $Y = 1.97(\tau - 0.15)^{0.5} + 4.25$, where τ is the chemical reaction time (μs), we also determine the nanodiamond yield.

The CRZ length (mm) is related to the pressure in the Chapman-Jouguet plane (P, GPa), by the following dependence $L = -5.84 + 770/(P + 93.8)$.

The pressure in the Chapman-Jouguet plane is related to the CRZ length by the formula $P = -93.8 + 770/(L + 5.84)$.

The detonation velocity ($m{\cdot}s^{-1}$) correlates with the length of the chemical reaction zone by the equation $D = 1000\ L^2 - 2500L + 9400$.

The chemical reaction time is related to the detonation velocity $\tau = 0.075 + 84/(D - 5600)$.

The pressure in the Chapman-Jouguet plane is related to the detonation velocity by the equation $P = 0.0075D - 32.5$.

The CRZ length correlates with the chemical reaction time by the formula $L = 5\tau$, and the chemical reaction time from the CRZ length, respectively, as $\tau = 0.2L$.

5. Funding

This study received no external funding.

6. Conflict of interest

The authors declare no conflict of interests.

References

1. Danilenko VV. *Synthesis and sintering of diamond by explosion*. Moscow: Energoatom; 2003. 271 p. (In Russ.)

2. Babushkin AYu, Lyamkin AI. About diamond formation at detonation synthesis. *Vestnik KrasGU. Fiziko-matematicheskiye nauki*. 2003;(3):89-96. (In Russ.)

3. Kolomiichuk VI, Malkov IYu. Investigation of the synthesis of an ultrafine diamond phase under conditions of detonation of mixed compositions. *Fizika goreniya i vzryva =Combustion, Explosion, and Shock Waves*.1993;29(1):120-128. (In Russ.)

4. Frenklach M, Kematick R, Huang D, Howard W, et al. Homogeneous nucleation of diamond powder in the gas phase. *Journal of Applied Physics*. 1989;66(1):395-399. DOI:10.1063/1.343890

5. Breusov ON. To the question about the mechanism of dynamic synthesis of diamond from organic substances. *Chemical Physics*. 2002;21(11):110-115.

6. Tolochko BP, Titov VM, Chernyshev AP. Physicochemical model of formation of diamond particles at shock-wave impact on adamantine. *NanoCarbon and NanoDiamond 2006 Join International Conference September*. St.-Petersburg: Abstract; 2006. p. 9. (In Russ.)

7. Danilenko VV. *Explosion: physics, technique, technology*. Moscow: Energoatomizdat; 2010. 784 p. (In Russ.)

8. Babushkin VV, Lemyakin AI, Staver AM. Features of obtaining ultradisperse carbon-based material from explosives. *V All-Union Meeting on Detonation: Collection of Reports, Krasnoyarsk – August 5-12, 1991*. Chernogolovka: Intech Publ. house; 1991. V. 1. pp. 81-83. (In Russ.)

9. Vyskubenko BA, Danilenko VV, Lin EE, Mazanov VA, et al. Influence of scale factors on the size and yield of diamonds during detonation synthesis. *Fizika goreniya i vzryva = Combustion, Explosion, and Shock Waves*. 1992;28(2):108-109. (In Russ.)

10. Arnault J-C. *Nanodiamonds, advanced material analysis, properties and applications*: Elsevier; 2017. 476 p.

11. Oleinik GS, Bochechka AA. To the mechanism of formation of nanosized diamond particles of detonation synthesis obtained from the decomposition products of explosives. *Sverkhtverdye Materialy = Journal of Superhard Materials*. 2008;3(173):3-30. (In Russ.)

12. Anisichkin VF. On the mechanism of carbon release during detonation decomposition of substances. *Fizika goreniya i vzryva = Combustion, Explosion, and Shock Waves*. 1994;30(5):100-106. (In Russ.)

13. Batsanov SS. Features of solid-phase transformations initiated by shock waves. *Uspekhi Khimii = Russian Chemical Reviews*. 2006;75(7):673-686. (In Russ.)

14. Lin EE. On the cluster mechanism of diamond synthesis from various solid forms of carbon. *Fizika Tverdogo Tela = Physics of the Solid State*. 2000;42(10):1893-1898. (In Russ.)

15. Danilenko VV. Features of carbon condensation in detonation wave and optimal synthesis of nanodiamonds. *Sverkhtverdye Materialy = Journal of Superhard Materials*. 2006;(5):9-24. (In Russ.)

16. Anisichkin VF. The phenomenon of resonant solid-phase coalescence of small diamond particles in explosion products. *Khimicheskaya Fizika = Russian Journal of Physical Chemistry B*. 1993;12(5):605-608 (In Russ.)

17. Dolmatov VYu. Assessment of applicability of explosive charges for synthesis of detonation nanodiamonds. *Journal of Superhard Materials*. 2016;38(5):373-376. DOI:10.3103/S1063457616050099

18. Zhukov BP. *Energy condensed systems: brief encyclopedic word*. Moscow: Janus-K; 1999. 595 p. (In Russ.)

19. Dolmatov V. Specific power of explosive and its effect on nanodiamonds. *Universal Journal of Carbon Research*. 2023;66-71. DOI:10.37256/ujcr.1220233919

20. Loboiko BG, Lubyatinsky SN. Reaction zones of detonating solid explosives. *Combustion, Explosion and*

Shock Waves. 2000;36(6):716-733. DOI:10.1023/A:1002898505288

21. All-Russian conference "Explosion in a physical experiment". *On the possibility of determining the size of the detonation wave zone by indirect methods*. Available from: http://conf.nsc.ru/explosion/ru/scientific_program [25 September 2024]

22. Dolmatov VYu, Ozerin AN, Eidelman ED, Kozlov AS, et al. Predictive estimate of the calorific value of substances with negative oxygen balance depending on the value of oxygen balance. *Journal of Advanced Materials and Technologies*. 2022;7(2):122-134. DOI:10.17277/jamt.2022.02.pp.122-134

Information about the authors / Информация об авторах

Valerii Yu. Dolmatov, D. Sc. (Eng.), Head of research laboratory, Special Construction and Technology Bureau “Technolog”, St. Petersburg, Russian Federation; ORCID 0000-0001-8643-0404; e-mail: diamondcentre@mail.ru

Evgeny D. Eidelman, D. Sc. (Phys. and Math.), Professor, Saint Petersburg State Chemical and Pharmaceutical University of the Ministry of Healthcare of the Russian Federation, St. Petersburg, Russian Federation; ORCID 0000-0002-2030-9262; e-mail:eugeny.eidelman@pharminnotech.com

Dmitry V. Rudenko, Cand. Sc. (Econ.), Director-Chief Designer, Special Construction and Technology Bureau “Technolog”, St. Petersburg, Russian Federation; e-mail: rudenko@sktb-technolog.ru

Maria A. Blinova, third category research engineer, Special Construction and Technology Bureau “Technolog”, St. Petersburg, Russian Federation; ORCID 0009-0004-4224-0755; e-mail: mashablinova5@gmail.com

Долматов Валерий Юрьевич, доктор технических наук, начальник научно-исследовательской лаборатории, Специальное конструкторско-технологическое бюро «Технолог», Санкт-Петербург, Российская Федерация; ORCID 0000-0001-8643-0404; e-mail: diamondcentre@mail.ru

Эйдельман Евгений Давидович, доктор физико-математических наук, профессор, Санкт-Петербургский государственный химико-фармацевтический университет Министерства здравоохранения Российской Федерации, Санкт-Петербург, Российская Федерация; ORCID 0000-0002-2030-9262; e-mail: eugeny.eidelman@pharminnotech.com

Руденко Дмитрий Владимирович, кандидат экономических наук, директор, главный конструктор Специальное конструкторско-технологическое бюро «Технолог», Санкт-Петербург, Российская Федерация; e-mail: rudenko@sktb-technolog.ru

Блинова Мария Алексеевна, инженер-исследователь третьей категории, Специальное конструкторско-технологическое бюро «Технолог», Санкт-Петербург, Российская Федерация; ORCID 0009-0004-4224-0755; e-mail: mashablinova5@gmail.com

Received 04 October 2024; Accepted 29 October 2024; Published 20 December 2024

Original papers
Nanostructured, nanoscale materials and nanodevices

УДК 620.3:620.18 DOI: 10.17277/jamt.2024.04.pp.257-266

Phase composition of stainless steel subjected to ultrasonic nanocrystal surface modification with different processing density

© Denis A. Polonyankin[a]✉, Alexey A. Fedorov[a], Tatyana M. Gomonyuk[a,b]

[a] *Omsk State Technical University, 11, Mira Av., Omsk, 644050, Russian Federation,*
[b] *CJSC "Elekton", 17 DC, 150, Raduzhny, 600910, Russian Federation*

✉ dapolonyankin@omgtu.tech

Abstract: Improving physical and mechanical properties of austenitic stainless steels (ASS) by methods of surface severe plastic deformation (SSPD) is one of the key problematic topics in the field of surface engineering and nanocrystal materials. The complex nature of the structural states evolution under the conditions of SSPD restricts the possibilities of a specified nanostructuring of the type 18-10 ASS in a wide range of deformation impacts. The article presents the results of XRD and TEM analysis of AISI 321 near-surface layer after ultrasonic nanocrystal surface modification (UNSM) with different processing densities. The work used methods of X-ray diffraction analysis (XRD) and transmission electron microscopy (TEM) tested for examination of the structural and phase composition of the type 18-10 ASS subjected to UNSM. XRD and TEM indicate a two-phase $(\alpha' + \gamma)$ composition of the near-surface layer of AISI 321 steel processed by UNSM. The XRD technique has established the functional dependencies of the martensite volume fraction from 1) the processing density and 2) the strain energy density, the approximation of which by linear regression equations is performed with reliability $R^2 = 0.984$. According to TEM data, the structure of the near-surface layer of AISI 321 stainless steel subjected to UNSM with the maximum processing density used ($N = 9367$ mm^{-2}) is represented by a significant amount of martensite in the form of lamellae with the width of less than 100 nm and a high dislocation density. The results of this work can be used to develop and optimize the UNSM processing modes of the 18-10 ASS produced by subtractive, additive and hybrid additive-subtractive manufacturing technologies.

Keywords: ultrasonic nanocrystal surface modification; AISI 321 stainless steel; processing density; strain energy density; phase composition; austenite; deformation-induced martensite; phase volume fraction; lamellae nanostructure.

For citation: Polonyankin DA, Fedorov AA, Gomonyuk TM. Phase composition of stainless steel subjected to ultrasonic nanocrystal surface modification with different processing density. *Journal of Advanced Materials and Technologies*. 2024;9(4):257-266. DOI: 10.17277/jamt.2024.04.pp.257-266

Фазовый состав нержавеющей стали, подвергнутой ультразвуковому нанокристаллическому поверхностному модифицированию с различной плотностью обработки

© Д. А. Полонянкин[a]✉, А. А. Федоров[a], Т. М. Гомонюк[a,b]

[a] *Омский государственный технический университет,*
пр. Мира, 11, Омск, 644050, Российская Федерация,
[b] *ЗАО «Электон», кв-л 17, 150, Радужный, 600910, Российская Федерация*

✉ dapolonyankin@omgtu.tech

Аннотация: Повышение физико-механических свойств аустенитных нержавеющих сталей (АНС) методами интенсивного поверхностного пластического деформирования (ИППД) является одной из ключевых проблемных тематик в области инженерии поверхности и нанокристаллических материалов. Комплексный характер эволюции структурных состояний в условиях ИППД ограничивает возможности регламентированного наноструктурирования приповерхностного слоя АНС типа 18-10 в широком диапазоне деформационных воздействий. Представлены результаты рентгенофазового анализа (РФА) и просвечивающей электронной микроскопии (ПЭМ) приповерхностного слоя стали 12Х18Н10Т после ультразвукового нанокристаллического поверхностного модифицирования (УНПМ) с различной плотностью обработки. РФА и ПЭМ свидетельствуют о двухфазном $(\alpha' + \gamma)$ составе стали 12Х18Н10Т, подвергнутой УНПМ. Методом РФА установлены функциональные зависимости объемной доли мартенситной фазы: 1) от плотности обработки; 2) энергии деформации, аппроксимация которых уравнениями линейной регрессии выполняется с достоверностью $R^2 = 0{,}984$. По данным ПЭМ, структура приповерхностного слоя стали 12Х18Н10Т, подвергнутой УНПМ с максимальной используемой плотностью обработки ($N = 9367$ мм$^{-2}$), представлена значительным количеством мартенсита в форме ламелей шириной менее 100 нм и высокой плотностью дислокаций. Результаты данной работы могут использоваться для разработки и оптимизации технологических режимов УНПМ АНС типа 18-10, полученных субтрактивными, аддитивными и гибридными аддитивно-субтрактивными технологиями производства.

Ключевые слова: ультразвуковое нанокристаллическое поверхностное модифицирование; нержавеющая сталь 12Х18Н10Т; плотность обработки; плотность энергии деформации; фазовый состав; аустенит; мартенсит деформации; объемная доля фаз; ламельная наноструктура.

Для цитирования: Polonyankin DA, Fedorov AA, Gomonyuk TM. Phase composition of stainless steel subjected to ultrasonic nanocrystal surface modification with different processing density. *Journal of Advanced Materials and Technologies*. 2024;9(4):257-266. DOI: 10.17277/jamt.2024.04.pp.257-266

1. Introduction

Austenitic chromium-nickel steels belong to the most common type of austenitic stainless steels (ASS), the relative share of which in the world market exceeds 80 % [1]. Among austenitic stainless steels the most demanded are steels of type 18-10, alloyed with ~18 % chromium and 8 to 12 % nickel, the advantages of which are machinability and ductility, while the disadvantages are relatively low strength properties (hardness, yield strength, fatigue strength). Titanium-stabilized ASS of type 18-10 (including AISI 321 steel) are used in the petrochemical industry [2, 3], in conventional [4] and alternative energy generation [2], as well as in the nuclear industry [5, 6] and biomedicine [7].

The use of 18-10 ASSs in subtractive manufacturing is combined with their utilization in additive printing technologies, which have become widespread in the aerospace industry as well as in mechanical engineering [8]. Modern arc [9] and beam [10, 11] 3D printing technologies provide the possibility of precision manufacturing of complex-shaped products from AISI 321 steel in a wide range of standard sizes. Depending on the type of energy impact, the form factor of the source material and the method of its feeding during printing, it is possible to evolve inhomogeneous structure and high residual stresses, defects in the form of pores and microcracks, the formation of δ-ferrite [12], as well as large columnar grains [8], which cause anisotropy of ASS properties [13].

The main approach to eliminating the above-mentioned disadvantages of additive as well as traditional subtractive ASS production is a scientifically based selection of optimal technological modes and post-processing operations [8, 13, 14], which ensure the formation of the required quality of the working surface, phase composition of the near-surface layer and residual stresses acting in it [15]. At the same time, due to the low carbon content, it is very difficult to increase the strength of 18-10 ASS by final heat treatment [8], in contrast to plastic deformation [5]. At present, the formation of a regulated structural-phase state and optimization of mechanical properties of ASS of type 18-10 is quite effectively realized by methods of surface severe plastic deformation (SSPD), including ultrasonic nanocrystal surface modification (UNSM).

UNSM is one of the most popular methods of SSPD of metals and alloys (including ASS type 18-10) and formation of gradient nanostructured near-surface layer in them, which corresponds to nanotechnologies realized according to the “top-down” approach [16, 17]. It is important to note that a direct analog of UNSM is the technology of ultrasonic impact treatment (UIT) [7, 18]. The range of processes involved in the UNSM includes: 1) fragmentation of the initial grains with the formation of nanoscale structural elements, 2) microdeformation of the lattice, 3) formation of defects of various types, 4) structural phase transformations [17], but is not limited to them. During the UNSM process, the processed material is subjected to deformation effects with a strain rate ranging from 0.5 to 10^6 s^{-1} [19], which contributes to the formation of residual compressive stresses [20].

One of the main variable parameters of UNSM modes is the number of tip strikes per unit area of the processed surface (N) [21], also referred to as “strike density” [18]. It is important to note that the UNSM strike density is inversely proportional to the speed at which the tip moves over the surface [22] ("scanning speed" [19]). As reported in [21], the higher the surface density of UNSM, the greater the depth and degree of refinement of polycrystalline grains in the near-surface layer of steel, and the faster its transition to a nanostructured state. In addition, increasing the intensity of UNSM processing contributes to a rise in the volume fraction of deformation-induced martensite (DIM) in 18-10 ASS [23]. At the same time, UNSM performed with a strike density exceeding a certain critical value promotes the formation of surface defects in the form of fatigue cracks [24]. Thus, the establishment of optimal parameters of UNSM modes, including the surface density of processing of ASS type 18-10, is an important scientific and technological problem.

As shown by the literature review, information on the structural phase composition of 18-10 ASS subjected to UNSM with different processing density and strain energy is extremely limited. Moreover, there are no relevant experimental studies available in the public domain for AISI 321 steel. This determines the relevance and practical significance of this work, the purpose of which is to determine the dependence of the phase composition (volume fraction of austenite and deformation-induced martensite) on the processing density and strain energy, as well as to analyze the peculiarities of the structure of the near surface layer of AISI 321 steel subjected to UNSM.

2. Materials and Methods

2.1. Materials and processing parameters

To perform the experimental part of the work, a metal bar with a radius of 12.75 mm in delivery condition, made of stainless steel grade AISI 321 was used. The content of the main chemical elements in the steel was: 0.12 % C, 18.64 % Cr, 10.1 % Ni and 0.54 % Ti. From the pre-turned bar ($Ra \sim 2.2$ μm) was cut a shaft with the length of 150 mm. Then the shaft was processed by ultrasonic nanocrystal surface modification in different modes (given in Table 1), namely, with different speed (υ, m·min^{-1}) of relative movement of the cylindrical surface of the shaft and the tip made of alloy VK8. UNSM was carried out on the unit consisting of the technological module DTM-07, magnetostrictive transducer PMS15A-18 and a waveguide with a spherical shaped indenter (tip) of diameter $d = 6$ mm. During UNSM the following parameters of the processing mode were kept constant: 1) frequency of the ultrasonic generator ($f = 18$ kHz); 2) amplitude of the indenter oscillations ($\xi_m = 0.05$ mm); 3) force of pressing the ultrasonic tool to the processed surface (static load, $F_{st} = 30$ N); 4) longitudinal tool feed ($s = 0.09$ mm·rev^{-1}).

In the case of tip machining of a cylindrical surface (shaft), the speed of their relative displacement υ is determined through the radius ($[r]$ = m) and shaft rotation frequency ($[n]$ = rev·s^{-1}) by the formula $\upsilon = 2\pi r \cdot n$ ($[\upsilon]$ = m·rev·s^{-1}). Taking into account the frequency of ultrasonic vibrations of the tool (f, Hz), the radius and rotation frequency of the shaft, the strike density ($[N]$ = m^{-2}) during UNSM is calculated by the formula (1):

$$N = \frac{60f}{\upsilon s} = \frac{60f}{(2\pi r \cdot n)s}, \tag{1}$$

where $[s]$ = m·rev^{-1} is the longitudinal tool feed.

In turn, the strain energy density (E) transferred to the near-surface layer during its processing by the indenter is estimated according to the formula (2) [19, 21, 25]:

$$E = \frac{F_{st} N \xi_m}{d}, \tag{2}$$

where $[E]$ = J·m^{-3}, $[F_{st}]$ = N, $[N]$ = m^{-2}, $[\xi_m]$ = m, $[d]$ = m.

It should be noted that, as a rule, the surface processing density is recalculated per square millimeter [21, 22], and the strain energy density is expressed in J·mm^{-3} [25].

For clarity, the designations of the specimens subjected to UNSM with different surface processing densities will be used hereafter as presented in Table 1.

Table 1. UNSM modes, the relevant surface processing density and strain energy density

Specimen	n, rev·min^{-1}	υ, m·min^{-1}	N, mm^{-2}	E, J·mm^{-3}
N1	16	1,28	9367	2,34
N2	25	2,00	5995	1,50
N3	45	3,60	3330	0,83
N4	63	5,04	2379	0,59
N5	100	8,00	1499	0,37

2.2. Characterization techniques

XRD analysis of samples before and after UNSM with different processing densities was carried out using a Shimadzu Maxima XRD-7000 diffractometer equipped with a copper cathode X-ray tube ($\lambda = 0.15406$ nm). Before XRD, which is universally used to identify the phase composition of 18-10 ASS, the diffractometer was adjusted according to the internal standard technique using silicon powder. For comparative analytical study of the phase composition of the samples, the diffractograms were recorded in the standard θ-2θ mode using the following imaging parameters: voltage and current on the X-ray tube 50.0 kV and 40.0 mA, respectively, width of the divergence and receiving slits 1.0 deg and 0.3 mm, respectively, range and scanning speed $2\theta = (30 \div 100)$ deg and 0.50 deg·min^{-1}, respectively. The “Basic Process” operation of the software “XRD-6100/7000 Ver.7.00: main” was used to process all the obtained diffractograms, providing the possibility of profile smoothing, background subtraction, separation of $K\alpha_1$- and $\text{K}\alpha_2$-lines, as well as correction of systematic errors. The transcription reports of the raw diffractograms contain information on the integral intensity of the reflexes, their full width at half maximum, and the corresponding diffraction angles and interplanar spacing. The volume fractions of austenite and deformation-induced martensite in the near-surface layer of UNSM-treated samples were estimated by analogy with [26] using the formula:

$$V_\gamma = \frac{1.4 I_\gamma}{1.4 I_\gamma + I_{\alpha'}}, \tag{3}$$

where $I_\gamma, I_{\alpha'}$, V_γ and $V_{\alpha'} = (1 - V_\gamma)$ are integral intensities of (111)γ and (110)α' reflexes, as well as volume fractions of austenitic and martensitic phases, respectively. The strongest reflexes of austenitic (111) and martensitic (110) phases were additionally registered three times in the range of angles $2\theta = (40 \div 50)°$ with the following statistical processing of the obtained integral intensity values according to the method of indirect reproducible measurements.

The structural features of the surface layer of AISI 321 steel after UNSM were studied by transmission electron microscopy (TEM) with an accelerating voltage of 120 kV on a Philips SM-12 device. The preparation of the foil samples for the TEM study was carried out using the Quanta 200 3D complex according to the standard technique of obtaining cross-sectional (normal) profiles with a focused beam of gallium ions. The structural state of the N1 sample subjected to UNSM with the processing density $N = 9367$ mm^{-2} was studied by TEM.

3. Results and Discussion

Figure 1 demonstrates the diffractograms of AISI 321 stainless steel samples before and after UNSM with different processing densities. As Figure 1 shows, the diffractogram of the untreated sample corresponds to the FCC lattice of iron: the maxima in the region of diffraction angles 43.6°, 50.7°, 74.5°, 90.6° and 95.9° are formed by the lattice planes of the γ-phase of iron (austenite). The composition of the near-surface layer of all UNSM-treated samples is biphasic and, in addition to austenite, is represented by deformation-induced martensite with a BCC lattice, which is confirmed by the presence of reflexes in the diffractograms in the region of angles 44.5°, 64.5°, 81.8° and 98.4° corresponding to the lattice planes of α'-phase iron (martensite) [26, 27].

As the UNSM processing density increases, the diffractograms of AISI 321 steel samples (Figure 1) in the range of angles $2\theta = (40 \div 50)°$ show a multidirectional change in the intensity of reflexes formed by the lattice planes (111)γ and (110)α', which correlates with the literature data, for example [28]. Figure 2 shows the corresponding dependences of the volume fraction of phases on the strain energy density (Fig. 2*a*) and surface processing density (Fig. 2*b*) of samples of AISI 321 steel by the UNSM method. The reliability of approximation by the linear regression equation is $R^2 = 0.984$.

Thus, UNSM ensures the formation of DIM in the near-surface layer of all samples of AISI 321 steel. The martensite volume fraction is in direct dependence on the strain energy density, as well as on the surface processing density. To interpret the obtained functional dependences, let us turn to the physical basis of ultrasonic nanocrystal surface modification. During UNSM, the kinetic energy of the tool's mechanical vibrations performed with ultrasonic frequency is converted into the energy of the tip impact on the treated surface. Accumulation and dissipation of the kinetic energy transferred from the tip to the ASS near-surface layer is accompanied by the appearance of elastic and plastic deformations in it, as well as local adiabatic heating [19].

Meanwhile, the fraction of the initial mechanical energy that is not converted into heat and used for plastic deformation is stored inside the treated material and is called accumulated or latent energy [29], as well as strain energy [30].

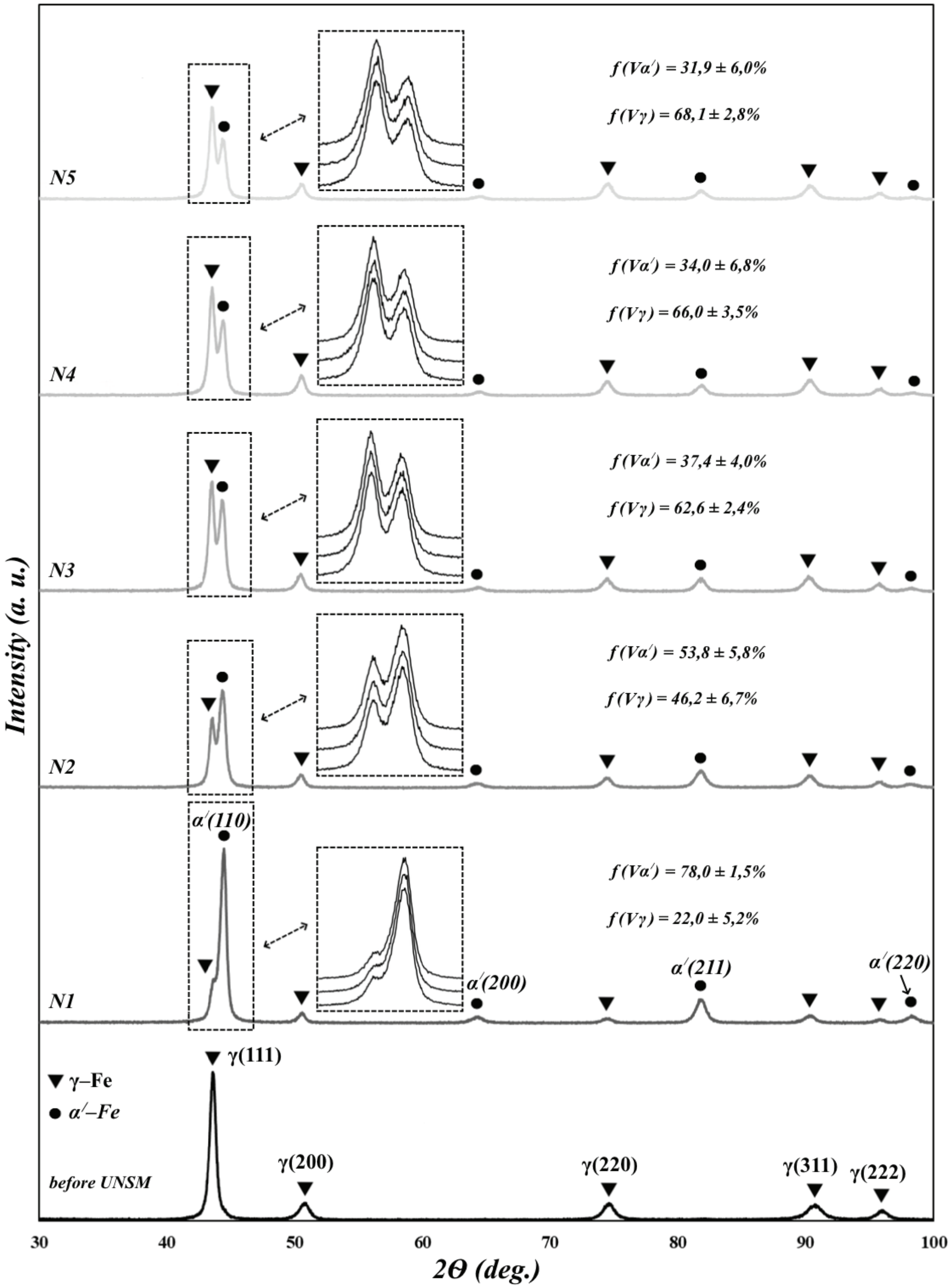

Fig. 1. Jointly presented XRD patterns of AISI 321 stainless steel before and after ultrasonic nanocrystal surface modification with different processing density

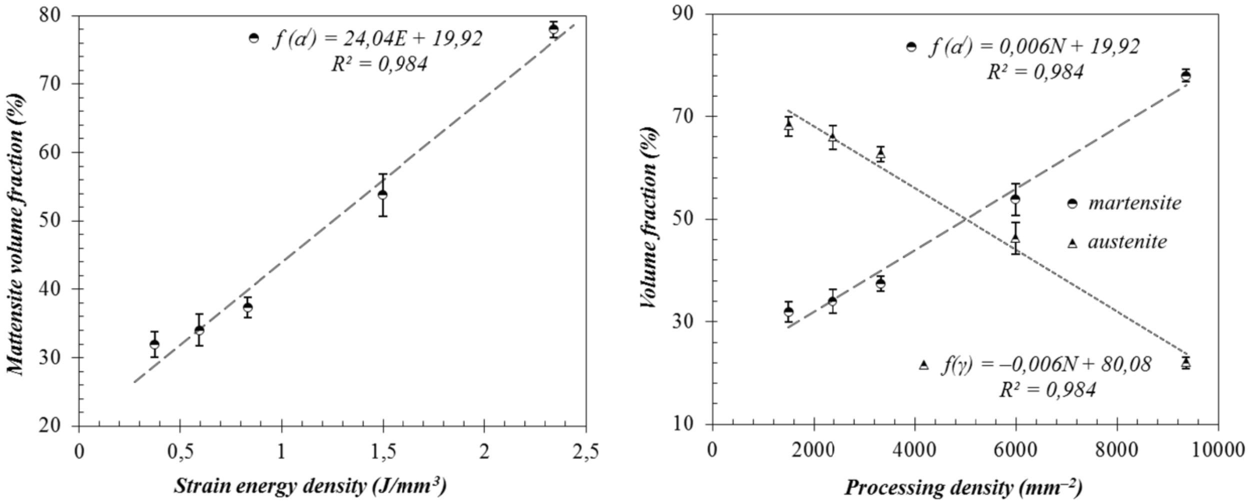

(a) *(b)*

Fig. 2. Dependencies of austenite and martensite volume fractions in AISI 321 steel near–surface layer from (*a*) strain energy density and (*b*) processing density induced by UNSM

At the same time, as noted in [31], it is possible to neglect thermal losses during ultrasonic impact treatment and to consider strain hardening of AISI 304 steel (analogous to the Russian grade 08Cr18Ni10), obtained by laser alloying in a powder bed and subjected to UNSM, on the basis of temperature-independent plasticity models. The authors of this work found that plastic deformation occurs only when the tip velocity and energy, as well as the applied stress, exceed a critical value corresponding to the yield strength of 08Cr18Ni10 steel, which changes dynamically with the increase of the processing time. It is worth noting that the strain energy accumulated in the dislocations is an additional factor contributing to the martensitic transformation [32].

Despite the fact that only a fraction of the total amount of strain energy is spent on the formation of martensite, the nucleation of which occurs predominantly at the intersection of shear bands [33], the nature of the $V\alpha' = f(E)$ dependence can be analyzed as follows. On the one hand, there is a phenomenological relationship between the value of the stored energy (strain energy) and the flow stress of various steels and alloys (including 18-10 ASS), which has a quadratic character $E \sim \sigma^2$ [29]. On the other hand, it has been established by experimental and computational methods that the volume fraction of martensite in strain-affected AISI 301LN (X2CrNiN18-7 according to DIN) [34] and AISI 304L (Russian analog 03Cr18Ni11) [32] steels is proportional to the square of the flow stress ($V\alpha' \sim \sigma^2$) under conditions of significant applied stresses. Thus, the dependence, shown in Fig. 2*a*, between the martensite volume fraction in the near-surface layer of AISI 321 steel and the energy density of its deformation by UNSM satisfies the relationship $V\alpha' \sim E$.

It is important to note that the linear correlation $V\alpha' \sim \sigma^2$ is not fulfilled in the whole range of values of the volume fraction of the martensitic phase, but under the condition of DIM is formed in the amount exceeding 30 %. An original interpretation of this effect based on the percolation theory is proposed in Talonen et al. [34] and Bönisch et al. [35]. The value of the volume fraction of deformation-induced martensite $V\alpha' = 0.3$ is considered as a certain critical value corresponding to the percolation threshold of the martensitic phase, which is 0.312 [34]. The authors associate the exceeding of this threshold with the formation of a certain "unitary cluster" (continuous network of martensitic phase) distributed throughout the deformed ASS volume. At this stage of plastic deformation of metastable austenitic stainless steels, the hardening effect becomes more pronounced due to the simultaneous deformation of both austenitic and martensitic phases, accompanied by an increase in the volume fraction of deformation-induced martensite [35].

As can be seen from the experimental data obtained in this work, all values of the volume fraction of DIM in the near-surface layer of AISI 321 steel after UNSM belong to the range $V\alpha' > 0.3$ and form a directly proportional dependence of the form $f(V\alpha') = 24.04E + 19.92$. In turn, the strain energy density is in a linear relationship with the surface processing density N (see formula (2) in the Materials and Methods section), which causes the $V\alpha' = f(N)$ dependence to be approximated by a similar first-order regression equation $f(V\alpha') = 0.006N + 19.92$ as shown in Fig. 2*b*.

At the same time, Li et al. [22] and Wang et al. [23] report on the nonlinear nature of the relationship between the volume fraction of DIM and the surface processing density (impact intensity or number of passes) of 18-10 ASS by UIT, while the experimental data are not approximated by a functional dependencies. A monotonic growth in the deformation-induced martensite volume fraction from 8.7 to 13.6 % and up to 17.2 % occurs with the increase in the surface processing density of UIT from 40000 to 57600 and then up to 75000 mm^{-2}, which contributes to a significant enhancement in the wear resistance and hardness of coatings formed by gas arc cladding of stainless steel (~15.5 % chromium and ~8 % nickel) [22].

Ultrasonic impact treatment of steel grade 08Cr18Ni10 at intensities of 3, 6 and 24 $\text{min}\cdot\text{cm}^{-2}$ provides an increase in the volume fraction of the martensitic phase from 83 to 96 % and up to 100 %, respectively, which has a nonlinear character and is accompanied by grain refinement and mechanical twinning [23]. In addition, the use of alternative methods of surface severe plastic deformation with varying processing density (coverage extent) also leads to a nonlinear change in the volume fraction of the martensitic phase. For example, in AISI 301 steel with austenite microstructure ($V\alpha' < 3\ \%$ after annealing, in delivery condition) shot peened with coverage up to 200 and 400 % and initial bead velocities of 65 and 75 $\text{m}\cdot\text{s}^{-1}$, a nonlinear increase in the deformation-induced martensite volume fraction is observed, reaching ~30 % relative to the corresponding initial value [36].

Thus, the authors of the above-mentioned works have studied the effect of ultrasonic impact and shot peening on the phase composition of 18-10 ASS, in which the volume fractions of the martensitic phase after processing in most cases either do not belong to the range $V\alpha' > 0.3$ [22, 36] or are close to the saturation limit ($83\ \% < V\alpha' \rightarrow 100\ \%$) [23]. In other words, there is no possibility to verify the experimental relation $V\alpha' = f(N)$ obtained by means of a comparative analysis with the results of alternative studies.

The results of TEM-analysis (Fig. 3) at the qualitative level confirm the data obtained by XRD method on the structural-phase composition of the near-surface layer of AISI 321 steel, subjected to UNSM. It is worth noting that in Fig. 3*a* in the lower left corner a thin layer of platinum formed on the surface of the specimen during its preparation is visualized.

As the bright-field TEM image (Fig. 3*a*) and the corresponding microdiffraction (MD, Fig. 3*b*) pattern show, the structure of the near-surface layer of the specimen N1 after UNSM with a processing density of $N = 9367\ \text{mm}^{-2}$ is biphasic ($\alpha' + \gamma$) with a predominant content of DIM. Figure 3*b* is an alternation of rings corresponding to the martensitic phase, however, weak austenitic reflexes $g = [200]\ \gamma$ are also present in the MD pattern. The TEM image (Fig. 3*a*) shows elongated martensitic lamellae with widths not exceeding 100 nm, oriented mainly parallel to the specimen surface, as well as a martensite dislocation structure with a high dislocation density of $\sim 10^{15}\ \text{m}^{-2}$.

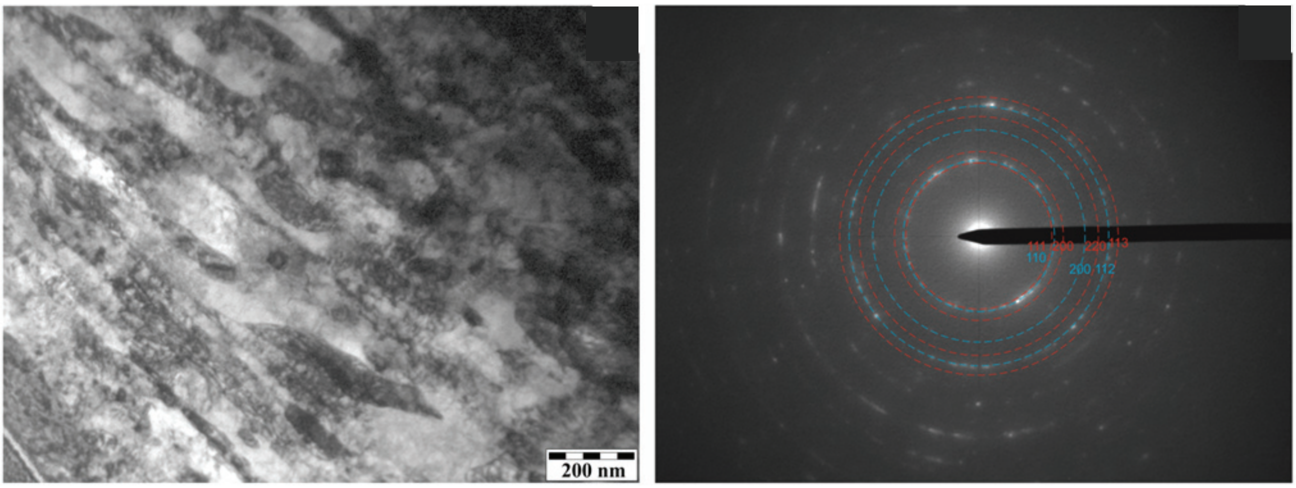

(a) (b)

Fig. 3. Near-surface layer's structure of AISI 321 stainless steel after UNSM with $N = 9367\ \text{mm}^{-2}$ processing density (specimen #1): (*a*) is TEM bright-field image of a cross-section parallel to the processing direction; (*b*) is the corresponding micro diffraction pattern with the reflections of α'- and γ-phases

Accordingly, as a result of SSPD by ultrasonic nanocrystal surface modification, a two-phase ($\alpha' + \gamma$) nanostructure is formed in the near-surface layer of AISI 321 steel. Thus, UNSM with the processing density $N = 9367$ mm^{-2} provides the formation in the surface layer of AISI 321 steel of a structural state characterized by a high content of deformation-induced martensite in the form of nano-sized lamellae (strips) and a developed dislocation structure.

4. Conclusion

During the experimental study of the phase composition of the near-surface layer of AISI 321 steel, a linear correlation between the volume fraction of martensite phase ($V\alpha'$), strain energy (E) and processing density (N) was established by the UNSM method. Approximation of the corresponding dependencies by first order regression equations $f(V\alpha') = 24.04E + 19.92$ and $f(V\alpha') = 0.006N + 19.92$ in the range of $V\alpha' \cong (30 \div 80)$ % values is performed with reliability $R^2 = 0.984$. The interpretation of the obtained results is carried out using the concept of "percolation threshold", as well as on the basis of phenomenological relationships between the yield stress and the strain energy, as well as with the volume fraction of the martensitic phase.

The results of TEM analysis at the qualitative level confirm the data obtained by XRD on the two-phase ($\alpha' + \gamma$) composition of AISI 321 steel subjected to ultrasonic nanocrystal surface modification. UNSM with processing density $N = 9367$ mm^{-2} provides structural transformation of the near-surface layer of AISI 321 steel containing a significant amount of deformation-induced martensite in the form of lamellae with width less than 100 nm and developed dislocation structure.

The obtained results can be used for improvement of physical-mechanical and functional properties, as well as for optimization of technological and operational characteristics of products made of 18-10 ASS using traditional subtractive, additive and hybrid additive-subtractive production technologies.

5. Funding

This study received no external funding.

6. Acknowledgements

The authors of the article express their gratitude to the staff of the Nanotech Research Center of the Federal State Budgetary Institution of Science "Institute of Strength Physics and Materials Science, Siberian Branch of the Russian Academy of Sciences" (ISPMS SB RAS, Tomsk) and personally to Dr. I. Litovchenko for conducting the research and assistance in interpreting the results obtained by transmission electron microscopy.

7. Conflict of interests

The authors declare no conflict of interests.

References

1. Beck T, Smaga M, Antonyuk S, Eifler D, et al. *Influence of Manufacturing and Load Conditions on the Phase Transformation and Fatigue of Austenitic Stainless Steels*. Cham: Springer; 2023. p. 257-288. DOI:10.1007/978-3-031-35575-2_11

2. Qiu Y, Yang H, Tong L, Wang L. Research progress of cryogenic materials for storage and transportation of liquid hydrogen. *Metals*. 2021;11(7):1101-1114. DOI:10.3390/met11071101

3. Shalaby HM. Failure investigation of 321 stainless steel pipe to flange weld joint. *Engineering Failure Analysis*. 2017;80:290-298. DOI:10.1016/j.engfailanal.2017.06.047

4. Min KS, Kim KJ, Nam SW. Investigation of the effect of the types and densities of grain boundary carbides on grain boundary cavitation resistance of AISI 321 stainless steel under creep–fatigue interaction. *Journal of Alloys and Compounds*. 2004;370(1-2):223-229. DOI:10.1016/j.jallcom.2003.09.129

5. Titouche N-E, Boukharouba T, Amzert SA, Hassan AJ, et al. Direct drive friction welding effect on mechanical and electrochemical characteristics of titanium stabilized austenitic stainless steel (AISI 321) research reactor thick tube. *Journal of Manufacturing Processes*. 2019;41:273-283. DOI:10.1016/j.jmapro.2019.03.016

6. Gurovich BA, Kuleshova EA, Frolov AS, Maltsev DA, et al. Investigation of high temperature annealing effectiveness for recovery of radiation-induced structural changes and properties of 18Cr–10Ni–Ti austenitic stainless steels. *Journal of Nuclear Materials*. 2015;465:565-581. DOI:10.1016/j.jnucmat.2015.06.045

7. Acharya S, Suwas S, Chatterjee K. Review of recent developments in surface nanocrystallization of metallic biomaterials. *Nanoscale*. 2021;13(4):2286-2301. DOI:10.1039/D0NR07566C

8. Laleh M, Sadeghi E, Revilla RI, Chao Q, et al. Heat treatment for metal additive manufacturing. *Progress in Materials Science*. 2023;133:101051. DOI:10.1016/|j.pmatsci.2022.101051

9. Wang X, Hu Q, Liu W, Yuan W, et al. Microstructure and corrosion properties of wire arc additively manufactured multi-trace and multilayer stainless steel 321. *Metals*. 2022;12(6):1039. DOI:10.3390/met12061039

10. Ma G, Li L, Chen Y. Effects of beam configurations on wire melting and transfer behaviors in dual beam laser welding with filler wire. *Optics & Laser Technology*. 2017;91:138-148. DOI:10.1016/j.optlastec.2016.12.019

11. Moskvina VA, Melnikov EV, Astafurov SV, Panchenko MYu, et al. Stable high-nickel austenitic steel produced by electron beam additive manufacturing using dual wire-feed system. *Materials Letters*. 2021;305: 130863. DOI:10.1016/j.matlet.2021.130863

12. Osipovich K, Kalashnikov K, Chumaevskii A, Gurianov D, et al. Wire-feed electron beam additive manufacturing: A review. *Metals*. 2023;13(2):279. DOI:10.3390/met13020279

13. Zhou C, Jiang F, Xu D, Guo C, et al. A calculation model to predict the impact stress field and depth of plastic deformation zone of additive manufactured parts in the process of ultrasonic impact treatment. *Journal of Materials Processing Technology*. 2020;280:116599. DOI:10.1016/j.jmatprotec.2020.116599

14. Tiamiyu AA, Eduok U, Szpunar JA, Odeshi AG. Corrosion behavior of metastable AISI 321 austenitic stainless steel: investigating the effect of grain size and prior plastic deformation on its degradation pattern in saline media. *Scientific Reports*. 2019;9(1):12116. DOI:10.1038/s41598-019-48594-3

15. Ye C, Zhang C, Zhao J, Dong Y. Effects of post-processing on the surface finish, porosity, residual stresses, and fatigue performance of additive manufactured metals: a review. *Journal of Materials Engineering and Performance*. 2021;30(9):6407-6425. DOI:10.1007/s11665-021-06021-7

16. Shi X, Xiao Z, Wu J. *The use of nanotechnology to improve the bulk and surface properties of steel for structural applications*. In: Nanotechnology in Eco-Efficient Construction. Cambridge: Woodhead Publishing Ltd; 2013. p. 75-107. DOI:10.1533/9780857098832.1.75.

17. Cao Y, Ni S, Liao X, Song M, et al. Structural evolutions of metallic materials processed by severe plastic deformation. *Materials Science and Engineering: R: Reports*. 2018;133:1-59. DOI:10.1016/j.mser.2018.06.001

18. Wu B, Zhang J, Zhang L, Pyoun Y-S, et al. Effect of ultrasonic nanocrystal surface modification on surface and fatigue properties of quenching and tempering S45C steel. *Applied Surface Science*. 2014;321:318-330. DOI:10.1016/j.apsusc.2014.09.068

19. Kishore A, John M, Ralls AM, Jose SA, et al. Ultrasonic nanocrystal surface modification: processes, characterization, properties, and applications. *Nanomaterials*. 2022;12(9):1415. DOI:10.3390/nano12091415

20. Yuan Y, Li R, Bi X, Yan M, et al. Review on numerical simulation of ultrasonic impact treatment (UIT): Present situation and prospect. *Journal of Materials Research and Technology*. 2024;30:1319-1340. DOI:10.1016/j.jmrt.2024.03.107

21. Kim C, Park S, Pyoun Y, Shim D. Effects of ultrasonic nanocrystal surface modification on mechanical properties of AISI D2 steel. *International Journal of Precision Engineering and Manufacturing*. 2021;22(7): 1271-1284. DOI:10.1007/s12541-021-00536-8

22. Li L, Guo S, Jia L, Zhang L, et al. Enhanced wear behavior of a stainless steel coating deposited on a medium-carbon low-alloy steel using ultrasonic impact treatment. *Coatings*. 2023;13(12):2024. DOI:10.3390/coatings13122024

23. Wang GQ, Lei MK, Guo DM. Interactions between surface integrity parameters on AISI 304 austenitic stainless steel components by ultrasonic impact treatment. *Procedia CIRP*. 2016;45:323-326. DOI:10.1016/j.procir.2016.02.351

24. Sun L, Huang L, Wu P, Huang R, et al. Progress on the effect and mechanism of ultrasonic impact treatment on additive manufactured metal fabrications. *Crystals*. 2023;13(7):995. DOI:10.3390/cryst13070995

25. Kim MS, Park SH, Pyun YS, Shim DS. Optimization of ultrasonic nanocrystal surface modification for surface quality improvement of directed energy deposited stainless steel 316L. *Journal of Materials Research and Technology*. 2020;9(6):15102-15122. DOI:10.1016/j.jmrt.2020.10.092

26. Diao M, Guo C, Sun Q, Jiang F, et al. Improving mechanical properties of austenitic stainless steel by the grain refinement in wire and arc additive manufacturing assisted with ultrasonic impact treatment. *Materials Science and Engineering: A*. 2022;857:144044. DOI:10.1016/j.msea.2022.144044

27. Polonyankin DA, Fedorov AA, Blesman AI, Nesov SN. Structural coloration of AISI 321 steel surfaces textured by ultrasonic impact treatment. *Optics & Laser Technology*. 2022;150:107948. DOI:10.1016/j.optlastec.2022.107948

28. Li L, Kim M, Lee S, Bae M, et al. Influence of multiple ultrasonic impact treatments on surface roughness and wear performance of SUS301 steel. *Surface and Coatings Technology*. 2016;307:517-524. DOI:10.1016/j.surfcoat.2016.09.023

29. Sendrowicz A, Myhre AO, Yasnikov IS, Vinogradov A. Stored and dissipated energy of plastic deformation revisited from the viewpoint of dislocation kinetics modelling approach. *Acta Materialia*. 2022;237:118190. DOI:10.1016/j.actamat.2022.118190

30. Xia P, Canillas Rodríguez FJ, Sabirov I. Microstructure evolution and adiabatic heating during dynamic biaxial deformation of a 304 stainless steel. *Materials Science and Engineering: A*. 2020;793:139829. DOI:10.1016/j.msea.2020.139829

31. Zhou C, Wang J, Guo C, Zhao C, et al. Numerical study of the ultrasonic impact on additive manufactured parts. *International Journal of Mechanical Sciences*. 2021;197:106334. DOI:10.1016/j.ijmecsci.2021.106334

32. Fang XF, Dahl W. Strain hardening and transformation mechanism of deformation-induced martensite transformation in metastable austenitic stainless steels. *Materials Science and Engineering: A*. 1991; 141(2):189-198. DOI:10.1016/0921-5093(91)90769-J

33. Ahmedabadi PM, Kain V, Agrawal A. Modelling kinetics of strain-induced martensite transformation during plastic deformation of austenitic stainless steel. *Materials & Design*. 2016;109:466-475. DOI:10.1016/j.matdes.2016.07.106

34. Talonen J, Hänninen H, Nenonen P, Pape G. Effect of strain rate on the strain-induced $\gamma \rightarrow \alpha'$-

martensite transformation and mechanical properties of austenitic stainless steels. *Metallurgical and Materials Transactions A*. 2005;36(2):421-432. DOI:10.1007/s11661-005-0313-y

35. Bönisch M, Barriobero-Vila P, Dhekne PP, Stark A, et al. Tension-compression asymmetry of metastable austenitic stainless steel studied by in-situ high-energy X-ray diffraction. *International Journal of Plasticity*. 2023;170:103767. DOI:10.1016/j.ijplas.2023.103767

36. Fargas G, Roa JJ, Mateo A. Effect of shot peening on metastable austenitic stainless steels. *Materials Science and Engineering: A*. 2015;641:290-296. DOI:10.1016/j.msea.2015.05.079

Information about the authors / Информация об авторах

Denis A. Polonyankin, Cand. Sc. (Pedagogy), Associate Professor, Omsk State Technical University (OmSTU), Omsk, Russian Federation; ORCID 0000-0001-6799-3105; e-mail: dapolonyankin@omgtu.tech

Alexey A. Fedorov, Cand. Sc. (Tech.), Associate Professor, OmSTU, Omsk, Russian Federation; ORCID 0000-0002-6681-087X; e-mail: aafedorov@omgtu.ru

Tatyana M. Gomonyuk, Design Engineer, CJSC “Elekton”, Raduzhny, Russian Federation; Postgraduate Student, OmSTU, Omsk, Russian Federation; ORCID 0000-0002-6703-0242; e-mail: gomonyuk1998@mail.ru

Полонянкин Денис Андреевич, кандидат педагогических наук, доцент, Омский государственный технический университет (ОмГТУ), Омск, Российская Федерация; ORCID 0000-0001-6799-3105; e-mail: dapolonyankin@omgtu.tech

Федоров Алексей Аркадьевич, кандидат технических наук, ОмГТУ, Омск, Российская Федерация; ORCID 0000-0002-6681-087X; e-mail: aafedorov@omgtu.ru

Гомонюк Татьяна Михайловна, инженер-конструктор, ЗАО «Электон», Радужный, Российская Федерация; аспирант, ОмГТУ, Омск, Российская Федерация; ORCID 0000-0002-6703-0242; e-mail: gomonyuk1998@mail.ru

Received 03 September 2024; Accepted 07 October 2024; Published 20 December 2024

Original papers
Advanced structural materials, materials for extreme conditions

УДК 544.3-971.2 DOI: 10.17277/jamt.2024.04.pp.267-275

Features and mechanism of combustion of energetic materials based on tungsten and polytetrafluoroethylene

© Stepan A. Seropyan[a]✉, Ivan V. Saikov[a], Gulnaz R. Saikova[a], Evgenii V. Petrov[a]

[a] *Merzhanov Institute of Structural Macrokinetics and Materials Science, Russian Academy of Science,*
8, Academician Osipyan St., Chernogolovka, 142432, Russian Federation

✉ stepan.seropyan@yandex.ru

Abstract: Multifunctional energetic materials (reactive materials) under normal conditions are inert mixtures, but under strong mechanical or thermal impact they are capable of intensive exothermic reactions. For the development of reactive materials and optimization of their composition it is necessary to take into account the sequences of chemical reactions. The features of combustion in powder reactive material based on tungsten, polytetrafluoroethylene and aluminum have been investigated. Since the metal components react with the decomposition products of polytetrafluoroethylene, this stage was studied in separate experiments on combustion of metals with CF_4 tetrafluoromethane. The use of tetrafluoromethane instead of polytetrafluoroethylene made it possible to determine that in the Al–CF_4 system the reaction starts at 900–1000 °C, and in the W–Al system at 700 °C. Intensive evaporation of polytetrafluoroethylene in the W–PTFE–Al system prevents the reaction of tungsten with aluminum, which leads to ignition at 900–1000 °C. Combustion of two-component systems W–Al and Al–CF_4 showed that the heat released during their interaction is insufficient for self-sustaining synthesis. Combustion of W–Al samples in tetrafluoromethane environment is realized in self-sustained mode. The reaction of tungsten with aluminum gives the initial impulse, and the main heat source is the interaction of aluminum with tetrafluoromethane.

Keywords: ignition; combustion; reactive materials; reaction mechanism; energy materials.

For citation: Seropyan SA, Saikov IV, Saikova GR, Petrov EV. Features and mechanism of combustion of energetic materials based on tungsten and polytetrafluoroethylene. *Journal of Advanced Materials and Technologies*. 2024;9(4):267-275. DOI: 10.17277/jamt.2024.04.pp.267-275

Особенности и механизм горения энергетических материалов на основе вольфрамаи политетрафторэтилена

© С. А. Серопян[a]✉, И. В. Сайков[a], Г. Р. Сайкова[a], Е. В. Петров[a]

[a] *Институт структурной макрокинетики и проблем материаловедения им. А. Г. Мержанова РАН,*
ул. Академика Осипьяна, 8, Черноголовка, 142432, Российская Федерация

✉ stepan.seropyan@yandex.ru

Аннотация: Многофункциональные энергетические материалы (реакционные материалы) при нормальных условиях являются инертными смесями, а при сильном механическом или тепловом воздействии способны к интенсивной экзотермической реакции. Для разработки реакционных материалов и оптимизации их состава необходимо учитывать последовательности химических реакций. Исследованы особенности горения в порошковом реакционном материале на основе вольфрама, политетрафторэтилена и алюминия. Поскольку металлические компоненты должны вступать в реакцию с продуктами разложения политетрафторэтилена, эта стадия выделена в отдельные эксперименты по горению металлов с тетрафторметаном CF_4. Использование тетрафторметана вместо политетрафторэтилена позволило установить, что в системе Al–CF_4 реакция начинается при 900…1000 °C, а в системе W–Al при 700 °C. Интенсивное испарение политетрафторэтилена в системе W–ПТФЭ–Al препятствует реагированию вольфрама с алюминием, что приводит к воспламенению при 900…1000 °C. Горение двухкомпонентных систем W–Al и Al–CF_4 показало, что выделяющееся при их взаимодействии тепло недостаточно для самоподдерживающегося синтеза. Горение образцов W–Al в среде тетрафторметана реализуется в самоподдерживающемся режиме. Реакция вольфрама с алюминием дает начальный импульс, а основным источником тепла является взаимодействие алюминия с тетрафторметаном.

Ключевые слова: воспламенение; горение; реакционные материалы; механизм реакции; энергетические материалы.

Для цитирования: Seropian SA, Saikov IV, Saikova GR, Petrov EV. Features and mechanism of combustion of energetic materials based on tungsten and polytetrafluoroethylene. *Journal of Advanced Materials and Technologies.* 2024;9(4):267-275. DOI: 10.17277/jamt.2024.04.pp.267-275

1. Introduction

Multifunctional reaction materials (RM) under normal conditions are inert mixtures, but under strong mechanical or thermal impact they are capable of intense exothermic reaction [1]. There are three main types of RMs: thermite [2–4], intermetallic [5–7] and metal-polymer mixtures [8–12]. Metal-polymer RMs typically consist of polytetrafluoroethylene (PTFE) and one or more metals. This is a relatively new class of materials that differs from traditional energetic compositions (pyrotechnic compositions, rocket fuel, explosives) by high energy density and safety under normal conditions. High-velocity impact initiates an intense redox reaction (up to deflagration and explosion), releasing a large amount of thermal energy [13].

PTFE, being a source of strong oxidizers (carbon, fluorine), enables oxidation of metals with a high thermal effect (about 8 $MJ \cdot kg^{-1}$ for the Al–PTFE system), which is significantly higher than that of TNT [14, 15]. In addition, PTFE is a technological additive – it improves the compactibility of powder compositions to a virtually pore-free state and acts as a protector from external influences (moisture, atmosphere). A metal-polymer mixture can combine sufficient strength, electrical and thermal conductivity of metal with high antifriction properties and chemical resistance of PTFE [16].

Despite its obvious advantages, Al–PTFE RM pressed from powders and sintered has low density and strength [17]. To improve the characteristics of RM, high-density additives in the form of tungsten, nickel, etc. powder are used [16, 18]. In [18], it was shown that with an increase in the content of tungsten or nickel in the Al–PTFE mixture, the strength and density of the composite increases, however, this leads to a decrease in the thermal effect of the reaction and sensitivity to impact initiation.

In addition, an urgent task is to increase the completeness of the reaction: during combustion of RM based on PTFE and high-density additives (W, Hf), the products contain a significant amount of unreacted metal.

A promising RM is a composition based on tungsten and PTFE. Calculations show that the optimal composition is a mixture with a tungsten content of 80 and 20 wt. % PTFE, which demonstrates a high combustion temperature (2115 °C) and a share of condensed products [19]. The main calculated products of this composition are condensed tungsten carbide W_2C (53 wt. %) and graphite (3 wt. %), as well as gaseous tungsten fluorides WF_6 (14 wt. %), WF_5 (20 wt. %), WF_4 (9 wt. %). However, experiments have shown that binary W-PTFE systems are difficult to initiate by shock-wave loading and activating additives are required to increase the reactivity. Such an additive can be aluminum powder, which allows increasing the reactivity of difficult-to-initiate RMs [20, 21]. The completeness of the reaction and the level of energy release of such multicomponent RMs are difficult to predict; they depend heavily, among other things, on the initiation method (heating, impact).

Thus, to develop energy compositions and optimize their composition, it is necessary to take into account the sequences of chemical reactions. Since combustion is a chemical process, it is necessary to take into account the chain nature of PTFE combustion: thermal destruction occurs with a fast stage of chain decomposition of the polymer into monomer links [22]. Therefore, for further improvement of the compositions of new reaction mixtures, an integrated approach to solving the problem is required: the use of specific patterns of chain processes that contribute to an increase in the efficiency of additives. Since the metal components of the RM must react with the decomposition products of PTFE, this stage can be separated into separate experiments on the combustion of metals with the final product of PTFE decomposition - tetrafluoromethane CF_4 (TFM). The aim of the paper is to study the features of combustion and the reaction mechanism in RM based on tungsten and PTFE.

2. Materials and Methods

As a result of the calculation in the ISMAN-THERMO program [23], a powder mixture based on tungsten, PTFE, and aluminum with sufficient exothermic effect and forming solid end products with high specific gravity was taken as an object of study (Table 1). The maximum adiabatic combustion temperature (T_{ad}) of 2866 °C corresponds to the composition with 10 wt. % Al with a high proportion of condensed products.

The initial components for RMs were tungsten powders PV-2 (particle size ≤ 50 μm), polytetrafluoroethylene Fluralite (≤ 5 μm) and aluminum ASD-1 (≤ 50 μm). Dry mixing of the powders was carried out in a "drunken barrel" mixer for 3 hours with a drum rotation speed of 30 rpm with a ball to powder mass ratio of 5 : 1.

To measure the combustion rate, parallelepiped-shaped samples with dimensions of 5×5×20 mm and a relative density of 0.7–0.8 were prepared using a manual hydraulic press (PGR-10, Lab Tools, St. Petersburg, Russia). Two blind holes with a diameter of 1 mm and a depth of 2 mm were drilled on the side surface of the samples for thermocouples (BP5/20 with a diameter of 100 μm), the distance between the holes was 14–15 mm (Fig. 1*a*). The samples were installed in a 20-liter reactor [24]. Air was pumped out of the reactor to a value of 2×10^4 Pa, and then either an inert gas (argon) or tetrafluoromethane (CF_4) was pumped in. The sample was initiated from the side end with a graphite plate by passing an electric current (Fig. 1*b*). The distance from the initiation point to the first thermocouple was about 3–4 mm. Signals from thermocouples were recorded at a frequency of 250 Hz via a QMBox analog-to-digital converter (R-Technology, Moscow, Russia). The X-ray phase analysis (XPA) was performed using DRON-3M. Samples were scanned in the range from 20° to 80° (2Θ) with a step of 0.02°. The quantitative analysis was performed using the corundum number method.

The ignition temperature was measured using the method described in [25, 26] on samples with a diameter of 5 mm and a height of 1.5–2.0 mm. The samples were ignited in a reactor (Fig. 2). The samples were placed on a 50 μm thick VR5/20 thermocouple in a boron nitride crucible and heated at a rate of 70–100 $°C\cdot s^{-1}$ using a graphite plate to achieve thermal explosion conditions.

Table 1. Calculated adiabatic combustion temperature and fraction of condensed products of W-PTFE-Al

Composition, wt. %	T_{ad}, °C	Condensed product, wt. %	Gas product, wt. %
76W-19PTFE-5Al	2776	C – 1 W_2C – 77	AlF_3 – 16; C_2F_2 – 1 CF_2 – 1; WF_4 – 3 WF_5 – 1
72W-18PTFE-10Al	2866	C – 2 W_2C – 74	AlF – 7; AlF_2 – 5 AlF_3 – 11
64W-16PTFE-20Al	1710	W_2C – 66 Al_4C_3 – 4	AlF – 29
56W-14PTFE-30Al	1382	AlF – 23	W_2C – 57

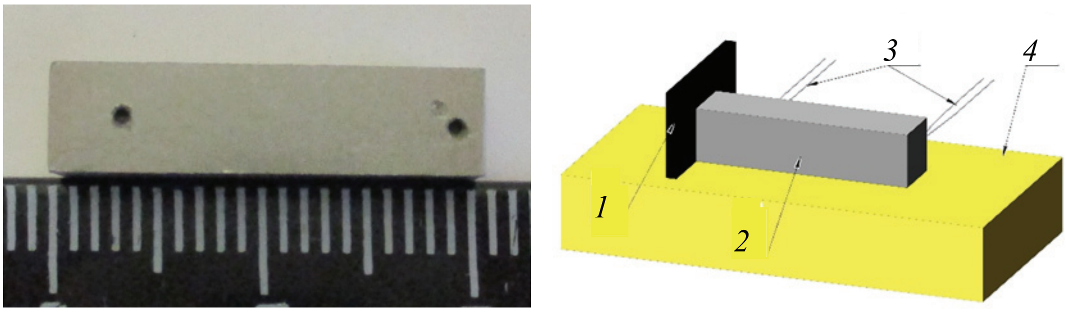

(a) *(b)*

Fig. 1. Combustion rate measurement: *a*) sample; *b*) combustion rate measurement scheme: *1* – graphite heater, *2* – sample, *3* – thermocouples BP5/20, *4* – refractory substrate

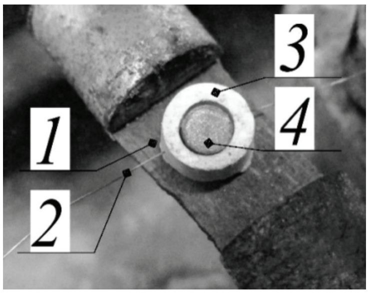

Fig. 2. Measurement of the ignition temperature:
1 – graphite heater; *2* – thermocouple;
3 – boron nitride crucible; *4* – sample

3. Results and Discussion

Under normal conditions, PTFE is inert because the chain of carbon atoms is surrounded by fluorine atoms, which block access to possible oxidants. However, when PTFE ($–(CF_2–CF_2)_n–$) is heated, thermal degradation of the polymer occurs, which begins with free-radical initiation. This process is followed by a rapid stage of chain rupture into monomer units from the free-radical end of the polymer chain. Thus, the rupture of the polymer chain leads to the formation of a large number of different free radicals. The main one is ($R–CF_2$) – difluorocarbene radical [22].

$$–(CF_2–CF_2)_n– \rightarrow nCF_3–CF_2\bullet; \quad (1)$$

$$2CF_2 = CF_2 \rightarrow C_4F_8 \bullet\bullet \text{ or cyclo-}C_4F_8; \quad (2)$$

$$CF_2 = CF_2 + CF_2 \bullet\bullet \rightarrow CF_2 = CF–CF_2\bullet. \quad (3)$$

The final product of PTFE decomposition is the monomer tetrafluoroethylene (TFE):

$$–(CF_2–CF_2)_n– \rightarrow nCF_2 = CF_2. \quad (4)$$

Since the system is constantly heated, TFE also undergoes decomposition. The final products of TFE decomposition are carbon and tetrafluoromethane CF_4 [27]:

$$CF_2 = CF_2 \rightarrow C + CF_4. \quad (5)$$

Thus, aluminum and tungsten react with the decomposition products of PTFE:

$$4Al + 3CF_4 \rightarrow 4AlF_3 + 3C. \quad (6)$$

$$W + C \rightarrow WC. \quad (7)$$

With excess W content:

$$WC + W \rightarrow W_2C. \quad (8)$$

The results of calculating the adiabatic combustion temperature and the proportion of products formed when replacing PTFE with TFM showed that the $W–CF_4$ composition behaves similarly to W-PTFE and demonstrates a relatively low combustion temperature (1464 °C) (Table 2). The main calculated products of this composition are condensed tungsten carbides, as well as gaseous tungsten fluorides (Table 2). The calculations showed that an increase in the aluminum content leads to a sharp decrease in the adiabatic combustion temperature (Fig. 3).

Ignition in the $W–CF_4–Al$-based system began with the melting of aluminum and its interaction with tungsten to a temperature of 1200–1300 °C, regardless of the aluminum content (Fig. 4*a*). Then, a drop in temperature to 1100–1150 °C was recorded. A further increase in temperature to 1200–1400 °C was associated with the combustion of aluminum with TFM. An increase in the aluminum content increased the rate and duration of the reaction. Ignition of the W-PTFE-Al system began at a temperature of 800–1000 °C, since at this temperature intense evaporation of PTFE and the formation of TFM, which interacted with aluminum, begin (Fig. 4*b*).

Table 2. Calculated values of the adiabatic combustion temperature and the proportion of condensed products of the $W–CF_4–Al$

Composition, wt. %	T_{ad}, °C	Condensed product, wt. %	Gas product, wt. %
$80W–20CF_4–0Al$	1464	$WC – 32; W_2C – 23$	$WF_5 – 3; WF_6 – 41$
$76W–19CF_4–5Al$	2416	$W_2C – 67$	$AlF_3 – 16; WF_4 – 8WF_5 – 7; WF_6 – 1$
$72W–18CF_4–10Al$	2777	$W_2C – 74$	$AlF – 5; AlF_2 – 5$ $AlF_3 – 16$
$68W–17CF_4–15Al$	1777	$W_2C – 70$	$AlF – 20; AlF_2 – 2$ $AlF_3 – 8$
$64W–16\ CF_4–20Al$	1277	$W_2C – 66; Al – 4$	$AlF – 24; AlF_3 – 5$

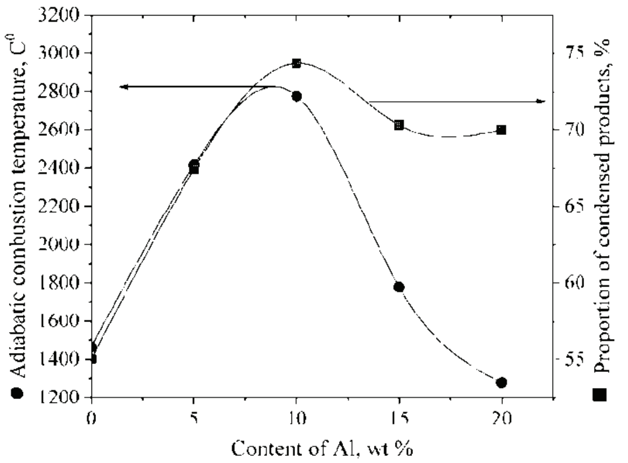

Fig. 3. The adiabatic combustion temperature and the proportion of condensed products in the W–CF_4–Al system depending on the aluminum content

According to the thermograms of the studied mixtures, it is evident that when PTFE is replaced by TFM, the combustion intensity increases (Fig. 4*a*). This is manifested in an increase in the slopes and height of the peaks of the curves, as well as in a decrease in the ignition temperature. The lower intensity of ignition of the mixture with PTFE is associated with the process of polymer decomposition and the removal of decomposition products from the reaction zone.

To confirm the above mechanisms and the role of TFM in increasing the ignition intensity, tungsten and aluminum were heated both together and separately (Fig. 5*a*). When tungsten was heated in TFM, ignition did not occur, and the temperature increased only due to continuous heating. When aluminum was heated in TFM, ignition began at a temperature of 900 °C and reached 1300 °C, and then the temperature dropped to 1100 °C with a subsequent increase to 1300 °C. The main ignition products in the Al–CF_4 system were AlF_3 and Al_4C_3 (Fig. 5*b*). The Al–W and Al–W–CF_4 systems ignited at 600–700 °C when heated.

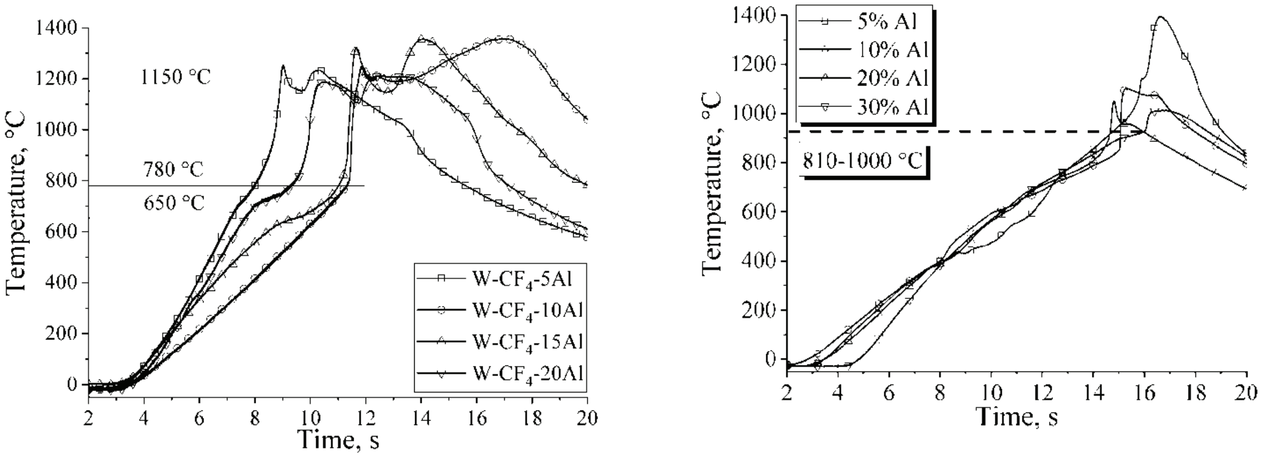

(a) *(b)*

Fig. 4. Thermograms of ignition of system samples: *a*) W–CF_4–Al, *b*) W–PTFE–Al

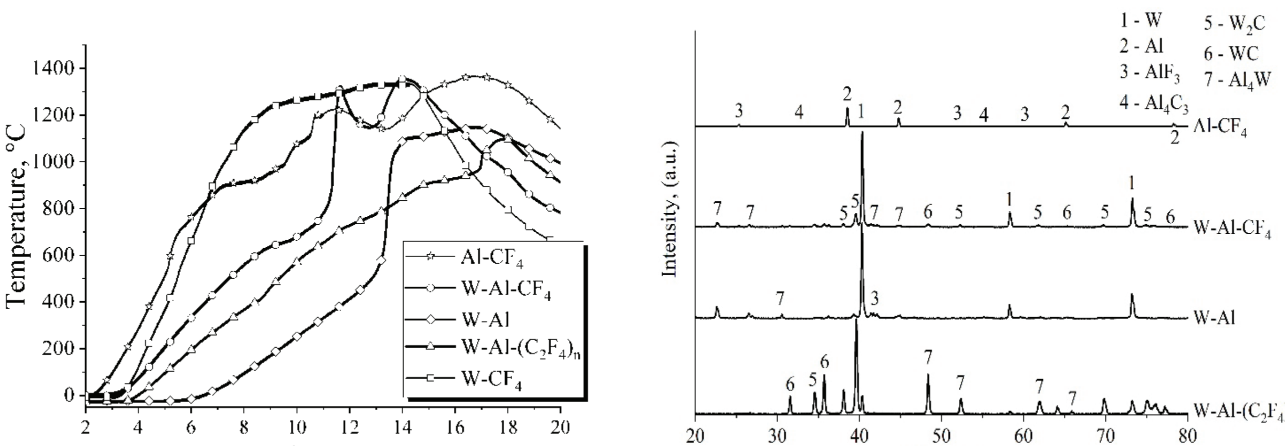

(a) *(b)*

Fig. 5. *a*) Thermograms of ignition of samples, *b*) XRD of combusted samples

The main product in the mixture without TFM was the intermetallic Al_4W, and when TFM was used, tungsten carbides were formed (Fig. 5*b*). The conducted ignition experiments show that the intense evaporation of PTFE in the W–PTFE–Al system prevents the interaction of tungsten with aluminum. Thus, the interaction of aluminum with TFM provides enough heat to form tungsten carbides and aluminides.

The experimental results showed that the Al–CF_4, 72 wt. % W – 10 wt. % Al systems are capable of ignition when heated, unlike W–CF_4 (Fig. 6*a*). As can be seen from the thermograms, the reactions of tungsten with aluminum and aluminum with TFM do not occur in a self-sustaining mode. High temperatures are not required for ignition of the W-Al system, but due to the low exothermicity of this reaction, the synthesis is not realized in a self-sustaining mode. To implement the self-sustaining mode in the Al–CF_4 system, a temperature significantly exceeding the melting point of aluminum is required; such conditions are created only near the heating element.

The experimental results on combustion of the system based on W–CF_4–Al with different aluminum content show the possibility of implementing a self-sustaining reaction with the participation of three components (Fig. 6*b*). The reaction was initiated by the interaction of tungsten with aluminum, and the self-sustaining synthesis mode occurs due to the reaction of aluminum with TFM with a combustion temperature of about 1200–1300 °C (Fig. 6*a*). The combustion rate is minimal for the composition with 5 wt. % Al – about 0.3 $mm \cdot s^{-1}$. The maximum combustion rate for the composition with 20 wt. % Al was 1.4 $mm \cdot s^{-1}$, while for the compositions with 10 and 15 wt. % Al they were 0.5 and 0.6 $mm \cdot s^{-1}$, respectively.

The sample of the W–CF_4–Al system with a content of 5 wt. % Al combusted partially, and the unreacted part showed tarnish colors (Fig. 7*a*). The samples with a content of 10, 15, and 20 wt. % Al combusted completely, forming a white coating on the surface, and the samples elongated from 20 to 30 mm (Fig. 7*b*).

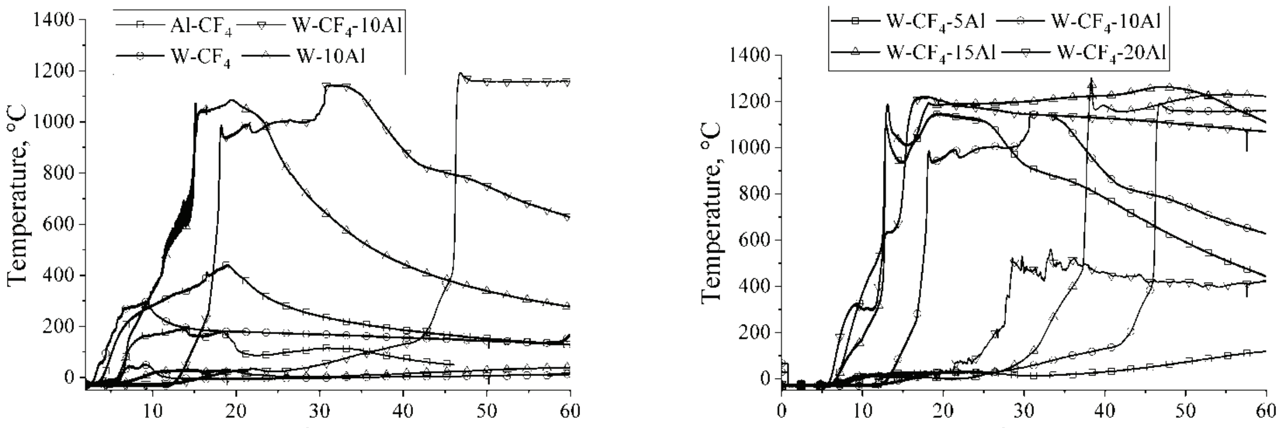

(a) *(b)*

Fig. 6. Combustion thermograms of the system: *a*) W–CF_4, Al–CF_4, W–10Al, W–CF_4–10Al; *b*) W–CF_4–5/10/15/20Al

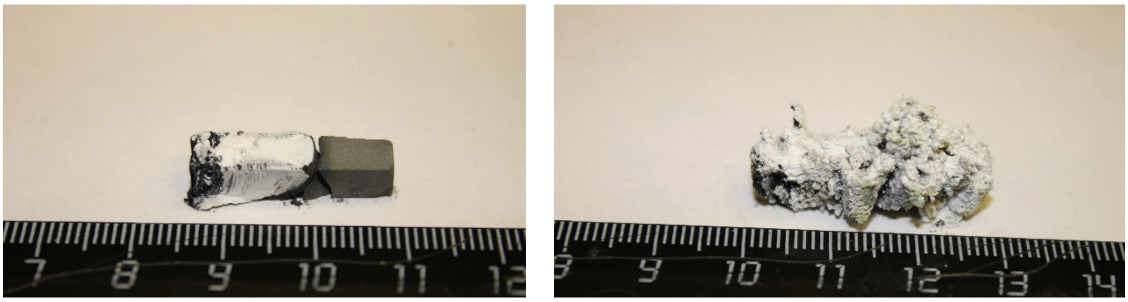

(a) *(b)*

Fig. 7. Samples after combustion W–CF_4–Al: *a*) 5 % Al, *b*) 20 % Al

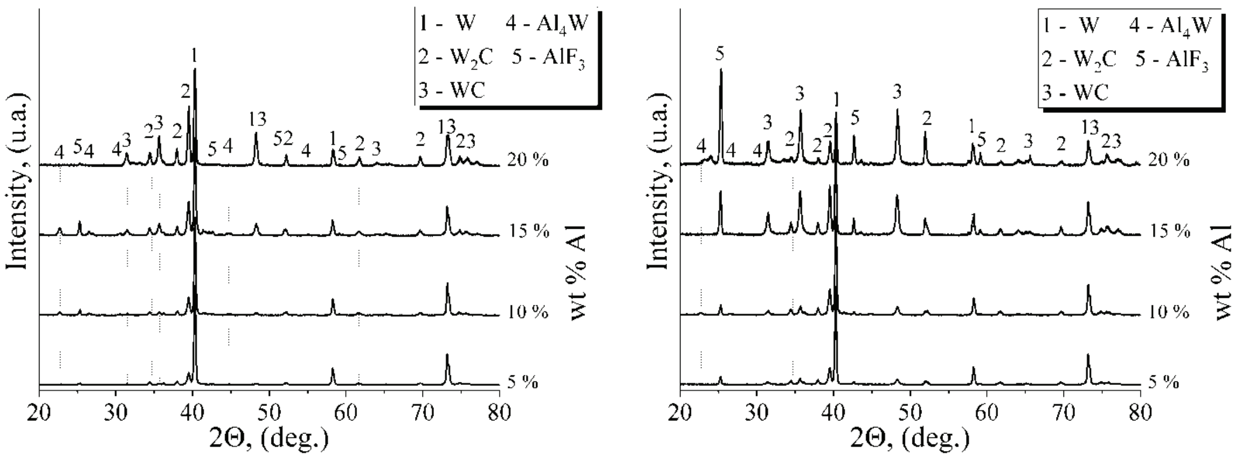

(a) *(b)*

Fig. 8. XRD of the inner (*a*) and outer (*b*) parts of the W–CF_4–Al samples separately

Table 3. Quantitative analysis of combustion products of the W–CF_4–Al system

Sample	Phase content, wt. %				
	W Cubic Im-3m	W_2C Hexagonal P-31m	WC Hexagonal P-6m2	AlF_3 Rhombohedral R-3c	Al_4W Monoclinic Cm
5 % Al outer	57	16	5	23	–
5 % Al inner	79	16	1	4	–
10 % Al outer	46	20	4	23	7
10 % Al inner	55	16	2	15	12
15 % Al outer	22	18	12	48	–
15 % Al inner	34	20	4	25	17
20 % Al outer	8	6	10	75	–
20 % Al inner	40	40	15	5	–

Due to the nature of combustion of the samples, X-ray fluorescence analysis was carried out separately for their external and internal parts (Fig. 8). Based on the intensity of the peaks of the formed products, it can be concluded that increasing the aluminum content reduces the amount of unreacted components both outside and inside the sample (Fig. 8).

The quantitative analysis of the outer part of the sample showed that an increase in the aluminum content leads to an increase in the proportion of AlF_3 from 5 to 75 wt. %. The proportion of WC increased from 4–5 to 10–12 wt. %, and the proportion of W_2C in the compositions with 5, 10 and 15 wt. % Al was from 16 to 20 wt. %. In the composition with 20 wt. % Al, the proportion of W_2C decreased to 6 wt. %. The quantitative analysis of the inner part of the sample shows that at 5 and 20 wt. % Al, the proportion of AlF_3 was about 5 wt. %. This fact indicates that aluminum fluoride is formed mainly on the surface of the sample. An increase in the Al content in the sample leads to an increase in the formation of Al_4W, WC and W_2C to 17, 15 and 40 wt. %, respectively. As expected, the proportion of unreacted components is higher inside the sample (Table 3).

4. Conclusion

The combustion features and reaction mechanism in a reactive material based on tungsten with aluminum and polytetrafluoroethylene are investigated. At high temperatures, PTFE decomposes by a radical-chain mechanism, where the main decomposition product is the tetrafluoroethylene monomer. With further heating of tetrafluoroethylene, it decomposes to carbon and TFM. When PTFE is replaced by TFM, the ignition of the W–CF_4–Al system begins with the interaction of tungsten with aluminum at 700 °C with a temperature increase to

1300 °C, and at 900–1100 °C, aluminum burns in TFM with an increase to 1300 °C. In the W–PTFE–Al system, ignition begins only at 900 °C due to intense evaporation of PTFE and loosening of the sample, which prevents the interaction of tungsten with aluminum.

Combustion of two-component W–Al and Al–CF_4 systems showed that the heat released during their interaction is insufficient for self-sustaining synthesis. Combustion of W-Al samples in the TFM environment is realized in a self-sustaining mode. The reaction of tungsten with aluminum gives the initial impulse, and the main source of heat is the combustion of aluminum in the TFM, which provides conditions for the formation of tungsten carbides. Increasing the aluminum content in the W–CF_4–Al system increases the completeness of synthesis and the combustion rate from 0.3 to 1.4 mm·s^{-1}.

5. Funding

This work was supported by Russian Science Foundation No. 24-29-00787, https://rscf.ru/project/24-29-00787/

6. Conflict of interests

The authors declare no conflict of interests.

References

1. Zhang H, Wang H, Ge C. Characterization of the dynamic response and constitutive behave or of PTFE/Al/W reactive materials. *Propellants, Explosives, Pyrotechnics*. 2020;45(5):788-797. DOI:10.1002/prep.|201900334

2. Glavier L, Taton G, Ducéré J-M, Baijot V, et al. Nanoenergetics as pressure generator for nontoxic impact primers: comparison of Al/Bi_2O_3, Al/CuO, Al/MoO_3 nanothermites and Al/PTFE. *Combustion and Flame.* 2015;162(5):1813-1820. DOI:10.1016/j.combustflame.2014.12.002

3. Bacciochini A, Radulescu MI, Yandouzi M, Maines G, et al. Reactive structural materials consolidated by cold spray: Al–CuO thermite. *Surface and Coatings Technology*. 2013;226:60-67. DOI:10.1016/j.surfcoat.2013.03.036

4. Wang H, Jian G, Egan GC, Zachariah MR. Assembly and reactive properties of Al/CuO based nanothermite microparticles.. *Combustion and Flame*. 2014;161(8):2203-2208. DOI:10.1016/j.combustflame.2014.02.003

5. He W, Liu P, He G, Gozin M, et al. Highly reactive metastable intermixed composites (MICs): preparation and characterization. *Advanced Materials*. 2018;30(41):1706293. DOI:10.1002/adma.201706293

6. Li J, Li W, Wang X. Effects of shock stress and microstructure on shock response of Al–Hf reactive materials. *Journal of Alloys and Compounds*. 2024;970:172569. DOI:10.1016/j.jallcom.2023.172569

7. Tu J, Qiao L, Shan Y, Xin C, et al. Study on the impact-induced energy release characteristics of $Zr_{68.5}Cu_{12}Ni_{12}Al_{7.5}$ amorphous alloy. *Materials*. 2021;14(6):1447. DOI:10.3390/ma14061447

8. Cai Y, Feng X, He C, Zhang S, et al. A 7.62 mm energetic bullet filled with PTFE-Mg-based reactive materials for anti-drone application. *Journal of Materials Research and Technology*. 2024;30:8749-8759. DOI:10.1016/j.jmrt.2024.05.240

9. Wu J, Fang X, Gao Z, Wang H, et al. Investigation on mechanical properties and reaction characteristics of Al–PTFE composites with different Al particle size. *Advances in Materials Science and Engineering*. 2018;2018(1):2767563. DOI:10.1155/2018/2767563

10. Zhang X-B, Liu J-X, Wang L, Li S-K. Reaction mechanism, insensitivity and mechanical property of PTFE–Mg–W composites with magnesium particles surface modification. *Rare Metals*. 2023;42(2):688-696. DOI:10.1007/s12598-017-0962-1

11. Zhuang Z, Xu K, Liu B, Shi Y, et al. Improved reactivity and energy release performance of core-shell structured fuel-rich Si/PTFE energetic composites. *Combustion and Flame*. 2023;255:112889. DOI:10.1016/j.combustflame.2023.112889

12. Feng B, Qiu C, Zhang T, Hu Y, et al. Sensitivity of Al–PTFE upon low-speed impact. *Propellants, Explosives, Pyrotechnics*. 2019;44(5):630-636. DOI:10.1002/prep.201800335

13. Zhang Z, He Y, He Y, Guo L, et al. Compressive mechanical properties and shock-induced reaction behavior of Zr/PTFE and Ti/PTFE Reactive Materials. *Materials*. 2022;15(19):6524. DOI:10.3390/ma15196524

14. Wang L, Liu J, Li S, Zhang X. Investigation on reaction energy, mechanical behavior and impact insensitivity of W–PTFE–Al composites with different W percentageю *Materials & Design*. 2016;92:397-404. DOI:10.1016/j.matdes.2015.12.045

15. Li Y, Ou Y, Wu J, Zhang Y. Modeling and simulation of laser-ignited Al-PTFE reactive material in vacuum. *Case Studies in Thermal Engineering*. 2024;61:104827. DOI:10.1016/j.csite.2024.104827

16. Adamenko NA, Kazurov AV, Agafonova GV, Savin DV. Structure formation in nickel-polytetrafluorethylene composite materials upon explosive pressing of powders. *Inorganic Materials: Applied Research*. 2020;11(4):982-990. DOI:10.1134/S2075113320040036

17. Hastings DL, Dreizin EL. Reactive structural materials: preparation and characterization. *Advanced Engineering Materials*. 2018;20(3):1700631. DOI:10.1002/adem.201700631

18. Wu J, Wang H, Fang X, Li Y, et al. Investigation on the thermal behavior, mechanical properties and reaction characteristics of Al–PTFE composites enhanced by Ni particle. *Materials*. 2018;11(9):1741. DOI:10.3390/ma11091741

19. Yu ZS, Fang X, Gao ZR, Wang HX, et al. Mechanical and reaction properties of Al/TiH_2/PTFE underquasi-static compression. *Advanced Engineering Materials*. 2018;20(7):1800019. DOI:10.1002/adem.201800019

20. Alymov MI, Vadchenko SG, Saikov IV, Kovalev ID. Shock-wave treatment of tungsten/fluoropolymer powder compositions. *Inorganic Materials: Applied Research*. 2017;8(2):340-343. DOI:10.1134/S2075113317020022

21. Saikov I, Seropyan S, Malakhov A, Saikova G, et al. Energetic materials based on W/PTFE/Al: thermal and shock-wave initiation of exothermic reactions. *Metals*. 2021;11(9):1355. DOI:10.3390/met11091355

22. Madorsky SL. *Thermal degradation of organic polymers*. New York: Interscience Publishers; 1964. 348 p.

23. Shiriev AA, Mukasyan AS. Thermodynamics of SHS processes. *Concise Encyclopedia of Self-Propagating High-Temperature Synthesis*. New York: Elsevier; 2017. p. 385-387.

24. Seropyan S, Saikov I, Andreev D, Saikova G, et al. Reactive Ni–Al-based materials: strength and combustion behavior. *Metals*. 2021;11(6):949. DOI:10.3390/met11060949

25. Vadchenko SG, Alymov MI, Saikov IV. Ignition of some powder mixtures of metals with teflon. *Inorganic Materials: Applied Research*. 2018;9(3):517-522. DOI:10.1134/S2075113318030309

26. Alymov MI, Vadchenko SG, Gordopolova IS. Ignition and combustion of W–Teflon–Al mixtures. *Izvestiya vysshikh uchebnykh zavedeniy. Poroshkovaya metallurgiya i funktsional'nye pokrytiya*. 2018;2:54-60. DOI:10.17073/1997-308X-2018-2-54-60 (In Russ.)

27. Archer G, Hildebrand JH. The solubility and entropy of solution of carbon tetrafluoride and sulfur hexafluoride in nonpolar solvents. *Journal of Physical Chemistry*. 1963;67(9):1830-1833. DOI:10.1021/j100803a021

Information about the authors / Информация об авторах

Stepan A. Seropyan, Junior Research, Merzhanov Institute of Structural Macrokinetics and Materials Science RAS (ISMAN), Chernogolovka, Russian Federation; ORCID 0000-0002-3714-3983; e-mail: stepan.seropyan@yandex.ru

Ivan V. Saikov, Cand. Sc. (Eng.), Leading Researcher, Deputy Director, ISMAN, Chernogolovka, Russian Federation; ORCID 0000-0003-1473-2854; e-mail: revan.84@mail.ru

Gulnaz R. Saikova, Cand. Sc. (Eng.), Senior Researcher, ISMAN, Chernogolovka, Russian Federation; ORCID 0000-0002-6542-7123; e-mail: gulnaz-84@mail.ru

Evgenii V. Petrov, Cand. Sc. (Eng.), Senior Researcher, Academic Secretary, ISMAN, Chernogolovka, Russian Federation; ORCID 0000-0002-7070-0972; e-mail: petrov@ism.ac.ru

Серопян Степан Арутюнович, младший научный сотрудник, Институт структурной макрокинетики и проблем материаловедения им. А. Г. Мержанова РАН (ИСМАН), Черноголовка, Российская Федерация; ORCID 0000-0002-3714-3983; e-mail: stepan.seropyan@yandex.ru

Сайков Иван Владимирович, кандидат технических наук, ведущий научный сотрудник, заместитель директора, ИСМАН, Черноголовка, Российская Федерация; ORCID 0000-0003-1473-2854; e-mail: revan.84@mail.ru

Сайкова Гульназ Рафиковна, кандидат технических наук, старший научный сотрудник, ИСМАН, Черноголовка, Российская Федерация; ORCID 0000-0002-6542-7123; e-mail: gulnaz-84@mail.ru

Петров Евгений Владимирович, кандидат технических наук, старший научный сотрудник, ученый секретарь, ИСМАН, Черноголовка, Российская Федерация; ORCID 0000-0002-7070-0972; e-mail: petrov@ism.ac.ru

Received 17 September 2024; Accepted 11 October 2024; Published 20 December 2024

Original papers
Biological materials; nanomedicine, and novel technologies for clinical and medical applications

УДК 538.9 DOI: 10.17277/jamt.2024.04.pp.276-285

The mechanism of interaction of a new drug coating components for medical stents based on polyvinylpyrrolidone with introduced carbon nanotubes and drugs

© Irina V. Zaporotskova[a]✉, Mariia F. Chesheva[a], Lusine S. Elbakyan[a]

[a] *Volgograd State University,*
100, Universitetskiy Av., Volgograd, 400062, Russian Federation

✉ irinazaporotskova@gmail.com

Abstract: Almost all stents with medicinal coatings used in Russia are manufactured abroad and have a high cost, which cannot meet the needs of Russian patients and their financial capabilities. The search and development of new types of medical stent coatings, as well as the establishment of their production in the Russian Federation is relevant. It is necessary to create thin-film drug coatings of stents with an extended time of drug emission for the treatment of various diseases. As a component providing prolonged and dosed desorption of the drug from the surface of the stent, it is best to use a carrier polymer. The paper investigates the possibility of using a promising modern material – carbon nanotubes – as a component of the medicinal coating of a medical stent, which will provide not only an improvement in the physical and mechanical properties of the coating, but also a prolonged effect of the drug by increasing its desorption time. Theoretical studies on the mechanisms of creating drug coatings for stents based on the polyvinylpyrrolidone copolymer, which include drugs (tegafur, dexamethasone) and carbon nanotubes, have been carried out. The quantum chemical calculation method – the density functional theory DFT, which is applied worldwide for calculating nanosystems, was used for research.

Keywords: medical stents; drug coating; carbon nanotubes; tegafur; dexamethasone; polyvinylpyrrolidone.

For citation: Zaporotskova IV, Chesheva MF, Elbakyan LS. The mechanism of interaction of a new drug coating components for medical stents based on polyvinylpyrrolidone with introduced carbon nanotubes and drugs. *Journal of Advanced Materials and Technologies*. 2024;9(4):276-285. DOI: 10.17277/jamt.2024.04.pp.276-285

Механизм взаимодействия компонентов нового лекарственного покрытия медицинских стентов на основе поливинилпирролидона с введенными углеродными нанотрубками и лекарственными препаратами

© И. В. Запороцкова[a]✉, М. Ф. Чешева[a], Л. С. Элбакян[a]

[a] *Волгоградский государственный университет,*
пр. Университетский, 100, Волгоград, 400062, Российская Федерация

✉ irinazaporotskova@gmail.com

Аннотация: Практически все используемые в России стенты с лекарственными покрытиями произведены за рубежом и имеют высокую стоимость, что не может удовлетворять потребностям российских пациентов и их финансовым возможностям. В связи с этим актуальным является поиск и разработка новых типов покрытий медицинских стентов, а также налаживание их производства в РФ. Необходимо создание тонкопленочных лекарственных покрытий стентов с увеличенным временем испускания лекарственного препарата для лечения различных заболеваний. В качестве компонента, обеспечивающего пролонгированную и дозированную десорбцию лекарственного препарата с поверхности стента, лучше всего использовать полимерный носитель. В работе исследована возможность применения перспективного материала современности – углеродных нанотрубок – в качестве компонента лекарственного покрытия медицинского стента, который обеспечит не только улучшение физико-механических свойств покрытия, но и пролонгированное действие лекарственного препарата за счет увеличения времени его десорбции. Выполнены теоретические исследования механизмов взаимодействия компонентов лекарственных покрытий стентов на основе биополимера поливинилпирролидона, в состав которых входят лекарственные препараты (тегафур, дексаметазон) и углеродные нанотрубки. Исследования выполнены в рамках квантово-химического расчетного метода теории функционала плотности (DFT), который широко используется во всем мире для расчета наносистем.

Ключевые слова: медицинские стенты; лекарственное покрытие; углеродные нанотрубки; тегафур; дексаметазон; поливинилпирролидон.

Для цитирования: Zaporotskova IV, Chesheva MF, Elbakyan LS. The mechanism of interaction of a new drug coating components for medical stents based on polyvinylpyrrolidone with introduced carbon nanotubes and drugs. *Journal of Advanced Materials and Technologies*. 2024;9(4):276-285. DOI: 10.17277/jamt.2024.04.pp.276-285

1. Introduction

The development of medicine today is associated with the introduction of high-tech types of care. Among such types of care for patients, one can name stenting, which is used to expand the lumen of blood vessels and ducts in the human body. Thus, stenting is used in cardiology and gastroenterology practice. One of the reasons for the need to use stents may be narrowing of ducts or vessels due to oncological neoplasms. In oncological diseases, a local drug delivery system through a stent with a coating that releases antitumor drugs can be successfully used, which allows for treatment without adverse systemic effects [1]. However, at present, almost all stents with drug coatings used in Russia are manufactured abroad and are expensive, which cannot meet the needs of Russian patients and their financial capabilities. It is necessary to search for new types of stent coatings and establish their production in the Russian Federation. The search and study of new composite coatings for medical stents related to the selection of drug coating components (polymer carrier, drugs corresponding to the stenting tasks, possible modifying elements) used in cardiac surgery for stenting of blood vessels, gastroenterology for endobiliary prosthetics and oncology to increase the lumen of various ducts compressed as a result of tumor growth, which can provide a high-quality, durable thin-film coating with an increased drug desorption time, are extremely relevant.

One of the main disadvantages of the medical stenting procedure is the risk of serious complications such as thrombosis and restenosis. It is believed that the polymer coating on the stent surface causes an inflammatory reaction at the site of injury creating the potential for restenosis. Drug-eluting stent reduces the percentage of restenosis to less than 10% in initial clinical trials [2].

Recently, the introduction of nanomaterials into drugs has been increasingly used for safer and more effective treatment of tumors. Nanomaterial-based therapy that provides target selectivity in action has been used since traditional chemotherapy faces several inevitable problems such as short half-life, cytotoxicity, lack of selective targeting, poor solubility and multidrug resistance [3].

The analysis of the available literature and in vitro results have shown that carbon nanotubes (CNTs) incorporated into the coating play an important role in stent bioactivity. Such coatings can significantly reduce the loss of therapeutic agents as they pass through the vessel during stent deployment, which significantly affects the occurrence of restenosis [4]. It can be assumed that the use of nanomaterial as a component of the stent drug coating can change the solubility, drug release profiles, diffusion, bioavailability and immunogenicity. This can lead to lower toxicity, fewer side effects, improved biodistribution and a longer life cycle of drugs [5, 6]. Known inexpensive biopolymers into which the drug is introduced can be used as a polymer matrix of the stent drug coating. The authors have previously conducted comparative theoretical and practical studies in which various polymer matrices of stent coatings were considered, including polylactic acid, polycaprolactone and chitosan, which proved the possibility of creating a thin-film drug coating that also uses a drug and carbon nanotubes [7, 8]. In this paper, polyvinylpyrrolidone is considered as a base polymer.

We assume that carbon nanotubes, which act as a modifying component of the coating, due to their unique strength and adhesive properties [9–11], can provide greater mechanical resistance of the coating and prolonged release of the drug.

The analysis of literary sources showed that chemotherapy is best at slowing down and stopping the growth of malignant neoplasms. The use of chemotherapeutic drugs on stent coatings can contribute to local (point) prevention of the disease without affecting other vital organs [12, 13]. Medicines such as tegafur and dexamethasone are the most suitable for the treatment of cancer at various stages of the disease, as their use prevents the cell from growing from the inside. Dexamethasone can also be used as a post-chemotherapy treatment to counteract certain side effects. That is why these medicines (tegafur, dexamethasone) were chosen as a component of the drug coating of the stent used in oncological practice created on the basis of the biopolymer polyvinylpyrrolidone modified with carbon nanotubes. To prove the possibility of creating a thin-film stent coating with an increased drug desorption time that can be used in oncology practice, we created models of drug coating based on the selected polymer matrix (polyvinylpyrrolidone) doped with carbon nanotubes, with the introduced antitumor drugs dexamethasone or tegafur. Then theoretical studies of the mechanisms of interaction of the main components of the ultra-thin drug coating of stents using quantum chemistry tools were conducted within the framework of density functional theory.

2. Materials and Methods

2.1. Initial materials

Polyvinylpyrrolidone (PVP) is a vinyl polymer obtained by radical vinyl polymerization from the monomer N-vinylpyrrolidone. The presence of a double bond and a heterocycle with a nitrogen atom in the elementary unit of the polymer, which is part of the amide group, impart unique properties to PVP [14, 15]. The use of PVP as a carrier polymer is of particular interest, since it fully meets the necessary requirements: PVP is indifferent to the human body, it is not broken down by enzymes in the body and is excreted through the kidneys unchanged, which minimizes the risk of toxicity and side effects [16].

CNTs in small quantities can be used to improve the strength coefficient and binding capacity of the components included in the thin-film coating of medical stents, as well as to ensure prolongation of the process of drug release from the coating [17, 18]. The unique antimicrobial activity of CNTs forms the basis for developments in protecting human health, and one of the main areas of using antimicrobial properties is the creation of bionanofilms [19]. Carbon nanotubes improve the adhesion of the coating to the stent surface, which in turn prevents the coating from peeling off during implantation [20, 21].

Tegafur is a cytostatic antitumor chemotherapeutic drug. Cytostatics, translated from Greek, mean “making the cell immobile” and have been used in oncology since 1947. These drugs disrupt the vital activity of the cell, forcing it to commit suicide – apoptosis [22, 23]. Tegafur has high lipophilicity, which ensures rapid passage through biological membranes and distribution in the body. It intensively penetrates most tissues and fluids, including the central nervous system and cerebrospinal fluid. Tegafur can enhance the effect of other antitumor drugs. The use of the drug tegafur allows for more “targeted” delivery of the drug to tumor cells [24–26].

Dexamethasone belongs to a group of synthetic hormones, which is a synthetic analogue of prednisolone. When interacting with specific cytoplasmic receptors, it forms a complex that penetrates the cell nucleus, causes expression or depression of mRNA, changing the formation of proteins on ribosomes that mediate cellular effects [27]. In the treatment of cancer, dexamethasone can be prescribed to people undergoing chemotherapy to counteract certain side effects of their anticancer treatment. Dexamethasone can enhance the antiemetic effect of 5-HT3 receptor antagonists, such as ondansetron (an antiemetic) [28]. Dexamethasone can also be used as a direct chemotherapeutic agent in certain hematological malignancies [29]. The drug can be administered in various ways: by aerosol inhalation, subcutaneously, intramuscularly, and intravenously. Intravenous and systemic drug therapy usually fails due to one or more of the following factors: low drug solubility, toxicity, short-term drug stability in vivo, poor drug pharmacokinetics, poor biodistribution, low bioavailability, rapid metabolism, and lack of selectivity for the disease target.

2.2. Density functional theory

In order to prove the possibility of creating a drug coating for stents with improved properties, such as biocompatibility and resistance to external influences, as well as predicting the physicochemical properties of materials before their synthesis and experimental study, we carried out quantum-chemical calculations of the interaction processes of the components of the drug coating (PVP, drug, CNT) using the density functional theory (DFT) [30, 31], which can significantly reduce the time and costs of experimental development of the coating.

The calculation method of the DFT from a quantum-mechanical point of view is the most convenient method and is widely used throughout the world for calculating nanosystems. The essence of this method is to use the electron density distribution in describing atomic-molecular systems. Due to the fact that any property of the ground state of a bound system of interacting electrons can only be described by the electron density ρ(r), the electron energy in the DFT method can be calculated as follows:

$$E[\rho] = T[\rho] + V_{\text{en}}[\rho] + V_{\text{ee}}[\rho], \qquad (1)$$

where $T[\rho]$ is kinetic energy, $V_{en}[\rho]$ is potential energy of electron-nuclear interactions, $V_{ee}[\rho]$ is energy of interelectronic interactions.

The used hybrid functional B3LYP is unique in that three exchange components are taken with weighting coefficients selected on the basis of experimental data, as a result of which the B3LYP method acquires the features of a semi-empirical method and its accuracy in most cases is significantly higher than in the case of methodologically "pure" functionals [31].

3. Results and Discussion

3.1. Interaction of polyvinylpyrrolidone with carbon nanotube

The first stage of geometry optimization of the polyvinylpyrrolidone fragment containing 21 elementary polymer units (21 monomers) revealed the presence of a certain region (the so-called half-cavity), which can act as an effective place for placing modifying systems in it. In our case, a single-walled carbon nanotube of the (6, 6) type is considered as such a system. The process of surface modification of the carbon nanotube with polyvinylpyrrolidone oriented with the named region to the nanotube was performed and analyzed with three possible locations of the PVP fragment relative to the CNT surface:

1) perpendicular to the nanotube axis, the polyvinylpyrrolidone fragment is oriented with the hydrogen atom (H) to the carbon atom (C) of the nanotube surface (Fig. 1*a*);

2) perpendicular to the nanotube axis, the polyvinylpyrrolidone fragment is oriented with the oxygen atom (O) to the carbon atom (C) of the nanotube surface (Fig. 1*b*);

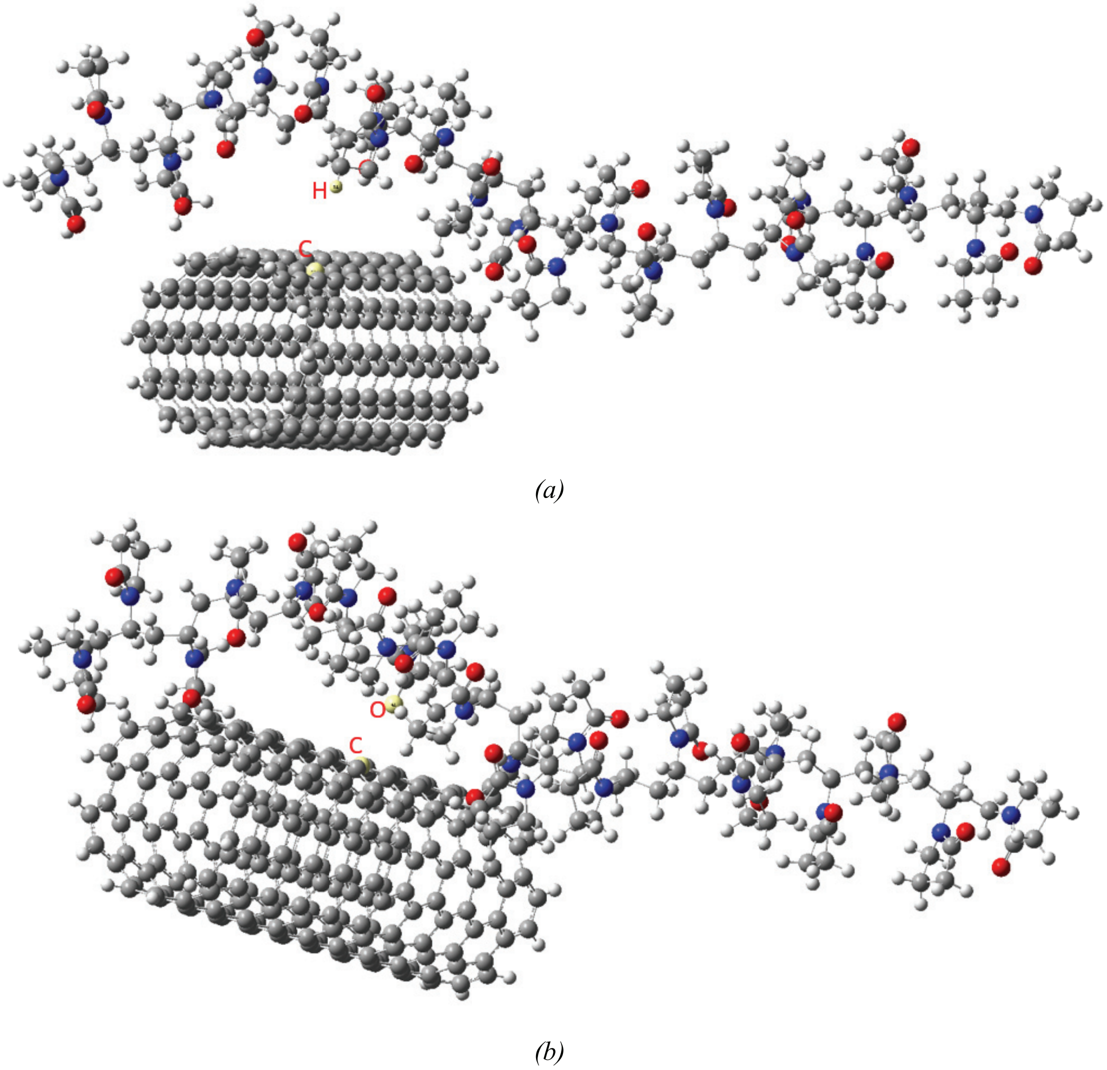

(a)

(b)

Fig. 1. Model of surface modification of (6, 6) carbon nanotube with polyvinylpyrrolidone when oriented:
a – by a hydrogen atom (H) to a carbon atom (C) of the nanotube surface;
b – by an oxygen atom (O) to a carbon atom (C) of the nanotube surface;

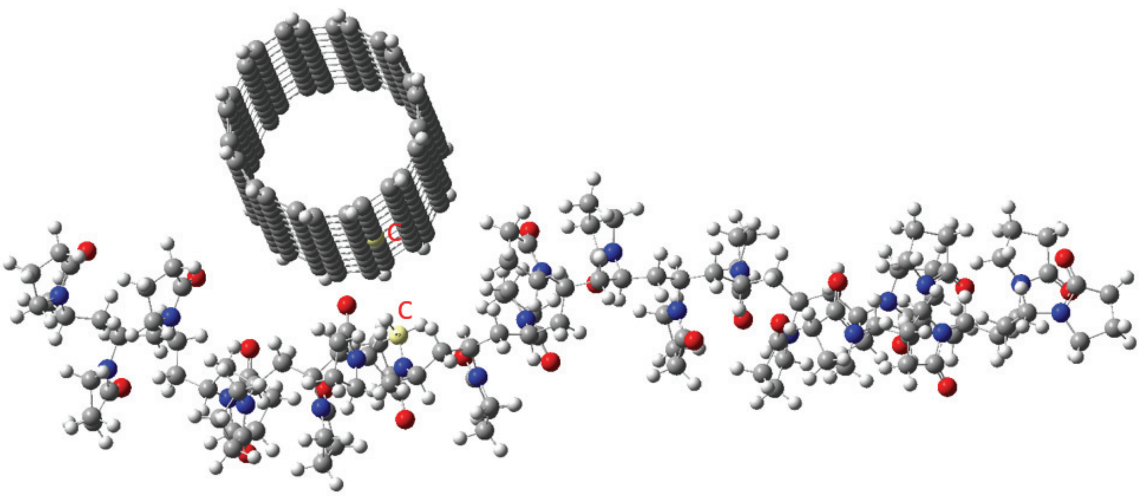

(c)

Fig. 1. *c* – by a carbon atom (C) to a carbon atom (C) of the nanotube surface

3) perpendicular to the nanotube axis, the polyvinylpyrrolidone fragment is oriented with the carbon atom (C) to the carbon atom (C) of the nanotube surface (Fig. 1*c*).

The length of the CNT molecular cluster was 22.16 Å. The cluster included nine layers of carbon hexagons along the longitudinal axis of the nanotube. To compensate for the broken chemical bonds along the cluster boundaries, pseudoatoms with a suitable valence were used. In this case, hydrogen atoms were chosen. The PVP fragment was approached step by step (with a step of 0.1 Å) to the selected atom of the nanotube surface, which made it possible to construct potential energy profiles of the considered processes for three possible orientation options (Fig. 2).

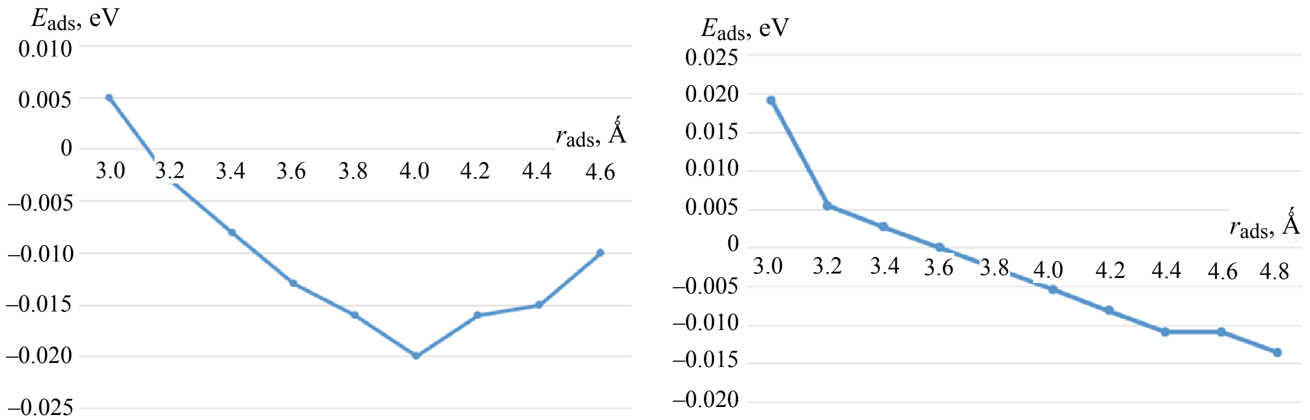

(a) *(b)*

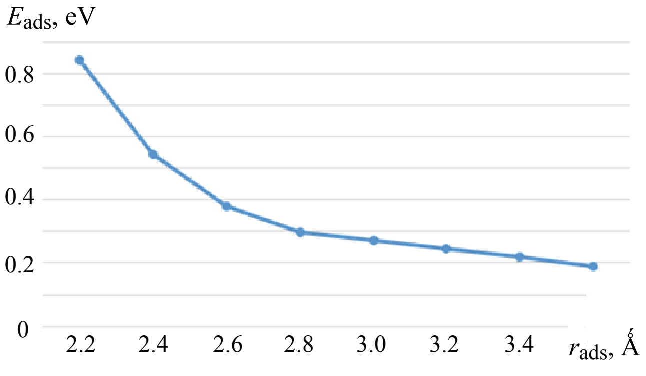

(c)

Fig. 2. Surface profiles of the potential energy of the process of a PVP fragment and CNT interaction (6, 6) when oriented: *a* – by the hydrogen atom (H) to the carbon atom (C) of the nanotube surface; *b* – by the oxygen atom (O) to the carbon atom (C) of the nanotube surface; *c* – by the carbon atom (C) to the carbon atom (C) of the nanotube surface

Table 1. The main parameters of the interaction of a PVP fragment with a carbon nanotube: r is interaction distance, E is interaction energy, q is charge of the active center after interaction

Orientation options	r, Å	E, eV	Charge of the active center after interaction, q
1) **H** – C	4,0	–0.02	0.081
2) **O** – C	–	–	–
3) **C** – C	–	–	–

The analysis of the curves allows us to establish the possibility of implementing the interaction of polyvinylpyrrolidone with a carbon nanotube, obtain the main parameters of the process and determine the most probable options for the arrangement of components during such interaction.

Table 1 shows the results of calculating the main parameters of the interaction between the polyvinylpyrrolidone fragment and the carbon nanotube.

The findings showed that the interaction is possible only for variant 1 of the arrangement of the PVP fragment relative to the CNT surface (with the orientation of the polyvinylpyrrolidone fragment by the H atom to the C carbon atom of the carbon nanotube): the curve has a minimum, which corresponds to a distance of 4 Å and energy of 0.02 eV. For the other orientation variants, there are no minima on the curves, which indicates the impossibility of interaction between PVP and CNT in such arrangements. A fairly large distance between polyvinylpyrrolidone and the nanotube corresponds to physical interaction between them without the formation of a chemical bond.

3.2. Polyvinylpyrrolidone complexes with carbon nanotube and drug

The mechanisms of creating a three-component complex including polyvinylpyrrolidone, a carbon nanotube and a drug (tegafur or dexamethasone) were studied by modeling the interaction process between the components of the complex. To perform theoretical calculations of the interaction of the components of the drug coating, a nanotube of the (6, 6) type was chosen, the length of the molecular cluster of which was also equal to 22.16 Å, and the dangling bonds at the cluster boundary were closed by pseudo-hydrogen atoms.

The dexamethasone (or tegafur) molecule was brought closer with a step of 0.1 Å to a stable complex consisting of a carbon nanotube cluster and a polyvinylpyrrolidone fragment including 21 monomer units orienting the oxygen atom of the molecule to the carbon atom of the CNT surface with its perpendicular arrangement relative to the longitudinal axis of the nanotube (Figs. 3, 4).

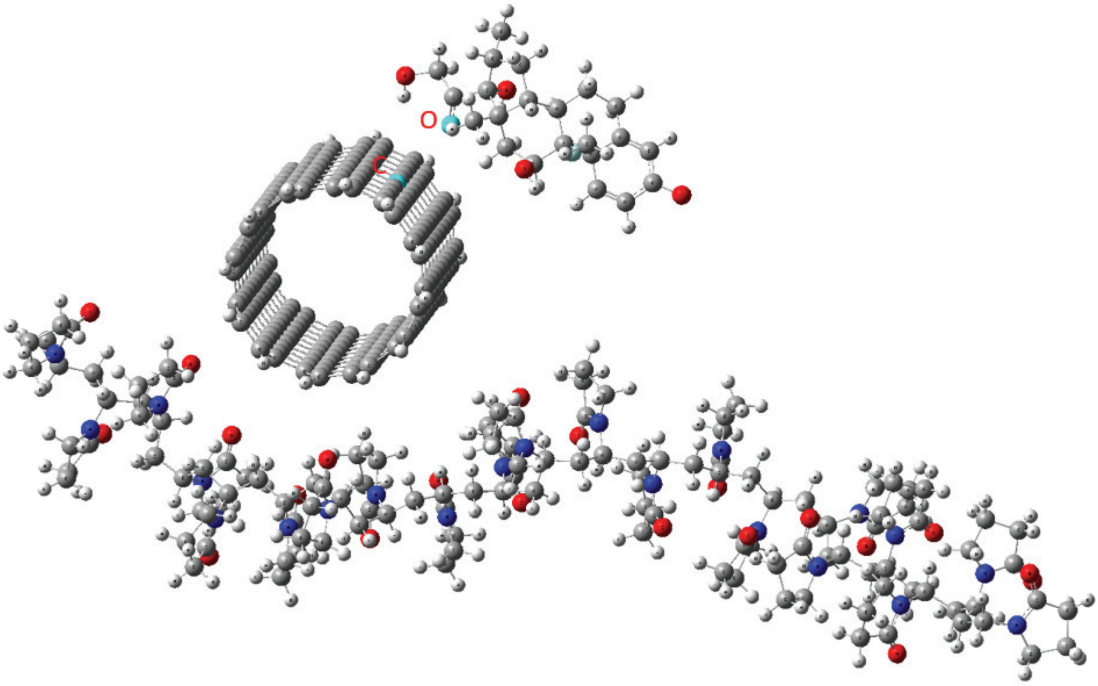

Fig. 3. Model of interaction of dexamethasone with the complex “polyvinylpyrrolidone + CNT”

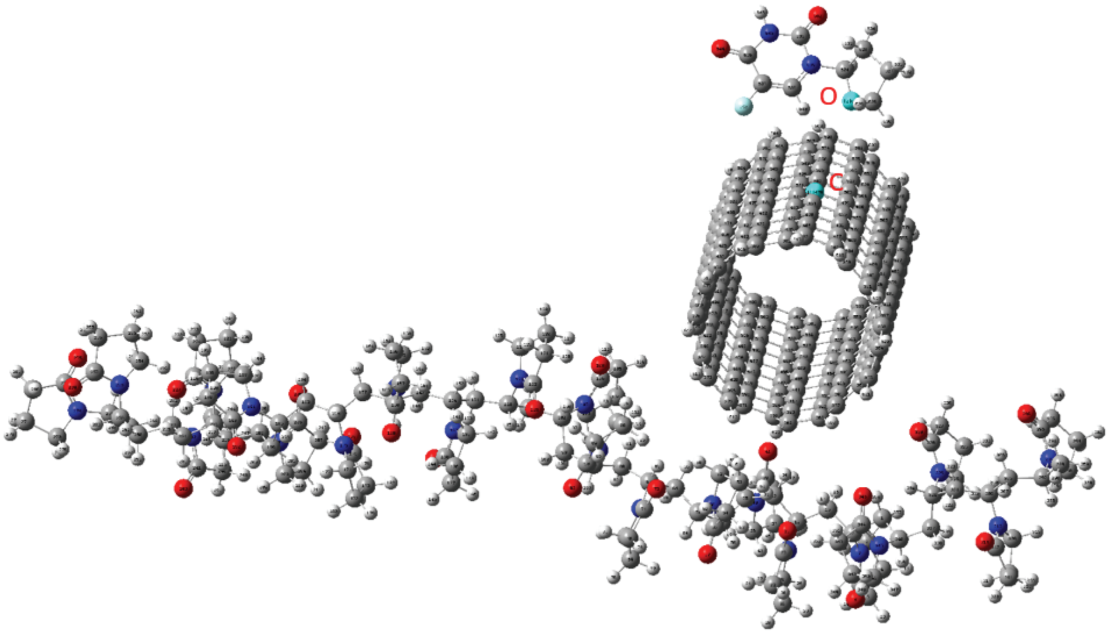

Fig. 4. Model of interaction of the tegafur molecule with the “polyvinylpyrrolidone + carbon nanotube” complex

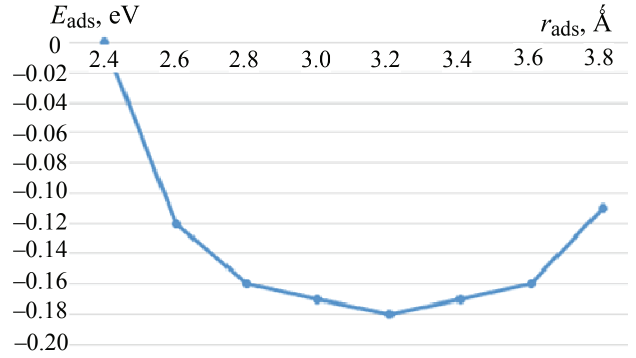

Fig. 5. The energy curve of the interaction of the dexamethasone molecule with the “polyvinylpyrrolidone + carbon nanotube” complex

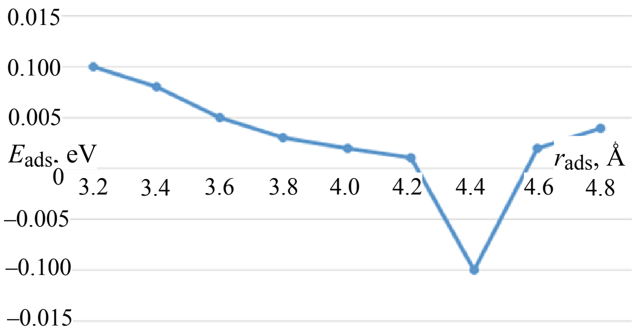

Fig. 6. Energy curve of the interaction of the tegafur molecule with the “polyvinylpyrrolidone + + carbon nanotube” complex

The obtained energy curves of the interaction process of the dexamethasone molecule with the “polyvinylpyrrolidone + carbon nanotube” complex are shown in Fig. 5. The optimal variant of PVP orientation relative to the CNT surface, determined in the previous step of the research, was chosen as the complex, when the polyvinylpyrrolidone fragment is located with the H atom to the C carbon atom of the carbon nanotube.

When analyzing the energy dependence, a minimum of the potential interaction energy ($E = –0.18$ eV) was found at a distance of 3.2 Å, which indicates the formation of a stable complex during physical interaction.

Similarly, the process of interaction of the complex components was studied when the tegafur drug approaches the stable complex “polyvinylpyrrolidone + + carbon nanotube”, as a result of which an energy curve of the process was constructed (Fig. 6).

The analysis of the curve revealed the presence of a minimum at a distance of 4.4 Å, corresponding to the energy of –0.01 eV, which proves the possibility of implementing the process of interaction of the drug with polyvinylpyrrolidone and a carbon nanotube.

The study of the interaction mechanisms of the complexes “dexamethasone + povinylpyrrolidone + + CNT” and “tegafur + polyvinylpyrrolidone + CNT” proved the possibility of physical interaction between the components of the complex. The addition of carbon nanotubes to the coating composition provides not only an increase in the durability of the coating on the surface of the medical stent, its mechanical strength, but also increases the duration of action of

Table 2. Main parameters of the interaction of the PVP + CNT complex with dexamethasone/tegafur drug molecules: r is the interaction distance of the drug molecule and the PVP + CNT complex when the oxygen molecule of the drug is oriented to the carbon atom of the nanotube

Interacting components	*r*, Å	*E*, eV	Charge of the active center after interaction, *q*
PVP + CNT+ Dexamethasone	3.2	–0.18	–0.261 **(O)**
PVP + CNT+ Tegafur	4.4	–0.01	–0.199 **(O)**

dexamethasone and tegafur due to their desorption from the CNTs surface included in the polymer complex "PVP + CNT + drug", as evidenced by the fact of physical, not chemical interaction of the drug molecule with the complex.

The results obtained during the model experiment containing the main parameters of the processes of interaction of the components of the drug coating are presented in Table 2.

The obtained calculation results are consistent with the conclusions presented in the works [32–34], which presented the results of an experimental study of the possibility of creating a drug coating based on PVP containing a drug and carbon nanotubes. In the works, the composition of a stable drug coating based on PVP was identified and the optimal concentration of carbon nanotubes was determined. A comparative analysis of various concentrations of CNTs introduced into the drug coating proved that applying a solution to the stent surface that includes PVP and contains, in addition to the drug, 0.01 wt. % carbon nanotubes leads to the creation of a high-quality coating that is sufficiently resistant to the effects of the external environment compared to the version without the addition of CNTs and including only polyvinylpyrrolidone and the drug [32–34].

Thus, it can be stated that the addition of carbon nanotubes to the coating composition provides an increase in the coating's resistance to external environments, better coupling of the coating with the surface of the medical stent itself, its mechanical strength, and also provides a prolonged action of the drug, as also evidenced by the results of the theoretical study. This allows us to recommend the use of carbon nanotubes as a modifying component of thin-film drug coatings of medical stents, leading to the creation of effective and inexpensive systems.

4. Conclusion

Medical stenting is one of the treatment methods in modern practice. The study of the interaction mechanisms of the components of complexes consisting of a polymer matrix of polyvinylpyrrolidone doped with carbon nanotubes with the introduced drugs dexamethasone or tegafur revealed the possibility of creating such drug coatings of stents due to the implementation of physical interaction between the components, which ensures the possibility of prolonged entry of the drug into the body during its desorption from the thin-film coating of the stent.

The study and comparison of the main characteristics of the interaction processes in the components of complexes consisting of CNTs and a carrier polymer allowed us to conclude that the best interaction of PVP with CNTs occurs when the polyvinylpyrrolidone fragment is oriented with a hydrogen atom to a carbon atom of the nanotube surface. For complexes including, in addition to PVP and CNTs, the antitumor drugs dexamethasone or tegafur, stable systems are formed at distances of 4.4 Å and 3.2 Å between "PVP + CNTs" and drug molecules (corresponding to interaction energies of –0.01 eV and –0.18 eV), and the fact of physical, rather than chemical, interaction of the drug molecule with the complex allows us to conclude that it is possible to increase the duration of action of the drugs dexamethasone and tegafur during their desorption from the surface of CNTs included in the polymer complex "PVP + CNTs + drug".

5. Funding

The work was carried out with the financial support of the Ministry of Education and Science of the Russian Federation (state assignment No. FZUU-2023-0001).

6. Conflict of interests

The authors declare no conflict of interests.

References

1. Seo EH, Na K. Polyurethane membrane with porous surface for controlled drug release in drug eluting stent. *Biomaterials Research*. 2014;18(1):15. DOI:10.1186/2055-7124-18-15

2. Virmani R, Farb A, Guagliumi G, Kolodgie FD. Drug-eluting stents: caution and concerns for long-term outcome: *Coronary Artery Disease*. 2004;15(6):313-318. DOI:10.1097/00019501-200409000-00003

3. Mir SA, Hamid L, Bader GN, Shoaib A, et al. Role of nanotechnology in overcoming the multidrug resistance in cancer therapy: a review. *Molecules*. 2022;27(19):6608. DOI:10.3390/molecules27196608

4. Paul A, Shao W, Shum-Tim D, Prakash S. The attenuation of restenosis following arterial gene transfer using carbon nanotube coated stent incorporating TAT/DNAAng1+Vegf nanoparticles. *Biomaterials*. 2012;33(30):7655-7664. DOI:10.1016/j.biomaterials.2012.06.096

5. Patra JK, Das G, Fraceto LF, Campos EVR, et al. Nano based drug delivery systems: recent developments and future prospects. *Journal of Nanobiotechnology*. 2018;16(1):71. DOI:10.1186/s12951-018-0392-8

6. Hua S, De Matos MBC, Metselaar JM, Storm G. Current trends and challenges in the clinical translation of nanoparticulate nanomedicines: pathways for translational development and commercialization. *Frontiers in Pharmacology*. 2018;9:790. DOI:10.3389/fphar.2018.00790

7. Zvonareva DA, Zaporotskova IV, An EE, Chesheva MF. Investigation of the possibility of creating a drug coating for coronary stents based on chitosan and heparin. *Interaction of ultrahigh frequency, terahertz and optical radiation with semiconductor micro- and nanostructures, metamaterials and biological objects: Collection of articles of the ninth All-Russian Scientific School-seminar, Saratov, May 24, 2022.* Saratov: "Saratov source" Publ. house; 2022. p. 223-226.

8. Zaporotskova IV, Suchkov SG, Boroznin SV, Zvonareva DA, et al. Study of the possibility of creating a drug coating of biliary stents based on the copolymer "polylactic acid - polycaprolactone" modified with carbon nanotubes and doxorubicin. *NBI technologies*. 2023;17(2):18-26. DOI :10.15688/NBIT.jvolsu.2023.2.3 (In Russ.)

9. Yetisgin AA, Cetinel S, Zuvin M, Kosar A, et al. Therapeutic nanoparticles and their targeted delivery applications. *Molecules*. 2020;25(9):2193. DOI: 10.3390/molecules25092193

10. Zhang X, Liu J, Li X, Li F, et al. Trastuzumab-coated nanoparticles loaded with docetaxel for breast cancer therapy. *Dose-Response*. 2019;17(3):155932581987258. DOI:10.1177/1559325819872583

11. Yao Y, Zhou Y, Liu L, Xu Y, et al. Nanoparticle-based drug delivery in cancer therapy and its role in overcoming drug resistance. *Frontiers in Molecular Biosciences*. 2020;7:193. DOI:10.3389/fmolb.2020.00193

12. Yokoyama S, Tamaru S, Tamaki S, Nakanishi D, et al. Genetic risk factors associated with antiemetic efficacy of palonosetron, aprepitant, and dexamethasone in japanese breast cancer patients treated with anthracycline-based chemotherapy. *Clinical Breast Cancer*. 2018;18(2):e157-e165. DOI:10.1016/j.clbc.2017.05.013

13. Chen P-H, Jhou H-J, Chung C-H, Wu Y-Y, et al. Benefit of uracil–tegafur used as a postoperative adjuvant chemotherapy for stage IIA colon cancer. *Medicina*. 2022;59(1):10. DOI:10.3390/medicina59010010

14. Voronov VK, Kim D, Yanushkin AS, Gerashchenko LA. *Properties and application of nanomaterials*. Moscow: TNT LLC; 2012. 220 p. (In Russ.)

15. Kedik SA, Zhavoronok ES, Sedishev IP, Panov AV, et al. Polymers for sustained drug delivery systems with prolonged action (review). Promising synthetic and natural polymers. *Razrabotka i registratsiya lekarstvennykh sredstv*. 2013;2(3):18-26. (In Russ.)

16. Alekseev KV, Gritskova IA, Kedik SA. *Polymers for pharmaceutical technology*. Moscow: IFT Publ. house; 2011. 512 p. (In Russ.)

17. Phan DC, Goodwin DG, Frank BP, Bouwer EJ, et al. Biodegradability of carbon nanotube/polymer nanocomposites under aerobic mixed culture conditions. *Science of the Total Environment*. 2018;639:804-814. DOI: 10.1016/j.scitotenv.2018.05.137

18. Zaporotskova I, Kalinichenko V, Kozhitov L, Zaporotskov P, Kislova T. On the influence of carbon nanotubes on the physical and mechanical properties of polypropylene. *NBI Technologies*. 2021;15(2):27-36. DOI: 10.15688/NBIT.jvolsu.2021.2.5 (In Russ.)

19. Valeeva AA, Dekhtyar TF. Carbon nanotubes in medicine. *Condensed matter physics and its applications: Proceedings of the IV International Scientific and Practical Conference, Sterlitamak, September 22-24, 2022.* Sterlitamak: Bashkir State UniversityPubl. house; 2022. p. 467-469. (In Russ.)

20. Chernozatonsky LA, Sorokin PB. *Carbon nanotubes: from fundamental research to nanotechnology*. Moscow: Nauka; 2007. p. 154-174. (In Russ.)

21. Zaporotskova IV. *Carbon and non-carbon nanomaterials and composite structures based on them: structure and electronic properties*. Volgograd: Volgograd State University Publ. house; 2009. 488 p. (In Russ.)

22. Ermachenkova KY, Simakova EK. The structure of the cytostatic drugs group (classification). *Innovations in science and practice: A collection of scientific articles based on the materials of the XII International Scientific and Practical Conference, Ufa, May 05, 2023. Volume Part 3*. Ufa: Bulletin of Science LLC; 2023. p. 14-20. (In Russ.)

23. Cytostatics. Available from: https://www.euroonco.ru/preparations-from-a-z/citostatiki [Accessed 20 May 2024] (In Russ.)

24. Semenov NN, Vakhabova YuV. The role of the drug tegafur/uracil in the treatment of malignant tumors. *Vmeste protiv raka: vracham vsekh spetsial'nostey*. 2008;(1):20-25. (In Russ.)

25. Romanov BK, Dmitrieva NB, Zatsepilova TA. Antitumor drugs. *Rossiyskiy meditsinskiy zhurnal*. 2018;24(3):146-150. DOI:10.18821/0869-2106-2018-24-3-146-150 (In Russ.)

26. Kakora S, Ulanova T, Kotlyarov A, Korniletsky I, et al. Experience of using antimetabolic agents in the therapy of antitumor diseases. *Mezhdunarodnyy nauchno-issledovatel'skiy zhurnal*. 2023;4(130):52. DOI:10.23670/IRJ.2023.130.35 (In Russ.)

27. Order of the Ministry of Health of the Russian Federation No. 103n dated February 28, 2019 "On approval of the procedure and deadlines for the development of clinical recommendations, their revision, the standard form of clinical recommendations and requirements for their structure, composition and scientific

validity included in clinical recommendations", Appendix A3 "Reference materials, including compliance with indications for use and contraindications, methods of application and doses of medicines, instructions for the use of the drug". Available from: http://publication.pravo.gov.ru [Accessed 2 June 2024] (In Russ.)

28. Italian Group for Antiemetic Research. Dexamethasone alone or in combination with ondansetron for the prevention of delayed nausea and vomiting induced by chemotherapy. *The New England Journal of Medicine*. 2000;342(21):59. DOI:10.1056/NEJM200005253422102

29. Harousseau JL, Attal M, Leleu X, Troncy J, et al. Bortezomib plus dexamethasone as induction treatment prior to autologous stem cell transplantation in patients with newly diagnosed multiple myeloma: results of an IFM phase II study. *Haematologica*. 2006;91(11):1498-505.

30. Koch WA. *Chemist's guide to density functional theory*. Weinheim: Wiley-VCH; 2001. p. 19-28.

31. Elbakyan LS. *Quantum chemical calculations using the GAUSSIAN software package and the GAUSSVIEW graphic.* Volgograd: Volgograd State University Publ. house; 2022. 79 p. (In Russ.)

32. Zvonareva DA, An EE, Chesheva MF, Zaporotskova IV. A new ultrathin medicinal coating of medical stents: the mechanism of interaction and application technology. *Methods of computer diagnostics in biology and medicine - 2021: collection of articles of the All-Russian School Seminar, Saratov, November 19, 2021.* Saratov: "Saratovsky Istochnik" Publ. house; 2021. p. 49-52.

33. Zvonareva DA, An EE, Zaporotskova IV. New ultrathin medical coating of PVP-based medical biliary stents with addition of carbon nanotubes*. AIP Conference Proceedings: The VII International Young Researchers' Conference – Physics, Technology, Innovations (PTI-2020), 18 May 2020*. Ekaterinburg: AIP Publishing. 2020;2313:080037. DOI: 10.1063/5.0032234

34. Zvonareva DA, An EE, Chesheva MF, Zaporotskova IV. Interaction mechanism and technology for application of new ultra-thin drug coating of medical biliary stents. *NBI Technologies*. 2022;(1):33-38. DOI:10.15688/NBIT.jvolsu.2022.1.6 (In Russ.)

Information about the authors / Информация об авторах

Irina V. Zaporotskova, D. Sc. (Phys. and Math.), Director of the Institute, Volgograd State University (VolSU), Volgograd, Russian Federation; ORCID 0000-0002-9486-2482; e-mail: irinazaporotskova@gmail.com

Mariia F. Chesheva, Assistant, VolSU, Volgograd, Russian Federation; ORCID 0000-0002-2695-1213; e-mail: chesheva@volsu.ru

Lusine S. Elbakyan, Cand. Sc. (Phys. and Math.), Associate Professor, VolSU, Volgograd, Russian Federation; ORCID 0009-0006-1014-240X; e-mail: lusniak-e@yandex.ru

Запороцкова Ирина Владимировна, доктор физико-математических наук, директор института, Волгоградский государственный университет (ВолГУ), Волгоград, Российская Федерация; ORCID 0000-0002-9486-2482; e-mail: irinazaporotskova@gmail.com

Чешева Мария Федоровна, ассистент, ВолГУ, Волгоград, Российская Федерация; ORCID 0000-0002-2695-1213; e-mail: chesheva@volsu.ru

Элбакян Лусине Самвеловна, кандидат физико-математических наук, доцент, ВолГУ, Волгоград, Российская Федерация; ORCID 0009-0006-1014-240X; e-mail: lusniak-e@yandex.ru

Received 05 September 2024; Accepted 04 October 2024; Published 20 December 2024

Original papers
Manufacturing processes and systems

УДК 544.723:544.34 DOI: 10.17277/jamt.2024.04.pp.286-295

Study of the trialkylamines adsorption on the surface of copper phthalocyanine using density functional theory methods

© Andrey A. Degtyarev[a]✉, Alexandra V. Trishina[a], Elizaveta I. Krovyakova[a]

[a] *Tambov State Technical University,*
Bld. 2, 106/5, Sovetskaya St., Tambov, 392000, Russian Federation

✉ ad.dycost@gmail.com

Abstract: The potential use of straight-chain trialkylamines to modify the oleophilic-hydrophilic properties of the surface of copper phthalocyanine was explored. Molecular modeling methods utilizing density functional theory were employed to investigate the characteristics of the adsorption process of trialkylamines with alkyl chain lengths of $n = 1 \div 8$. The change in Gibbs free energy for the adsorption of the studied surfactants from the aqueous phase onto the surfaces (001), $(20\bar{1})$ containing the metal atom was calculated. It was determined that adsorption of trialkylamines from the aqueous phase does not occur on the non-polar surfaces (001) and $(20\bar{1})$, with ΔG values ranging from 18 to 41 $\text{kJ}{\cdot}\text{mol}^{-1}$. For adsorption onto surfaces containing a metal atom, negative Gibbs free energy values are observed for tripentylamine and longer-chain trialkylamines (assuming complete loss of rotational and translational degrees of freedom) or for all except triethylamine (with partial retention of rotational degrees of freedom). However, for trialkylamines such as trihexylamine and longer, steric hindrances will be observed during adsorption onto surfaces with a metal atom. For all the examined trialkylamines, lower Gibbs free energy values for adsorption on surfaces with a metal atom were noted compared to non-polar surfaces, indicating selective adsorption of these surfactants on the surface of copper phthalocyanine. The study results indicate that tripentylamine exhibits the best characteristics for the oleophilization of the surface of copper phthalocyanine.

Keywords: copper phthalocyanine; surface oleophilization; surfactants; density functional theory; crystallographic surface; trialkylamines; adsorption; Gibbs free energy.

For citation: Degtyarev AA, Trishina AV, Krovyakova EI. Study of the trialkylamines adsorption on the surface of copper phthalocyanine using density functional theory methods. *Journal of Advanced Materials and Technologies*. 2024;9(4):286-295. DOI: 10.17277/jamt.2024.04.pp.286-295

Исследование адсорбции триалкиламинов на поверхности фталоцианина меди методами теории функционала плотности

© А. А. Дегтярев[a]✉, А. В. Тришина[a], Е. И. Кровякова[a]

[a] *Тамбовский государственный технический университет,*
ул. Советская, 106/5, пом. 2, Тамбов, 392000, Российская Федерация

✉ ad.dycost@gmail.com

Аннотация: Рассмотрены возможности применения триалкиламинов неразветвленного строения для изменения олеофильно-гидрофильных свойств поверхности фталоцианина меди. Методами молекулярного моделирования с использованием теории функционала плотности исследованы характеристики процесса адсорбции триалкиламинов с длиной алкильной цепи $n = 1…8$. Рассчитано изменение свободной энергии Гиббса для адсорбции исследуемых поверхностно-активных веществ из водной фазы на поверхностях (001), $(20\bar{1})$ и содержащей атом металла. Определено, что на неполярные поверхности (001) и $(20\bar{1})$ адсорбция триалкиламинов из водной фазы не происходит ($\Delta G = 18…41$ кДж/моль). Для адсорбции на поверхность, содержащую атом металла, отрицательные значения энергии Гиббса наблюдаются для трипентиламина и выше (при условии полной потери вращательных и поступательных степеней свободы) или для всех, кроме триэтиламина (при частичном сохранении вращательных степеней свободы). Однако для тригексиламина и выше при адсорбции на поверхность с атомом металла будут наблюдаться стерические затруднения. Для всех рассмотренных триалкиламинов наблюдаются более низкие значение энергии Гиббса для адсорбции на поверхность с атомом металла, чем на неполярные поверхности, что говорит об избирательной адсорбции данных поверхностно-активных веществ на поверхность фталоцианина меди. По результатам исследования выявлено, что наилучшими характеристиками для олеофилизации поверхности фталоцианина меди обладает трипентиламин.

Ключевые слова: фталоцианин меди; олеофилизация поверхности; поверхностно-активные вещества; теория функционала плотности; кристаллографическая поверхность; триалкиламины; адсорбция; энергия Гиббса.

Для цитирования: Degtyarev AA, Trishina AV, Krovyakova EI. Study of the trialkylamines adsorption on the surface of copper phthalocyanine using density functional theory methods. *Journal of Advanced Materials and Technologies*. 2024;9(4):286-295. DOI: 10.17277/jamt.2024.04.pp.286-295

1. Introduction

For organic pigments, one of the most important characteristics is the hydrophilic-oleophilic properties of the particle surfaces. These properties affect parameters such as the size and strength of agglomerates and aggregates, as well as the dispersibility and stability of pigment particles in the binder.

The surface properties can be modified using additive agents, with various surfactants being the most common. These surfactants adsorb onto the surface and alter its characteristics [1]. A frequent goal is to enhance the oleophilicity of the pigment surface to achieve dispersion in alkyd binders. This enhancement is useful for both stabilizing dispersions and for energy-efficient methods of producing pigmented alkyd materials, such as in the flushing process. The flushing process not only helps avoid one of the most costly stages of pigment production–drying–but also allows for the production of higher-quality pigmented materials. This is because undesirable processes like recrystallization, crystal growth, crystal agglomeration, and surface amorphization (the Bailby effect) do not occur during this process [2]. For the flushing process, the optimal surfactant concentration is considered to be one that forms a chemisorbed monolayer on the pigment surface [2]. It is also important for the surfactant adsorption to occur in the aqueous phase, as this significantly facilitates the transfer of crystals from the aqueous phase to the oil phase.

To impart oleophilic properties to a highly hydrophilic surface, such as those of inorganic pigments and fillers (titanium white, lead chromate, etc.), cationic surfactants are typically used, as they possess basic properties while the surface is acidic. For copper phthalocyanine (the Pigment Blue 15, CuPc), the surfactants that enhance the oleophilic properties of the surface are trialkylamines, which can chemisorb on surfaces containing copper atoms. However, the proposed mechanism of their interaction with the surface is not acid-base but rather involves the overlap of the *d*-orbitals of the copper atom and the nitrogen atom [3, 4].

Copper phthalocyanine molecules are well known to adsorb onto various metals [5–7], metal oxides [8], silicon oxide [9], as well as graphite surfaces [10]. However, the adsorption of any substances on copper phthalocyanine itself has been studied relatively little. It is known that it can absorb ammonia [8] and alcohols [9] from the gas phase, but the mechanisms of these processes have not been thoroughly investigated.

This study investigates the geometric and thermodynamic characteristics of the adsorption process of trialkylamines with straight-chain alkyl groups on various surfaces of copper phthalocyanine. The goal is to determine the adsorption mechanisms and the potential use of these substances as oleophilizers in an aqueous environment, which could facilitate the transfer of pigment particles from the aqueous phase to the alkyd phase during the flushing process.

2. Materials and Methods

To determine the mechanism and characteristics of the adsorption process, molecular modeling methods were employed. Among the two possible approaches, periodic slab and cluster methods, the latter was chosen due to its greater flexibility in terms of calculation methods and software.

Unbranched trialkylamines with the same number of atoms in each alkyl group and a general formula of $(CH_3–(CH_2)_n–)_3N$ were used as model surfactants, where n varies from 0 (trimethylamine) to 7 (trioctylamine).

There are many crystalline modifications of copper phthalocyanine (α, β, γ, ε, η) [11–14]; however, we focus on the β modification, as it has the most practical applications as a pigment. This form has a monoclinic crystal lattice (space group P1c1) with parameters: $a = 19.407$ Å, $b = 4.79$ Å, $c = 14.628$ Å, $\beta = 120.93°$ [11]. A schematic representation of the crystallographic planes for this modification is shown in Fig. 1.

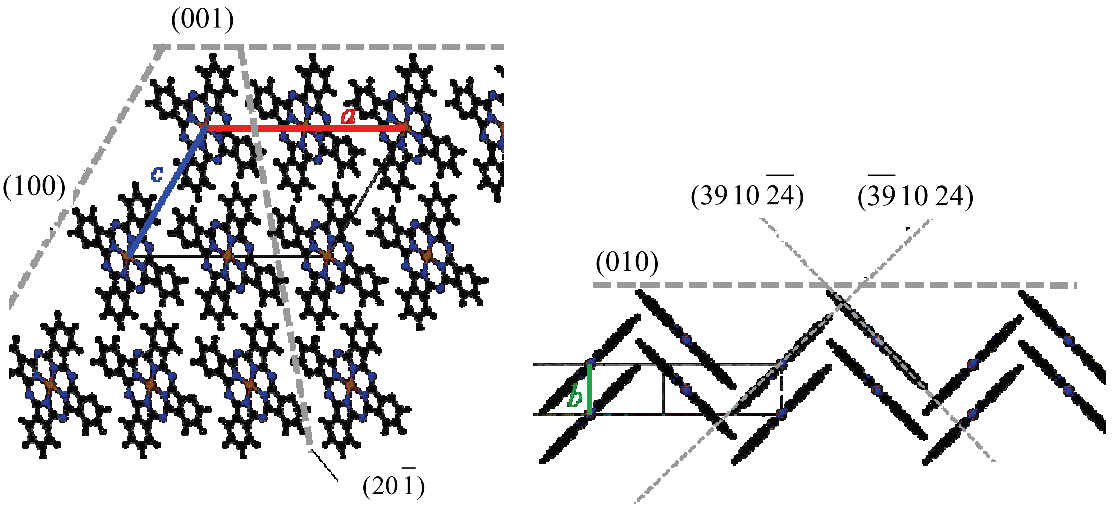

(a) *(b)*

Fig. 1. Direction of crystallographic planes in the β-copper phthalocyanine

The packing of molecules in the crystal of the β modification occurs in vertical "stacks," which are arranged in a "zigzag" pattern with respect to each other (Fig. 1*b*). In this structure, three types of surfaces are most likely along the "stacks" (Fig. 1*a*). However, studies using powder X-ray diffraction show a nearly complete absence of the (100) surface in the β modification crystal [14].

The vectors [*hkl*] perpendicular to the molecular plane are given as [–3.91, 1, 2.38] and [3.91, 1, –2.38] (calculated by approximating the coordinates of the atoms in a system corresponding to the crystallographic axes). The nearest integer indices for surfaces parallel to the molecules will thus be $(\overline{39}\,10\,24)$ and $(39\,10\,\overline{24})$ (Fig. 1*b*). Surfaces with such large index values are unlikely to be encountered in a real crystal; however, it can be assumed that the copper atoms are situated on the pseudo-(010) surface, which is not a pure crystallographic plane but, at the nanoscale, consists of alternating planes (Fig. 1*b*), similar to how the (110) surface of γ-alumina actually represents alternating (111) planes [15].

Thus, it is necessary to consider the adsorption of trialkylamines on the surfaces (001), $(20\bar{1})$, and parallel to the molecular plane. To do this, we will use the clusters presented in Fig. 2.

For modeling sorption on the molecular plane and surface $(20\bar{1})$, a single "stack" is sufficient (Fig. 2*a* and Fig. 2*b*). When interacting with surface (001), the sorbate molecules (except for the smallest ones) will inevitably interact with the neighboring "stack" (Fig. 2*c*), which is why a larger cluster was selected.

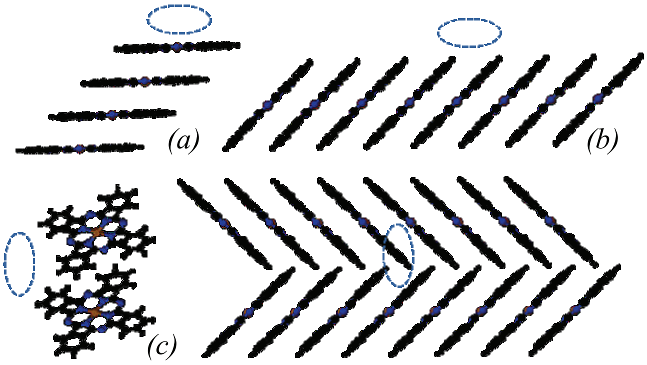

Fig. 2. Scheme of clusters for modeling sorption: *a* – per metal atom (4 molecules CuPc), *b* – per surface $(20\bar{1})$ (8 molecules CuPc), *c* – per surface (001) (16 molecules CuPc), the expected position of the sorbate molecule is shown

The method used to determine the geometric and thermodynamic characteristics of the sorption process was density functional theory (DFT), which has proven to be effective in studying sorption processes [16–19]. This approach has a relatively low computational cost, allowing for the modeling of molecular complexes that include several hundred atoms.

The optimization of the geometry of the sorbate-sorbent complexes was performed at the following levels of theory:

– XTB2 [20] – a fast method that provides a good estimate of the non-covalent dispersion interactions between the sorbate and the sorbent;

– r^2SCAN-3c [21] – a composite method that includes a meta-GGA functional, a triple-ζ basis set, and two types of corrections: for dispersion interaction and for basis set superposition error (BSSE).

As a control, for some structures, single-point energy calculations were carried out at a higher level of theory: ωB97x-D4/def2-SVPD – a spatially separated hybrid functional ωB97x [22] with the Grimme D4 dispersion correction [23, 24] and a double-ζ basis set from the Karlsruhe family, including diffuse functions [25, 26]. Since this method does not include built-in corrections for BSSE, they were calculated manually following the methodology [27].

Since the modification of particle surfaces in an aqueous suspension is assumed, continuous models were used to simulate the effect of the solvent: ALPB [28] for XTB, SMD [29] for r^{2}SCAN-3c, and ωB97x-D4/def2-SVP.

Despite the use of relatively inexpensive modeling methods, the calculation of eight- and sixteen-molecule clusters is quite labor-intensive. To reduce computational costs, a hybrid method called ONIOM [30] was applied, which allows different parts of the molecular system to be modeled at different levels. In our case, a two-layer model was used, where the first (high-level) layer consisted of the sorbent molecule and the two closest sorbate molecules.

All calculations were performed using the ORCA 5.0 software package [31].

The following designations will be used for the methods:

– QMMM1: r^{2}SCAN-3c – first layer, XTB2 – second layer;

– QMMM2: ωB97x-D4/def2-SVPD – first layer, XTB2 – second layer.

When calculating thermodynamic parameters, we assume that no new chemical bonds are formed during sorption, and therefore the vibrational-rotational energy levels change only slightly, allowing us to accept the change in enthalpy as equal to the difference in electronic energy. The change in the entropic component will occur due to the loss of translational and rotational degrees of freedom for the sorbate molecule. The translational degrees of freedom are completely lost, but there is still some probability of rotation of the sorbate molecule when interacting with the cluster in Fig. 2, as the surface on which sorption occurs is devoid of irregularities, allowing for rotation about an axis perpendicular to the surface. This rotation will become increasingly constrained as the length of the alkyl chain increases (due to dispersion interactions with the surface and steric hindrance from neighboring "stacks") and will cease for sufficiently large sorbate molecules.

Rotational entropy changes little when transitioning from the gas phase to solution [32], so for its determination, the values of gas-phase entropy provided by the ORCA program can be used. The translational entropy for the liquid phase differs significantly from that of the gas phase; its calculation was performed using the methodology based on the free volume occupied by the dissolved substance in the solvent [32]:

$$V_{\text{free}} = \left(\sqrt[3]{V_{\text{cav}}} - \sqrt[3]{V_{\text{mol}}}\right)^3; \tag{1}$$

$$S_{\text{trans}} = R \ln\left(\frac{V_{\text{free}}}{\Lambda^3}\right) + \frac{5}{3} R, \tag{2}$$

where $\Lambda = h/\sqrt{2\pi m k_B T}$, h is Planck's constant, k_B is Boltzmann's constant, m is the mass of the molecule, T is absolute temperature, V_{mol}, V_{cav} are the molecular volume and cavitation volume, respectively.

The volume of the molecule and the cavitation volume are calculated using the same methodology, treating them as cavities from which the solvent will be displaced [33]; the difference lies in the values of atomic radii. The Bader atomic radii [34] are used for the molecular volume, while radii based on the use of a surface of constant electronic density (isodensity surface) [35] are used for calculating the cavitation volume. Volumes were calculated in ORCA using the vdw_gaussian scheme [36].

Thus, the change in Gibbs free energy during the adsorption of a surfactant molecule on the surface of copper phthalocyanine will be calculated based on the following dependencies:

– in the case of complete loss of rotational degrees of freedom

$$\Delta G_{\text{ads}} = \Delta E_{\text{ads}} - T\left(-S_{\text{trans}} - S_{\text{rot}}\right) = \Delta E_{\text{ads}} + T\, S_{\text{tr}}; \tag{3}$$

– in the case of partial loss of rotational degrees of freedom

$$\Delta G_{\text{ads}} = \Delta E_{\text{ads}} - T\left(-S_{\text{trans}} - 2/3 S_{\text{rot}}\right) = \Delta E_{\text{ads}} + T\, S_{\text{t2/3r}}, \tag{4}$$

where ΔE_{ads} is the change in electronic energy upon the formation of the sorbate-sorbent complex.

3. Results and Discussion

As a result of the conformational analysis at the level of theory ωB97x-D4/def2-SVPD, it was found that in the aqueous phase, the most stable conformers of trialkylamines are the molecules with the arrangement of alkyl groups relative to the nitrogen atom, as shown in Fig. 3.

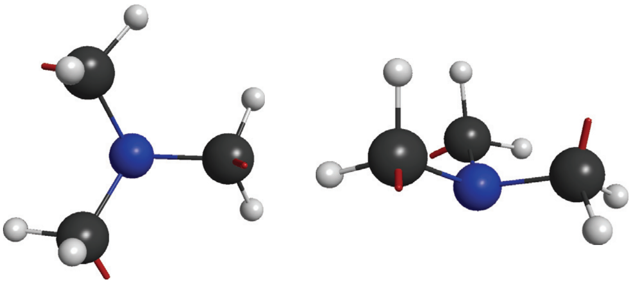

Fig. 3. Scheme of the arrangement of alkyl groups relative to the nitrogen atom for the most low-energy conformation of linear trialkylamines

In this arrangement, the average C–N–C angle is 110.7° (for triethylamine), which is close to its value in the solid phase (112.6°) [37]. For the other trialkylamines, the angles range from 108.6° to 110.8°, indicating an absence of steric strain, which is characteristic of branched trialkylamines [38]. With the exception of trimethylamine, all trialkylamines have C_1 symmetry, while trimethylamine exhibits C_3 symmetry; however, based on experimental data, it can be said that the transition between different types of symmetry occurs quite easily [37].

The scheme of the interaction of trialkylamines with the active center containing a copper atom is presented in Fig. 4.

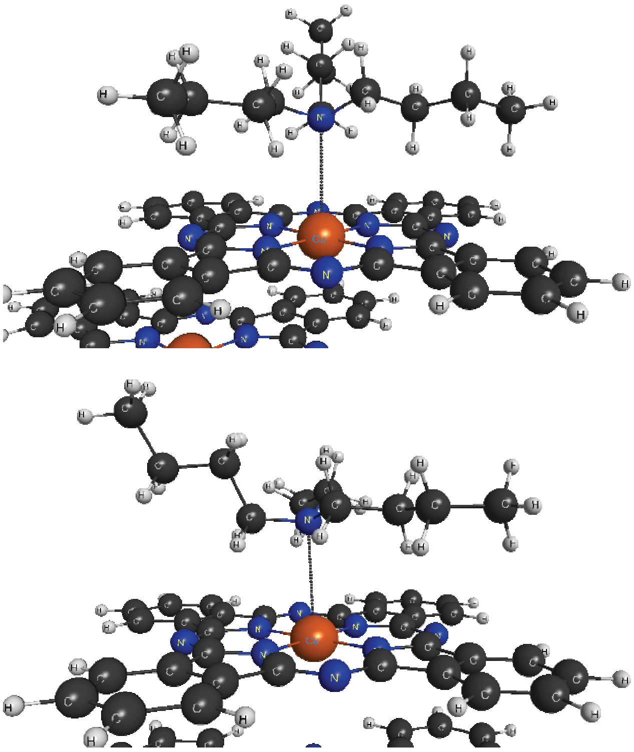

Fig. 4. Scheme of sorbate-sorbent interaction on a surface containing a metal atom using the example of tributylamine

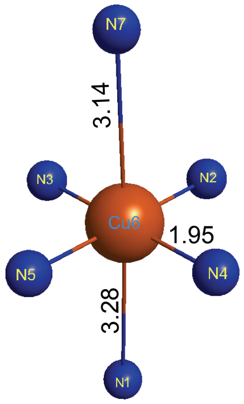

Fig. 5. Six-coordinated copper atom in a tributylamine complex with a surface, distances in angstroms

According to the scheme (Fig. 4), the sorption occurs in such a way that the nitrogen atom of the trialkylamine, which has a lone pair of electrons, is positioned near the copper atom. The copper atom has a six-coordinate structure, where four nitrogen atoms from the phthalocyanine molecule containing that atom (1.95 Å), the nitrogen atom of a neighboring phthalocyanine molecule (3.28 Å), and the nitrogen atom of the trialkylamine (3.14 Å) act as ligands (Fig. 5).

The structure of the complexes with the other trialkylamines is similar to the provided complex with tributylamine. The mechanism of ammonia adsorption on the surface of copper phthalocyanine through the metal atom was proposed in reference [8]. Trialkylamines, if their nitrogen atom is available for interaction, should behave similarly.

The distances between the surface copper atom and the nitrogen atom of the trialkylamines are presented in Table 1.

The tributylamine molecule is the largest that can fully fit on a single copper phthalocyanine molecule. The tripentylamine molecule slightly extends beyond the edges of the "pack", but does not contact neighboring molecules. For larger molecules, steric hindrances may occur during sorption on this surface (Fig. 6).

Table 1. Geometric parameters of trialkylamine sorption on the surface of copper phthalocyanine

Alkyl chain length	Cu–N length, Å
1	2.70
2	3.12
3	3.24
4	3.14
5	3.13
6	3.13
7	3.13
8	3.13

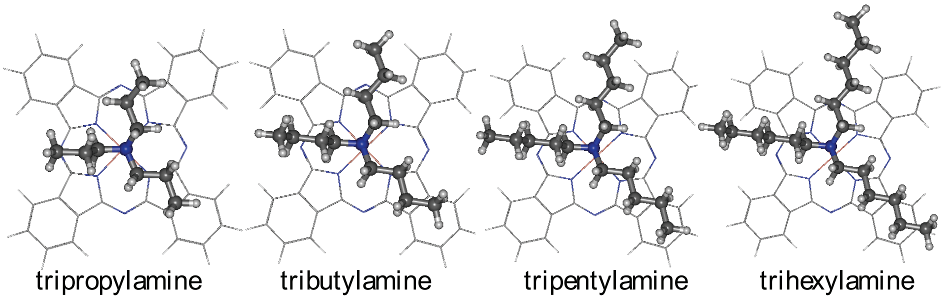

Fig. 6. Top view of some trialkylamine complexes with the copper phthalocyanine surface

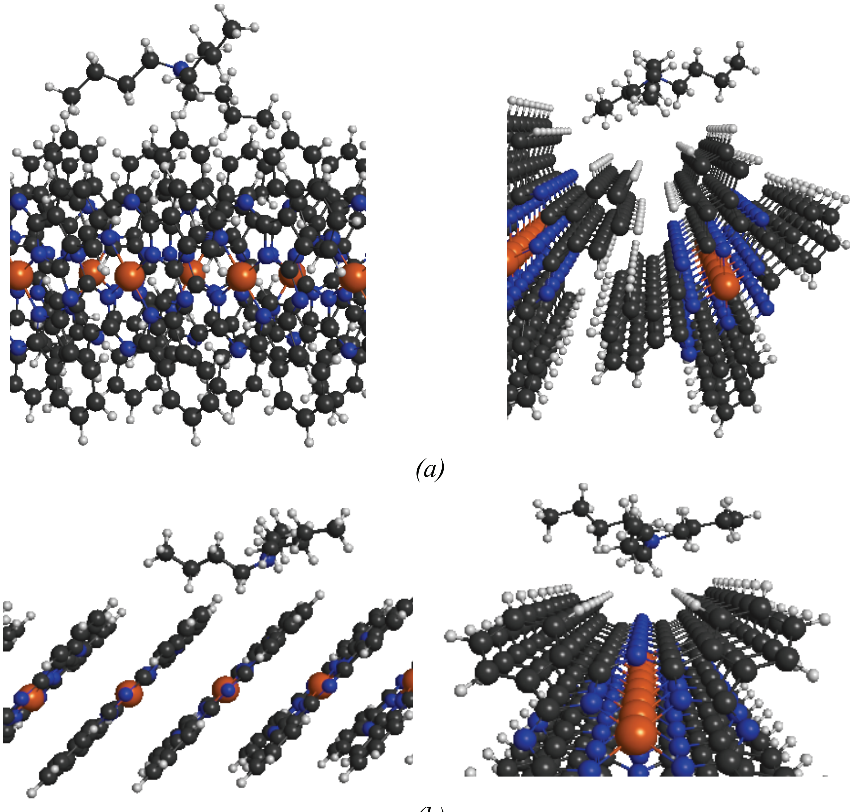

Fig. 7. Complexes of tributylamine with the surface of $(20\bar{1})$ (*a*) and (001) (*b*) copper phthalocyanine

When sorbing on surfaces (001) and $(20\bar{1})$, the only polar atoms with which the trialkylamine molecule can interact are the nitrogen atoms. However, due to steric hindrances, the strength of the nitrogen-nitrogen interaction is too low, and the main contribution to the sorption energy will come from the dispersion interactions between the nonpolar parts of the sorbate and the sorbent. The structure of the trialkylamine complexes with surfaces (001) and $(20\bar{1})$ is shown in Fig. 7.

The formation energies for the presented trialkylamine complexes with the surface of copper phthalocyanine are shown in Figs. 8–10.

As can be seen from the graphs in Fig. 8, the XTB2 method yields significantly overestimated values of sorption energy on metal atom surfaces. Methods QMMM1 and QMMM2 provide nearly identical values when including BSSE (Basis Set Superposition Error) corrections. Without BSSE consideration, the calculation error in energy is quite significant, as expected with such a small basis set. For other surfaces, calculations were conducted using only QMMM1 and XTB2 methods, with the energy values obtained by these methods differing less significantly compared to the metal atom surface. Overall, sorption energy on non-polar surfaces (001) and $(20\bar{1})$ is substantially lower than on metal atom surfaces. Surface (001) is slightly more favorable than $(20\bar{1})$.

Gibbs sorption energies calculated using dependencies (3), (4) with electronic energies computed by the QMMM1 method are presented in Fig. 11.

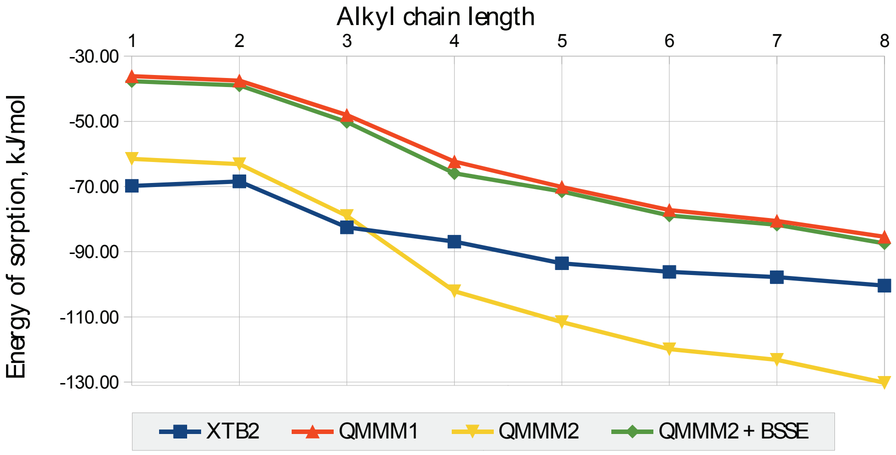

Fig. 8. Sorption energy of trialkylamines on the surface of copper phthalocyanine containing a metal atom

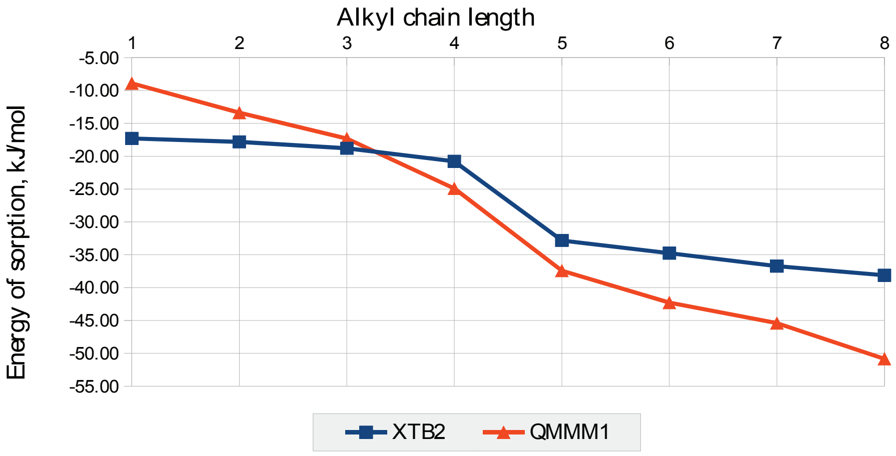

Fig. 9. Sorption energy of trialkylamines on the surface of $(20\bar{1})$ copper phthalocyanine

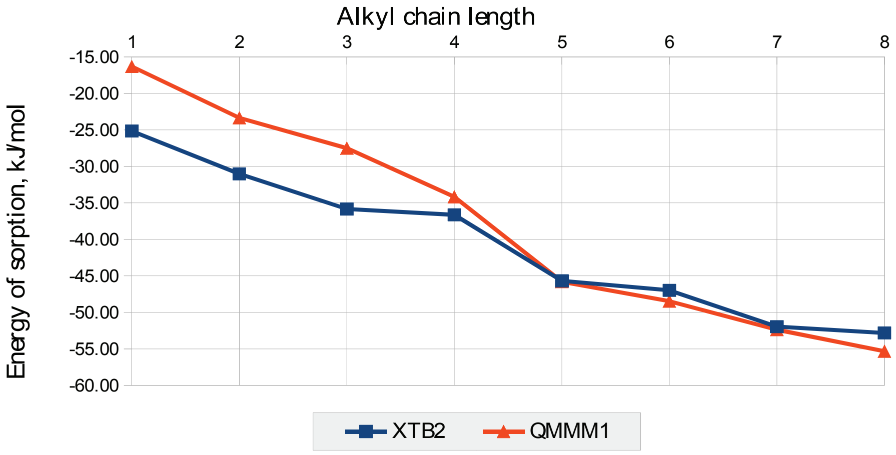

Fig. 10. Sorption energy of trialkylamines on the surface of (001) copper phthalocyanine

Based on the Gibbs energy values, it can be concluded that sorption of trialkylamines from the aqueous phase will not occur on surfaces (001) and $(20\bar{1})$ (minimum ΔG value = 18.13 kJ·mol^{-1}, corresponding to an equilibrium constant ≈ 0.0007). The graph (Fig. 11) shows two regions for these surfaces: up to tributylamine with $\Delta G \approx 40$ kJ·mol^{-1} for surface $(20\bar{1})$ and ≈ 30 kJ·mol^{-1} for surface (001), after which the free energy decreases by approximately 10 kJ·mol^{-1}.

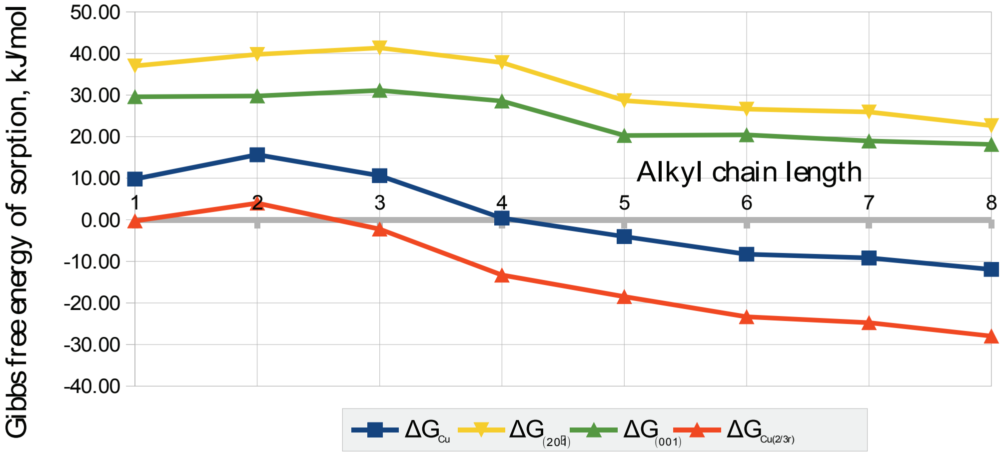

Fig. 11. Gibbs free energy of sorption of trialkylamines on various surfaces of copper phthalocyanine, calculated by the QMMM1 method

This is explained by the fact that small molecules are rigid and dispersion forces cannot deform them sufficiently to maximize interaction area with the surface. For molecules with alkyl chains longer than 5, deformation of the alkyl groups becomes advantageous, ensuring maximum interaction area between non-polar segments of the sorbate and sorbent.

Sorption of trialkylamines on the surface containing a metal atom is feasible (Fig. 11). Clearly negative values of Gibbs free energy (both with full and partial loss of rotational degrees of freedom) are observed starting from tripentylamine. However, steric hindrances may occur starting from trihexylamine and higher, which increase the energy of the sorbate-sorbent complex and make such processes less favorable. The poorest sorption characteristics are exhibited by triethylamine. Trimethylamine and tripropylamine can sorb on this surface with partial retention of rotational degrees of freedom. Tributylamine sorbs on this surface with complete loss of rotational degrees of freedom ($\Delta G = 0.4$ kJ·mol^{-1}) and well with partial retention of rotational degrees of freedom ($\Delta G = -13.32$ kJ·mol^{-1}).

4. Conclusion

In this study, molecular modeling methods using density functional theory were used to evaluate the adsorption characteristics of trialkylamines with alkyl chain length $n = 1 \div 8$. It was found that the best trialkylamine with an unbranched alkyl group for rendering the polar surface of copper phthalocyanine oleophilic is tripentylamine. Tributylamine and trihexylamine can also be used for this purpose, albeit with lower efficiency. The effectiveness of trialkylamines with longer alkyl groups remains questionable due to steric hindrances during adsorption on the polar surface. Thus, it is established that all trialkylamines only sorb on surfaces containing copper atoms, indicating selective adsorption of these surfactants on surfaces requiring oleophilization.

5. Funding

This research was funded by the Ministry of Education and Science of the Tambov Region, grant number MU2023-02/16 from the regional competition "Grants for Support of Applied Scientific Research of Young Scientists in 2023".

6. Conflict of interest

The authors declare no conflict of interests.

References

1. Lambourne R, Strivens TA. *Paint and surface coatings: theory and practice*. Saint Petersburg: William Andrew publ. house; 1999. 784 p. (In Russ.)

2. Indeikin EA, Leibzon LN, Tolmachev IA. *Pigmentation of paints and varnishes*. Leningrad: Khimiya; 1986. 160 p. (In Russ.)

3. Degtyarev AA, Trishina AV, Tarakanov AG. Research of the sorption activity of copper phthalocyanine. *Butlerovskiye soobshcheniya = Butlerov Communications*. 2018;55(7):22-30. DOI:10.37952/ROI-jbc-01/18-55-7-22 (In Russ.)

4. Degtyarev AA, Trishina AV, Dyachkova TP, Subocheva MYu, Obraztsova EYu. Predicting the possibility of oleophilizing surfaces of copper phthalocianin on the basis of reactivity descriptors. *Russian Journal of Physical Chemistry A*. 2020;94(8):1694-1698. DOI:10.1134/S0036024420080051

5. Vinogradov SV, Kononov MA, Pustovoi VI, Svetikov VV. Plasmonic spectroscopy of the water solutions of the copper phthalocyanine adsorbed on a silver surface. *Prikladnaya Fizika = Plasma Physics Reports*. 2018;(1):69-73 (In Russ.)

6. Koshida H, Takahashi Y, Okuyama H, Hatta S, et al. CuPc adsorption on Au(110)-(1 × 2): from a monomer to a periodic chain. *e-Journal of Surface Science and Nanotechnology*. 2022;20(1):25-30. DOI:10.1380/ejssnt.2022-010

7. Huang Y, Wruss E, Egger D, Kera S, et al. Understanding the adsorption of CuPc and ZnPc on noble metal surfaces by combining quantum-mechanical modelling and photoelectron spectroscopy. *Molecules*. 2014;19(3):2969-2992. DOI:10.3390/molecules19032969

8. Komolov AS, Lazneva EF, Gerasimova NB, Zimina MV, et al. Water-soluble copper phthalocyanine for optimization of gas-sensor characteristics of tin dioxide upon adsorption of ammonia. *Fizika tverdogo tela = Physics of the Solid State*. 2015;57(12):2550-2554. DOI:10.1134/S1063783415120203 (In Russ.)

9. Gavrilenko MA. Use of a copper phtalocyanine adsorption layer for subtraction of spirits in gasochromatographic analysis. *Izvestiya Tomskogo politekhnicheskogo universiteta = Bulletin of the Tomsk Polytechnic University*. 2006;309(4):98-100 (In Russ.)

10. Yin S, Wang C, Xu B, Bai C. Studies of CuPc adsorption on graphite surface and alkane adlayer. *The Journal of Physical Chemistry B*. 2002;106(35):9044-9047. DOI:10.1021/jp0202901

11. Brown CJ. Crystal structure of β-copper phthalocyanine. *Journal of the Chemical Society A*. 1968;2488-2493. DOI:10.1039/J19680002488

12. Defeyt C, Vandenabeele P, Gilbert B, Van Pevenage J, et al. Contribution to the identification of α-, β- and ε-copper phthalocyanine blue pigments in modern artists' paints by x-ray powder diffraction, attenuated total reflectance micro-Fourier transform infrared spectroscopy and micro-Raman spectroscopy. *Journal of Raman Spectroscopy*. 2012;43(11):1772-1780. DOI:10.1002/jrs.4125

13. Gorelik TE, Habermehl S, Shubin AA, Gruene T, et al. Crystal structure of copper perchlorophthalocyanine analysed by 3D electron diffraction. *Acta Crystallographica Section B Structural Science, Crystal Engineering and Materials*. 2021;77(4):662-675. DOI:10.1107/S2052520621006806

14. Zou T, Wang X, Ju H, Zhao L, et al. Controllable molecular packing motif and overlap type in organic nanomaterials for advanced optical properties. *Crystals*. 2018;8(1):22. DOI:10.3390/cryst8010022

15. Khivantsev K, Jaegers NR, Kwak J, Szanyi J, Kovarik L. Precise identification and characterization of catalytically active sites on the surface of γ-alumina**. *Angewandte Chemie International Edition*. 2021;60(32):17522-17530. DOI:10.1002/anie.202102106

16. Shor EA, Shor AM, Nasluzov VA. Quantum-chemical modeling of Ag/CeO_2 nanoscale catalysts. *Russian Journal of Physical Chemistry A*. 2023;97(5):836-845. DOI:10.1134/S0036024423050242

17. Rudenko EI, Dohlikova NV, Gatin AK, Sarvadiy SY, et al. Simulation of hydrogen and oxygen adsorption on palladium nanoparticles located on a graphite substrate with various defects. *Russian Journal of Physical Chemistry B*. 2023;17(4):845-852. DOI:10.1134/S1990793123040164

18. Nizovtsev AS. Interaction of carbon monoxide with transition metal phthalocyanines. *Journal of Structural Chemistry*. 2023;64(7):1275-1282. DOI:10.1134/S0022476623070119

19. Degtyarev AA, Zarapina IV, Zdereva AV. Modeling the sorption of low-molecular compounds on the surface of copper phthalocyanine by the method of density functional theory. *Butlerovskiye soobshcheniya = Butlerov Communications*. 2021;65(3):86-92. DOI:10.37952/ROI-jbc-01/21-65-3-86 (In Russ.)

20. Bannwarth C, Ehlert S, Grimme S. GFN$_{2-x}$TB–An accurate and broadly parametrized self-consistent tight-binding quantum chemical method with multipole electrostatics and density-dependent dispersion contributions. *Journal of Chemical Theory and Computation*. 2019;15(3):1652-1671. DOI:10.1021/acs.jctc.8b01176

21. Grimme S, Hansen A, Ehlert S, Mewes J-M. r^{2}SCAN-3c: A "swiss army knife" composite electronic-structure method. *The Journal of Chemical Physics*. 2021;154(6):064103. DOI:10.1063/5.0040021

22. Najibi A, Goerigk L. DFT-D4 counterparts of leading meta-generalized-gradient approximation and hybrid density functionals for energetics and geometries. *Journal of Computational Chemistry*. 2020;41(30):2562-2572. DOI:10.1002/jcc.26411

23. Caldeweyher E, Bannwarth C, Grimme S. Extension of the D3 dispersion coefficient model. *The Journal of Chemical Physics*. 2017;147(3):034112. DOI:10.1063/1.4993215

24. Caldeweyher E, Ehlert S, Hansen A, Neugebauer H, et al. A generally applicable atomic-charge dependent London dispersion correction. *The Journal of Chemical Physics*. 2019;150(15):154122. DOI:10.1063/1.5090222

25. Hellweg A, Rappoport D. Development of new auxiliary basis functions of the Karlsruhe segmented contracted basis sets including diffuse basis functions (def2-SVPD, def2-TZVPPD, and def2-QVPPD) for RI-MP2 and RI-CC calculations. *Physical Chemistry Chemical Physics*. 2015;17(2):1010-1017. DOI:10.1039/C4CP04286G

26. Rappoport D, Furche F. Property-optimized gaussian basis sets for molecular response calculations. *The Journal of Chemical Physics*. 2010;133(13):134105. DOI:10.1063/1.3484283

27. Boys SF, Bernardi F. The calculation of small molecular interactions by the differences of separate total energies. Some procedures with reduced errors. *Molecular Physics*. 1970;19(4):553-566. DOI:10.1080/00268977000101561

28. Ehlert S, Stahn M, Spicher S, Grimme S. Robust and efficient implicit solvation model for fast semiempirical methods. *Journal of Chemical Theory and Computation*. 2021;17(7):4250-4261. DOI:10.1021/acs.jctc.1c00471

29. Garcia-Ratés M, Neese F. Effect of the solute cavity on the solvation energy and its derivatives within

the framework of the gaussian charge scheme. *Journal of Computational Chemistry*. 2020;41(9):922-939. DOI:10.1002/jcc.26139

30. Mayhall NJ, Raghavachari K, Hratchian HP. ONIOM-based QM:QM electronic embedding method using Löwdin atomic charges: energies and analytic gradients. *The Journal of Chemical Physics*. 2010;132(11):114107. DOI:10.1063/1.3315417

31. Neese F. Software update: the ORCA program system – version 5.0. *WIREs Computational Molecular Science*. 2022;12(5):e1606. DOI:10.1002/wcms.1606

32. Liu S-C, Zhu X-R, Liu D-Y, Fang D-C. DFT calculations in solution systems: solvation energy, dispersion energy and entropy. *Physical Chemistry Chemical Physics*. 2023;25(2):913-931. DOI:10.1039/D2CP04720A

33. Herbert JM. Dielectric continuum methods for quantum chemistry. *WIREs Computational Molecular Science*. 2021;11(4):e1519. DOI:10.1002/wcms.1519

34. Mu WH, Chasse GA, Fang DC. Test and modification of the van der Waals' radii employed in the default PCM model. *International Journal of Quantum Chemistry*. 2008;108(9):1422-1434. DOI:10.1002/qua.21674

35. Tao JY, Mu WH, Chass GA, Tang TH, Fang DC. Balancing the atomic waistline: Isodensity-based scrf radii for main-group elements and transition metals. *International Journal of Quantum Chemistry.* 2013;113(7):975-984. DOI:10.1002/qua.24065

36. Lange AW, Herbert JM. A smooth, nonsingular, and faithful discretization scheme for polarizable continuum models: The switching/Gaussian approach. *The Journal of Chemical Physics*. 2010;133(24):244111. DOI:10.1063/1.3511297

37. Boese R, Bläser D, Antipin MY, Boese R, Antipin MY, Chaplinski V, de Meijere A. Non-planar structures of Et_3N and $Pr_{i3}N$: a contradiction between the X-ray, and NMR and electron diffraction data for $Pr_{i3}N$. *Chemical Communications*. 1998;(7):781-782. DOI:10.1039/a708399h

38. Banert K, Heck M, Ihle A, Shoker T, et al. Non-Planar structures of sterically overcrowded trialkylamines. *Chemistry – A European Journal*. 2021;27(11):3700-3707. DOI:10.1002/chem.202003933

Information about the authors / Информация об авторах

Andrey A. Degtyarev, Cand. Sc. (Eng.), Associate Professor, Tambov State Technical University (TSTU), Tambov, Russian Federation; ORCID 0000-0003-3690-4565; e-mail: ad.dycost@gmail.com

Alexandra V. Trishina, Assistant, TSTU, Tambov, Russian Federation; ORCID 0000-0003-3413-4763; e-mail: koroleva_tambov@mail.ru

Elizaveta I. Krovyakova, Student, TSTU, Tambov, Russian Federation; e-mail: krovakovaelizaveta@gmail.com

Дегтярев Андрей Александрович, кандидат технических наук, доцент, Тамбовский государственный технический университет (ТГТУ), Тамбов, Российская Федерация; ORCID 0000-0003-3690-4565; e-mail: ad.dycost@gmail.com

Тришина Александра Викторовна, ассистент, ТГТУ, Тамбов, Российская Федерация; ORCID 0000-0003-3413-4763; e-mail: koroleva_tambov@mail.ru

Кровякова Елизавета Ивановна, студент, ТГТУ, Тамбов, Российская Федерация; e-mail: krovakovaelizaveta@gmail.com

Received 02 September 2024; Accepted 10 October 2024; Published 20 December 2024

Journal of Advanced Materials and Technologies. Vol. 9, No. 4. 2024

Original papers
Manufacturing processes and systems

УДК 621.6.04.001 DOI: 10.17277/jamt.2024.04.pp.296-311

Quasidiffusion effects in fast gravitational flows of cohesionless particles of granular matter

© Viktor N. Dolgunin[a]✉, Andrey N. Kudi[a],
Andrey A. Zhilo[a], Konstantin A. Kudi[b], Vasily A. Pronin[a]

[a] *Tambov State Technical University, 1, Leningradskaya St., Tambov, 392000, Russian Federation,*
[b] *PJSC "MTS Bank", Bld. 1, 18, Andropova Av., Moscow, 115432, Russian Federation*

✉ dolgunin-vn@yandex.ru

Abstract: The study analyzes the physical mechanisms behind the quasi-diffusive separation of cohesionless spherical particles in thin-layer fast gravity flows on a rough chute with substantial structural and kinematic parameter nonuniformity, with their complex size and density discrepancies. Studies have been conducted into alternative conditions of quasi-diffusive interaction of particles in a fast gravitational flow on a rough chute, which are defined by the dominance of the particles' relative velocities in the direction of gravitational shear or their chaotic fluctuations in the interaction. It has been found that the intensity of the quasi-diffusive separation flux is in direct dependence on the particle collision frequency, which, in the general case of gravity flows of granular matter, is determined at the dominant value of the component of the relative shear velocity of particles and depends to a lesser extent on the velocity of their chaotic fluctuations. In non-ordinary conditions of fast gravity flow, which are formed in the flow of nonsmooth elastic particles in its upper part, called the "cloud" of particles, the frequency of particle collisions is determined at the dominant value of the velocity of their fluctuations. It is found that in thin-layer fast gravity flows the effect of quasi-diffusive separation due to structural nonuniformity of the flow can dominate over the segregation effect resulting from local nonuniformity of the medium.

Keywords: granular matter; fast gravitational flow; structural heterogeneity; quasi-diffusion separation; size and density separation; segregation; void fraction gradient.

For citation: Dolgunin VN, Kudi AN, Zhilo AA, Kudi KA, Pronin VA. Quasidiffusion effects in fast gravitational flows of cohesionless particles of granular matter. *Journal of Advanced Materials and Technologies*. 2024;9(4):296-311. DOI: 10.17277/jamt.2024.04.pp.296-311

Квазидиффузионные эффекты в быстрых гравитационных потоках несвязных частиц зернистых материалов

© В. Н. Долгунин[a]✉, А. Н. Куди[a], А. А. Жило[a], К. А. Куди[b], В. А. Пронин[a]

[a] *Тамбовский государственный технический университет,*
ул. Ленинградская, 1, Тамбов, 392000, Российская Федерация,
[b] *ПАО «МТС-Банк», Андропова пр., 18, корп. 1, Москва, 115432, Российская Федерация*

✉ dolgunin-vn@yandex.ru

Аннотация: Проанализированы физические механизмы квазидиффузионной сепарации когезионно несвязанных сферических частиц при комплексном их различии по размеру и плотности в тонкослойных быстрых гравитационных потоках на шероховатом скате с высокой неоднородностью структурно-кинематических параметров. Исследованы альтернативные условия квазидиффузионного взаимодействия частиц в быстром гравитационном потоке на шероховатом скате, отличающиеся доминированием при взаимодействии либо относительной скорости частиц в направлении гравитационного сдвига, либо скорости их хаотических флуктуаций. Установлено, что интенсивность потока квазидиффузионной сепарации находится в прямой зависимости от частоты столкновения частиц, которая в общем случае гравитационных течений зернистых материалов определяется при доминирующем значении компоненты относительной сдвиговой скорости частиц и в меньшей степени зависит от скорости их хаотических флуктуаций. В неординарных условиях быстрого гравитационного течения, которые формируются в потоке гладких упругих частиц в верхней его части, называемой «облаком» частиц, частота столкновений частиц определяется при доминирующем значении скорости их флуктуаций. Установлено, что в тонкослойных быстрых гравитационных потоках эффект квазидиффузионной сепарации, обусловленный структурной неоднородностью потока, может доминировать над эффектом сегрегации, являющимся следствием локальной неоднородности среды.

Ключевые слова: зернистый материал; быстрый гравитационный поток; структурная неоднородность; квазидиффузионная сепарация; сепарация по размеру и плотности; сегрегация; градиент доли пустот.

Для цитирования: Dolgunin VN, Kudi AN, Zhilo AA, Kudi KA, Pronin VA. Quasidiffusion effects in fast gravitational flows of cohesionless particles of granular matter. *Journal of Advanced Materials and Technologies*. 2024;9(4):296-311. DOI: 10.17277/jamt.2024.04.pp.296-311

1. Introduction

Granular matter, whose particles have no significant cohesive interactions, is frequently used in industrial technologies (chemistry, construction, food, mining, agriculture, etc.), in everyday life (cereals, legumes, nuts, salt, sugar, spices, etc.) and in the natural environment (sands, gravel, pebbles, rock fragments, etc.). Such materials look quite ordinary when they are considered at the level of individual particles, but at a closer look, they reveal original, mesoscopic properties, especially, when they are analyzed as a set of particles under certain interaction conditions [1, 2]. For example, depending on the interaction conditions, quartz sand particles can act as a solid base for building structures, as a liquid in an hourglass, and migrate as a gas of solid particles in the process of dune movement.

The most common form of particle interaction is their interaction under shear flow conditions of granular media. In this connection, for example, the piston flow of granular media is perceived as an idealized version of the flow.

In natural phenomena and technological processes in industry and agro-industrial complex, shear flows of granular matter most often occur in the form of fast gravitational flows. One of the main features of such flows is that particles interact intensively with each other and are involved in transverse mass transfer accompanied by quasi-diffusive effects of separation and mixing [3, 4]. The above effects are so significant that they can significantly influence the kinetics of the processing of granular matter and, moreover, can be used as a basis for the development of technological processes with original functional properties [5–7]. The analysis of literature sources shows that, despite the rather high scientific and applied significance of the study of quasi-diffusion effects under shear deformation of granular media, in most cases the studies are limited to modeling of quasi-diffusion mixing processes [8–10]. These circumstances explain that the physical mechanisms of quasi-diffusion effects of particle separation in fast gravitational flows of granular matter are the main object of the present study.

2. Analysis of methods for modeling separation effects in gravity flows of granular matter

The analysis of studies on modeling of separation dynamics in gravity flows of granular matter [5, 6, 8, 10] shows that in most of them the interaction of particles in the flow is modeled in the absence of attention to the structural nonuniformity of the flow. This is explained by the fact that in many cases of modeling dispersed media are analyzed in the state of gravitational shear at high and relatively stable values of pressure and low gradients of shear rate, when the assumption of structural uniformity of the medium can be quite correct. In addition, the analysis of gravitational flow mainly under conditions of its structural uniformity is explained by the great problems of identification of microstructural characteristics of fast gravitational flow of particles in states of unusual gas and liquid properties [2–4, 11].

The separation effects due to spatial nonuniformity of shear flows of granular matter were among the first to be identified by Stephens and Bridgewater [12]. Using an annular shear cell, the authors investigated the distributions of nonuniform particles in failure zones, where high shear rate gradients and void fractions result from intense particle interaction. The flow conditions formed in the failure zones of granular media significantly affect the kinetics of technological processes.

When studying the effects of separation and mixing of particles in the above-mentioned zones, the authors [12] found an unusual effect of movement of large particles of the mixture, which they called migration. The authors explained migration qualitatively as the effect of movement of large particles in the direction of the shear strain rate gradient. However, a sufficiently deep analysis of the physical mechanism of the detected effect was hindered by the unfavorable conditions for the analysis of obtaining measurement data. Firstly, problems in the analysis arose due to the highly complex shape of the shear flow, which resulted in the manifestation of difficult to estimate nonuniformity of the shear rate in the three-dimensional volume of the shear cell, for example, in the radial direction of the annular failure zone [12]. Secondly, and more importantly, a comprehensive analysis of the migration phenomenon was hindered by the limited amount of measurement information due to the lack of an opportunity to evaluate the influence of the structural nonuniformity of the failure zone on the effect in the form of the distribution of the void fraction or solid phase concentration in its volume. Therefore, the authors in [12] faced the problem of explaining the unusual distributions of mustard seed and polystyrene granules in the shear cell.

In addition, the simplest verification of the proposed migration mechanism by testing it on the results of studies of separation in gravity flow on a chute (e.g., Fig. 1*a*) does not make it possible to explain the opposite directions of migration of large particles near the bottom and open surface of the flow. When the shear rate varies monotonically along the bed thickness, large particles are displaced in the flow regardless of the shear strain rate gradient [13]. At the same time, it is important to note an obvious contradiction between the migration mechanism and the dispersion pressure mechanism proposed in [14], and according to which large particles move in the direction opposite to the shear strain rate gradient. Thus, with the unity of views on the driving force of separation due to the nonuniformity of the shear strain rate, the researchers in [12] and [14] determine the opposite direction of the process.

As a result, in the absence of a single abstract judgment regarding the physical nature of separation effects, the assumption of homogeneity of the characteristics of the gravitational flow structure is accompanied by serious problems in the mathematical description of the process. Consequently, it is often accompanied by the necessity to use different separation mechanisms in modeling the process depending on the distinctive properties of particles in invariant flow conditions. For example, when modeling the dynamics of separation of particles of different densities in a gravitational flow [15], the ascent mechanism is used, which formally reproduces the process of behavior of bodies with large and small densities in a liquid. At the same time, when describing the separation of particles by size under similar conditions, the mechanism of partial stress relaxation is used in [10].

In accordance with the mechanism of partial stresses, the stresses generated by gravitational shear are distributed on particles nonuniformity, if the latter are unequal in size. It is assumed that the stress distribution on nonuniform particles follows some law, according to which the stresses on particles of a certain size are proportional to some partial stress coefficient. It is important that in this case the values of the coefficients of the components of the particle mixture are not equal to their relative fraction [10]. In this case, the driving force of the process is expressed as a gradient of lithostatic pressure due to gravitational influence. It is assumed that particles of large size tend to generate partial stresses, whose share in the total stresses is greater than their concentration in the mixture, and are forced toward the lithostatic pressure gradient, i.e., toward the open surface of the flow [16]. Accordingly, small-sized particles generate partial stresses in the flow, the fraction of which in the total stresses is less than their volume fraction in the mixture. Such particles move in the direction of the lithostatic pressure gradient, i.e., to the lower layers of the flow, where the stresses have the maximum value.

The authors of relatively recent studies [8, 16], analyzing the physical mechanisms of buoyancy [15] and partial stress relaxation [10, 17], note their rather high flexibility, and conclude that they have a serious drawback, which is a consequence of the lack of attention to the separation effects initiated by the nonuniformity of shear flow parameters. Among such parameters, the authors in [8] emphasize the shear rate and granular temperature, which, in general, vary in the shear flow volume over a wide range. The necessity to consider the effects of spatial heterogeneity of shear flow characteristics on the separation dynamics was justified by many researchers of the separation process in gravity flows of granular media [8, 13, 16].

Assuming that the size and density separation proceeds according to different physical mechanisms, the authors in [8] considered it rational to divide the local stresses into two components: one component is contact stresses, and the other one is kinetic stresses. In this case, they assume that the size separation occurs under the action of the driving force caused by the action of kinetic stresses and expressed in the form of their gradient under the condition of disproportionate distribution of stresses on particles of different sizes. Kinetic stresses are stresses that are

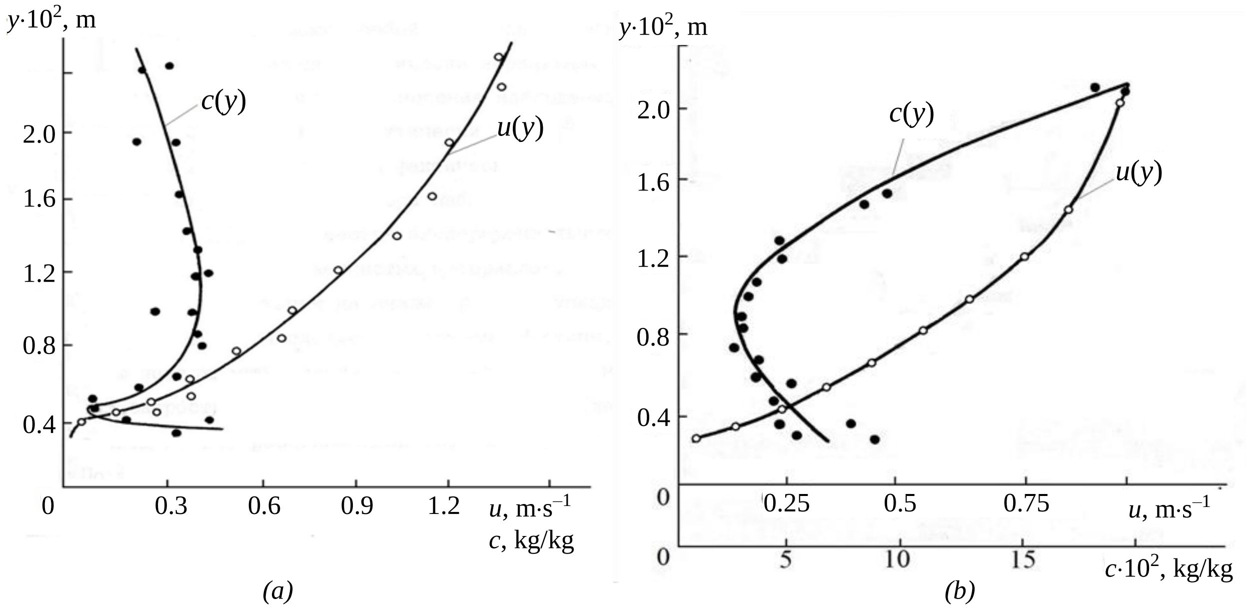

(a) *(b)*

Fig. 1. Profiles of velocity $u(y)$ and concentration $c(y)$ of particles in flows on a rough chute in binary mixtures:
a) large particles in a mixture of steel balls;
b) silica gel granules in a mixture with equally sized granules of superphosphate

generated in granular matter under conditions of rapid shear deformation as a result of transfer of impact impulses by colliding particles across the shear surface.

However, if we take into account that the intensity of impulse interaction between particles is proportional to the shear rate, we should conclude that the directions of gradients of kinetic stresses and shear rate coincide. Thus, a certain physical analogy between the mechanisms of migration [12] and partial kinetic stresses [8, 16] is revealed, and the critical remarks made earlier with respect to the migration mechanism largely apply to the mechanism of partial kinetic stresses as well.

According to [8], density separation proceeds under the action of contact stresses in accordance with the previously presented buoyancy mechanism [15]. The driving force of separation in this case is gravitational influence under conditions of disproportionate distribution of contact stresses on nonuniform particles. It is important to pay attention to the fact that when developing the separation mechanisms due to spatial inhomogeneity of shear flow, the authors limit themselves to the case of particle size difference, considering that spatial inhomogeneity of shear flow does not affect the separation by density. The validity of this approach is refuted by experimental data [13] (e.g., Fig. 1*b*), which confirms the effect of spatial inhomogeneity of flow on density separation.

Thus, the process of separation by size and density is described [8] through separate physical mechanisms [10] and [15], each of which is adapted for an autonomous description of the separation effect with respect to a certain distinctive property of particles.

Based on the corresponding physical representations, a mathematical model of particle separation by size and density was developed in [8]. The mathematical model is based on the equation describing the dynamics of distribution of nonuniform particles in a flow with nonuniform shear strain rate

$$\rho^i\left(v^{c,i}-v\right)=\frac{(\psi^{c,i}-\psi^{k,i})}{c_D}\frac{\partial\sigma_{yy}^k}{\partial y}+$$

$$+\frac{(\phi_m^i-\psi^{c,i})}{c_D}\rho g\cos\zeta-D\frac{\partial\rho^i}{\partial y}, \qquad (1)$$

where ρ, ρ^i are bulk density of granular medium and particles of the i-th component, respectively; g is gravitational acceleration; v, v^i are velocity of granular medium and particles of the i-th component in the direction of y separation, respectively; ϕ_m^i is concentration of the i-th component; $\psi^{c,i}, \psi^{k,i}$ are coefficients of partial contact and kinetic stresses for the i-th component of the mixture, respectively; σ_{yy}^k is kinetic stress; ζ is flow slope angle to the horizon; D is mixing coefficient; c_D is drag coefficient in the process of particle separation.

The partial stresses $\psi^{c,i}$, $\psi^{k,i}$ and the ϕ_m^i component concentration are expressed as relative dimensionless quantities.

According to the mathematical description (1), the concentration field of control particles of granular medium in shear flow is determined by the conjugation of the effects of particle transport by convection, separation and quasi-diffusive mixing, and the manifestation of separation effects is caused by the disproportionate distribution of two types of stresses on nonuniform particles. It is important to note that due to this approach, the description of the dynamics of the separation process is provided taking into account both the local nonuniformity of particles of the granular medium and the spatial inhomogeneity of kinematic characteristics in the shear flow of the matter.

However, verification of the mechanisms and kinetic dependences of the separation effects proposed in [8] due to both local and spatial inhomogeneity of the granular medium flow reveals their apparent contradictory nature. Verification was carried out by testing the mechanisms and kinetics based on the results of experimental studies presented in [13] (Fig. 1). Figure 1 shows experimental profiles of velocity and distributions of control particles in fast gravity flows of mixtures of particles of different sizes (Fig. 1*a*) and densities (Fig. 1*b*) on a rough chute. First of all, when. testing the model representations on which the separation dynamics equation (1) is based, it is important to pay attention to the experimental velocity profiles, which in both cases (Figs. 1*a* and 1*b*) have a parabolic shape with a monotonic change in the shear rate and its gradient directed toward the bottom of the flow. However, when the direction of the shear rate gradient in the flow is constant, different directions of the separation fluxes by size and density are observed. In the processes of separation by both size and density, the direction of movement of the particles of the control component at the bottom and at the open surface of the flows is opposite, which is impossible to explain from the position of model ideas about the mechanisms of separation by size and density, on which the mathematical description of the separation dynamics is based (1).

One of the reasons for such contradictions may be the lack of due attention to the structural nonuniformity of the granular medium flow when developing [8] the physical mechanism and mathematical model of separation. Given the fundamentally important role of shear rate nonuniformity with respect to the size separation kinetics, the assumption made does not seem to be correct enough. This conclusion is confirmed by many examples that show the presence of a pronounced dependence of the void fraction in the shear flow of a granular medium on the shear rate. Such examples are the results of experimental studies of the relationship between kinematic and structural parameters under conditions of both fast gravity flows on a rough chute and pseudoplastic shear deformations of granular matter [7, 13]. Since the volume fraction of particles in shear flow significantly affects [2] the conditions of their interaction and flow dynamics, the assumption of homogeneity of solid phase distribution in a flow with pronounced nonuniformity of shear rate, is one of the reasons for the inadequacy of modeling found in [8]. It is difficult to assume that the ratio of partial contact and kinetic stresses for particles of different size and density under conditions of structural inhomogeneity of the flow remains constant.

The lack of a sufficiently developed theoretical base does not allow for identification of a complex of kinetic parameters characterizing the intensity of separation and mixing effects and becomes the reason for the use of fitting coefficients. For example, according to the process dynamics equation (1), the number of such coefficients can be equal to four, if we take into account that the kinetic characteristics of the equation are complex functions not only of the shear rate, but also of the void fraction, which is in a complex dependence on the shear rate.

The above situation indicates the relevance of analytical and experimental studies of the mechanisms and kinetic regularities of size and density separation effects in fast shear flows of particles, the failure zones of which are characterized by high gradients of kinematic and structural characteristics. The purpose of the present study is to analyze the results of a comprehensive study of size and density separation in particle flows on a gravity chute under conditions of a vivid manifestation of inhomogeneity of flow parameters in its failure zones. Due to the dislocation of failure zones at the base and surface of such flows, thin-layer gravity flows are the most suitable for studies. With a relatively large volume fraction of failure zones in thin-bed flows, conditions for intensive separation of particles under the effects of inhomogeneity of flow parameters are formed in most of them. It is interesting to note that, in many formal features, the flow conditions occurring in a thin-bed fast gravity flow are similar to the conditions of shear flow in a annular shear cell [12] and differ from the latter by more favorable conditions for analysis in a two-dimensional flow.

3. Research methods and model materials

The regularities of particle size and density separation under the effects of gravity flow inhomogeneity are investigated using an experimental-analytical method [7]. The method provides access to a set of the most important information on flow parameters and particle separation effects on a rough chute in the form of velocity profiles, void fraction and distributions of nonuniform particles.

Under this method, experimental information is obtained using a setup that is an open inclined channel of rectangular cross-section with smooth side walls and a rough bottom. The channel is set at an angle to the horizon with some excess of the angle of repose of the material. To ensure the conditions of sticking at the bottom of the flow and intensive shear deformations in its volume, the roughness value of the channel base is equal to half of the diameter of the largest particles of granular medium. To feed the material into the channel the unit is equipped with a metering feeder. A horizontal cuvette with transverse partitions dividing the cuvette into cells is installed under the threshold of channel on the plumb line. Cells are used to receive falling particles in the stationary mode of steady-state material flow to obtain the corresponding distribution functions of material and test particles. The stationary regime of steady-state flow is confirmed by the fact that the distributions remain unchanged when the length of the rough chute is increased in the experiments.

The set of experimental information necessary for the implementation of the method, in addition to the mentioned distribution functions, includes the time of filling the cells of the cuvette, the width of the channel and its slope angle, the geometric parameters of the bed on the chute and the height of placement of the discharge threshold above the cuvette. Based on the obtained information, the profiles $u(y)$, $\varepsilon(y)$ and $c(y)$ are determined by analytical solution of the system of equations including the material balance equation, the law of a free-falling body and the equation of state of the granular medium under conditions of rapid gravitational shear [7]. The solution is obtained assuming the condition of zero longitudinal velocity of particles at their contact with bottom roughness ($u = 0$ at $y = 0$).

In the analysis, in addition to the original data, the results of the study obtained earlier [13] using mixtures (Table 1) with complex particle size and density differences: 1) in size (mixture 1); 2) mainly in density (mixture 2); 3) in size and density (mixture 3) were used.

The dynamics of the concentration field of test particles in shear gravity flow of granular matter is defined [7, 13] as the resultant effect of particle transport by convection j_c, separation j_s, caused by factors of both local and spatial heterogeneity of the flow, and quasi-diffusive mixing of j_d component:

$$\frac{\partial(c\rho)}{\partial t}+\operatorname{div}\left(\vec{j}_c\right)=-\operatorname{div}\left(\vec{j}_s\right)-\operatorname{div}\left(\vec{j}_d\right), \qquad (2)$$

where t is time; ρ is local value of bulk density, which is defined as a function of control particle concentration $c(x, y, t)$ under conditions of stationary distribution of void fraction in the flow $\varepsilon(y)$.

The kinetics of size and density segregation initiated by local flow inhomogeneity is modeled on the basis of the mechanism of shear flow segregation [7, 18, 19]. According to this mechanism, segregation is a consequence of the process of stress relaxation on particles – stress concentrators, which differ in properties from uniform particles of a conventionally homogeneous flow. In the relaxation process, an aggregate of particles is formed near the stress concentrator, and when interacting with it, the concentrator acquires a transverse momentum that initiates its displacement accompanied by a weakening of the stress state.

Table 1. Characterization of mixture matter

Matter	Mixture 1		Mixture 2		Mixture 3	
	Steel balls		Superphosphate	Silica gel	Superphosphate	Silica gel
Particle diameter, 10^3 m	6.6	7.0	+3.75 – 4.0		+3.75 – 4.0	+4.0 – 4.25
Weight concentration, %	56.6	43.4	95.6	4.4	95.6	4.4
Density, $\text{kg}\cdot\text{m}^{-3}$	7850		1800	785	1800	785
Slope angle, deg	31		35		35	

The control particle contacts the aggregate in points, the coordinates of which are determined by methods of statistical mechanics with regard to the local value of solid phase concentration and the ratio of sizes of the test particle and the particles of a conventionally uniform medium forming the aggregate. Through the contact points passes the axis of rotation of the particle under the action of ΔM excessive momentum of gravity, friction and impact momentums in the direction of segregation. As a result, when the process driving force ΔM and the process kinetic coefficient K_S are used, it is possible to reflect the influence of the complex of flow parameters and the full complex of particle properties on the segregation kinetics, which is expressed in the following form

$$\vec{j}_s = K_S c \rho \Delta M. \qquad (3)$$

Studies of the mechanism and kinetics of segregation [7, 18, 19] have contributed to the deepening of knowledge about its mechanism and kinetics and enabled to propose methods for determining the driving force and the segregation coefficient K_S. The results of the study indicate that for a wide range of particle properties of a certain material and its gravitational flow parameters, the coefficient K_S exhibits the properties of a kinetic constant.

It is worth noting that the action of the shear flow segregation mechanism is limited by the conditions of low values of the void fraction ($\varepsilon < 0.75$), allowing the formation of particle aggregate near the particle – stress concentrator [7, 18]. In this connection, it can be concluded that in the gravity flow regions with high values of the void fraction ($\varepsilon \geq 0.75$) the particles are in a state of intensive chaotic (quasi-diffusive) movements and, as a consequence, it seems possible to assume that the effects of their segregation are determined mainly by diffusion kinetics.

4. Results and Discussion

4.1. Mechanisms and kinetic regularities of quasi-diffusive separation by size and density due to structural nonuniformity of gravity flow of granular matter

Mathematical modeling of the process of separation by size and density in thin-bed flow of cohesionless particles on a gravity chute with pronounced inhomogeneity of flow parameters was carried out using equation (2). The equation was used to predict the dynamics of the concentration field of test particles under the action of a set of effects (separation, quasi-diffusion, convection). Taking into account the revealed shortcomings of the analyzed methods of modeling separation, its flow is represented by two components with fundamentally different nature of the driving force. To evaluate the degree of influence of the effects of nonuniformity of structural and kinematic parameters on the predictive properties of equation (2), we analyzed the possibilities of predicting experimental concentration profiles of control particles in mixtures 1 and 2 (Table 1) taking into account only the component of the separation flow formed under the action of the factor of local nonuniformity of the flow. The intensity of the named component of the separation flux is expressed (3) on the basis of the mechanism of shear flow segregation, which is described in the previous section of the paper. In accordance with the mechanism, the segregation flow is the result of formation and relaxation of local stress concentration centers.

The mathematical description of separation using the kinetic dependence (3) provides prediction of the dynamics of the concentration field of particles differing not only in size and density, but also in the full complex of properties during gravity flow. However, it is established that in some cases, mainly in conditions of thin-bed gravity flow, with their characteristic high inhomogeneity of flow parameters, there are problems of mathematical description of separation dynamics. Moreover, the problems of mathematical description are found with respect to separation by size and density.

The inadequacy of modeling is clearly manifested in the fact that the shear segregation mechanism cannot explain the separation flows of less dense particles in mixture 2 to the base and fine particles in mixture 1 to the flow surface. If we assume that the observed counter directions of separation of particles by size and density take place at unchanged direction of the shear rate gradient in the flow, then obvious contradictions of experimental data with the mechanisms of buoyancy and partial stresses are revealed [8, 12, 14, 15, 17]. The observed paradoxical counterflow separations in size and density initiated a comprehensive study of the separation effects due to the inhomogeneity of gravity flow parameters of granular media.

The separation effects due to the inhomogeneity of thin-bed gravity flows have been investigated by the experimental-analytical method [7, 13, 18, 19], the description of which is given in the previous section of the paper.

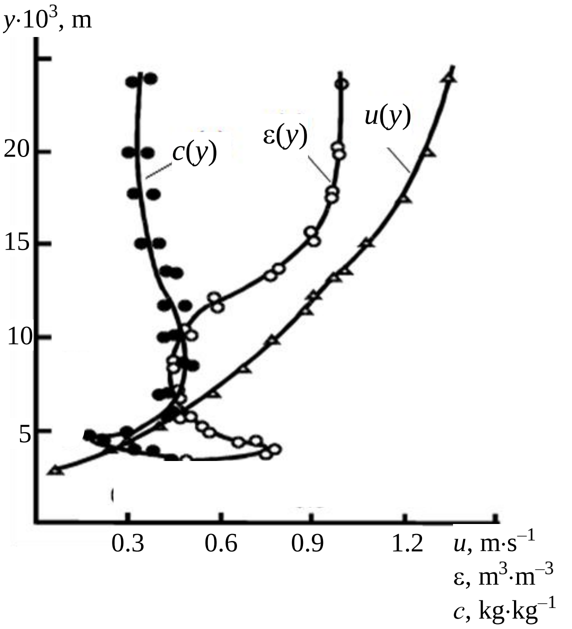

Fig. 2. Profiles of velocity $u(y)$, void fraction $\varepsilon(y)$ and large particle concentration distribution $c(y)$ in the fast gravity flow of mixture 1 (Table 1) on a rough chute

The structural and kinematic characteristics of the gravity flow of mixture 1 (Table 1) in the form of void fraction and velocity profiles are shown in Fig. 2. The same figure shows the distribution of large particles, which contain sufficient information about the separation effects that occur in the void zones in the flow on the rough slope [13]. The experimental data indicate an extremely high concentration of large-sized particles in the flow core, far exceeding their average concentration. Accordingly, in the directions from the flow core to its bottom and open surface, the concentration of small-sized particles increases significantly above the average value.

Experimental results and their discussion

The joint analyses of the profiles of void fraction and concentration distribution of large particles indicate that their shape can be considered as a mirror reflection of each other's characteristic features. It is obvious that for the profile of small particles distribution, a high analogy with the profile of void fraction can be observed.

Similar profiles $u(y)$, $\varepsilon(y)$ and $c(y)$ characterizing the gravity flow parameters and separation effects in the rarefied zones on the rough chute for mixture 2 (Table 1) are shown in Fig. 3. The results indicate that in the case of particle density differences, as well as in the case of particle size nonuniformity, the shape of the void fraction profile $\varepsilon(y)$ characteristic of steady-state fast gravity flow is observed. In the core of the flow a zone with the highest fraction of solid phase is formed, the content of which in the peripheral regions of the flow decreases with the formation of rarefied zones, especially near the open surface of the layer.

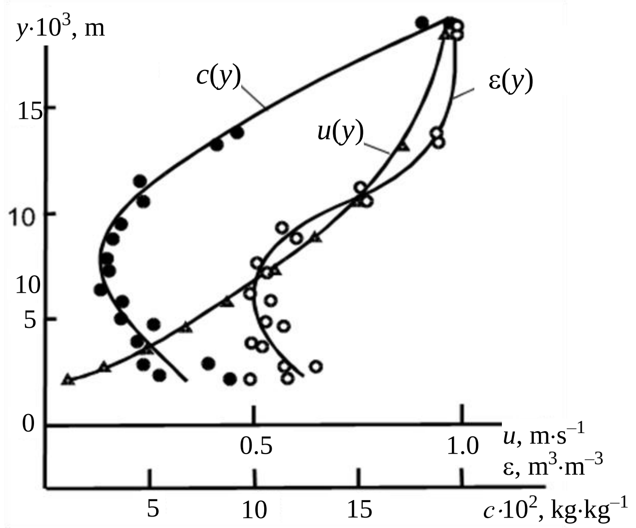

Fig. 3. Profiles of velocity $u(y)$, void fraction $\varepsilon(y)$ and low-density particle concentration distribution $c(y)$ in fast gravity flow of mixture 2 (Table 1) on a rough chute

The profile of particle distribution with low density $c(y)$ by characteristic features of the shape agrees with the profile of the void fraction $\varepsilon(y)$. The comparison of the profiles indicates a complete coincidence of the coordinates of the extreme values of the distribution functions of the void fraction $\varepsilon(y)$ and the concentration of test light particles $c(y)$. The minimum of the mentioned distribution functions is in the region of the core of the flow of granular matter on the rough chute. In the direction towards the bottom and the upper open surface of the flow, the values of these parameters increase significantly.

As a result of a complex analysis of the sets of profiles shown in Figs. 2 and 3 for flows of mixtures of particles nonuniform in size and density, it is possible to draw conclusions regarding the kinetic regularities of the observed separation effects.

Despite the unchanged direction of the shear rate gradient in the flow volume (in the direction of the bottom), in its regions near the open surface and the bottom, the size and density separation flows have opposite directions. It is noteworthy that particles with high inertial properties (larger and denser) in the process of separation move from the peripheral parts of the flow and concentrate in its central part.

Further abstraction of the experimental profiles shown in Figs. 2 and 3 suggests that, because of size and density separation, particles with large mass are concentrated in the core region of the flow with characteristically high values of void fraction. Correspondingly, there is a concentration of particles with low mass (small and low density) in the peripheral parts of the flow with characteristically high values of void fraction. In this connection it should be concluded that in the fast gravitational flow of granular medium there is an effect of structural nonuniformity, under the influence of which the separation flows of particles with small mass in the direction of the gradient of the void fraction and particles with large mass in the direction of the gradient of the volume fraction of solid phase are formed. In addition, when analyzing the variable values of the degree of curvature of profiles, it seems fundamentally important to pay attention to the importance of the void fraction gradients as a kinetic parameter that determines the intensity of the separation effect due to the inhomogeneity of shear flow parameters. This can be confirmed, for example, by density separation effects (Fig. 3), the high intensity of which can be explained by high values of the void fraction gradient $\varepsilon(y)$.

Among many extraordinary experimental results, the effect of moving of low-density particles from the core to the bottom of the flow attracts special attention (Fig. 3). It is important that in the steady-state flow regime the fraction of particles with low density increases towards the bottom until the concentration exceeds its average value in the mixture. The observed effect cannot be explained by using a set of previously analyzed separation mechanisms [8, 10, 12, 14, 15]. In this connection, there are sufficient grounds to develop the mechanism of separation as an effect of structural nonuniformity of rapid gravity flow of granular medium by analyzing the given experimental data.

A comprehensive analysis of a set of profiles $u(y)$, $\varepsilon(y)$, $c(y)$ (Figs. 2 and 3), characterizing structural-kinematic parameters and separation effects in fast gravitational flows of particles, gives grounds to assert that the movement of particles in the process of separation by size and density occurs under the action of the transfer potential, which has a direct relation to the gradient of the void fraction. The main type of interaction of particles in the rarefied zones of fast gravitational flows is their collision accompanied by the transfer of impact impulses. At chaotic exchange of impact impulses, particles differing in size and density will be in a state of chaotic fluctuations proceeding with different velocity of displacements. At collision of particles having different densities, the velocities of chaotic displacements for particles with low density, in general case, will be higher than for dense particles.

Collisions of particles at gravitational shear take place in confined conditions. In this connection, the total momentum acquired by a particle is determined in direct dependence on its surface area [13]. In this case, the average value of the fluctuation velocity of the *i*-th particle having diameter d_i and mass m_i is defined as: $V_i' \approx k d_i^2 m_i^{-1}$, where k is proportionality coefficient.

The nature of interaction of particles under conditions of fast gravitational shear has an obvious quasi-diffusive nature. At the difference in size and density, the fluctuation velocities and, accordingly, quasi-diffusion of particles will have different average values depending on their properties. In such a case, under conditions of structural nonuniformity of the shear flow, the quasi-diffusion separation effect is manifested, which has a physical nature with a high formal analogy with the nature of the molecular thermo-barodiffusion effect [20]. In the process of molecular thermo-barodiffusion, a diffusive separation flow of molecules with high fluctuation velocity is formed in the medium region, providing the possibility of fluctuations of molecules at large free path length. Molecules having a small velocity of chaotic movements are moved by the flow of separation in the medium region, in which the conditions for fluctuations of molecules at a small free path length are formed.

Under conditions of rapid shear deformation of granular medium in steady flow on a rough gravity chute, a zone with maximum values of solid phase fraction is formed in the central part of the bed. The size of the zone and the values of the solid phase fraction in it depend on the thickness of the bed and the value of the chute angle to the horizon. In this flow zone with the lowest values of the void fraction, conditions are created for the movement of particles inclined to quasi-diffusion with low velocity and amplitude of fluctuations. Consequently, according to the dependence of the fluctuation rate on the diameter and mass of particles ($V_i' \approx k d_i^2 m_i^{-1}$), conditions for quasi-diffusive fluctuations of particles with large mass are created in the central zone of the flow. At the same time, particles with small masses, which acquire large fluctuation velocities during collisions, participate in quasi-diffusive movements with large amplitude of oscillations and are displaced to the peripheral region of the flow, where conditions for fluctuations of particles with large free path length are formed.

4.2. Modeling of kinetics of quasi-diffusion separation process

This section of the paper presents variants of a mathematical model of quasi-diffusive separation by size and density for two idealized conditions of interaction of cohesionless spherical particles under rapid shear deformation of a granular medium with high structural nonuniformity. The analyzed conditions of particle interaction are of decisive importance in estimating the frequency of their collisions. In contrast to the previously presented studies [7, 13, 18], the present paper presents a comparative analysis of the variants of modeling the contact interaction of particles with the involvement of experimentally obtained information.

Variants of contact quasi-diffusion interaction of particles under conditions of rapid shear deformation are analyzed using the example of [13] of steady-state shear flow of a mixture of two components (components 1 and 2) having particles of diameter d_1 and d_2, density ρ_1, ρ_2, and mass m_1, m_2, with their concentration in the mixture c and $1-c$, respectively. The mixture of particles is subjected to rapid shear deformation in the shear direction x (Fig. 4). It is assumed that under the action of a set of variable factors (deformation rate du/dy and lithostatic pressure), structural nonuniformity of the flow occurs, expressed in an increase in the fraction of voids in the y direction.

It is assumed that under conditions of steady-state shear flow of particles, the convection mechanism of transfer dominates in the process of their mixing in the direction of the shear. In the y direction, perpendicular to the direction of the shear, nonuniform particles change their position in the flow due to the manifestation of quasi-diffusion effects of particle interaction, accompanied by their mixing and separation.

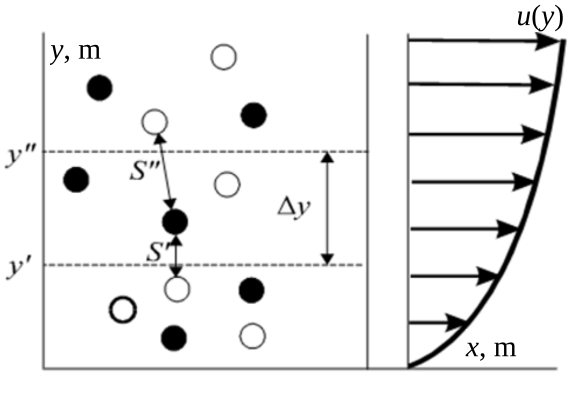

Fig. 4. To the mechanism illustration and formulation of kinetic regularities of quasi-diffusive separation by size and density due to structural nonuniformity of shear flow of particles

The latter assumption allows us to analyze the quasi-diffusive interaction of nonuniform particles in a fast shear flow under conditions of inhomogeneity of its structural and kinematic parameters, neglecting the effect of separation (segregation) due to the relaxation of stress concentrators. It should be noted that such conditions occur at high values of the void fraction ($\varepsilon \geq 0.75$), and in accordance with most physical mechanisms, segregation is a consequence of relaxation of contact stresses during the interaction of nonuniform particles in the flow.

In the process of analysis, an elementary layer bounded by the coordinates y' and y''. The surfaces bounding the layer are perpendicular to the y axis, and the layer thickness Δy satisfies the condition $\Delta y = y'' - y' << 2s$, where s is the distance between particles averaged over the volume of the layer [13].

The relative rate of quasi-diffusion of nonuniform particles $q_{\rm rel}$ necessary for the expression of the separation flux is determined under the condition $c(y)$ = const within the selected layer and the gradient of the quasi-diffusion transfer potential equal to 1. In accordance with the kinetic theory [20], the indicated flux is expressed in the following form:

$$q_{\rm rel} = 0.33(V_1' l_1 - V_2' l_2), \tag{4}$$

where V_i' and l_i are the fluctuation velocity and the path length of particles of the i-th component, respectively.

The formulation of relations describing the kinetic regularities of quasi-diffusive separation is obtained by analyzing the quasi-diffusive particle interaction under two variants of assumptions.

The first assumption [13] is that the fluctuation velocities of the particles are so large that they significantly exceed the mean value of their relative velocity Δu in the shear direction, i.e. $\overline{V}' >> \Delta u$, where $\Delta u = (\partial u / \partial y)\Delta y$. Under this assumption, conditions for the dominance of binary particle collisions are formed in the shear flow, which allows us to express the average value of the particle fluctuation velocity V_i' of the i-th component by the law of conservation of momentum. Using the average values of physical and mechanical characteristics and kinematic parameters of particles in the volume of the elementary layer, the following relation is obtained:

$$V_i' = \overline{V'}\,\frac{\overline{m}(c)}{m_i}, \tag{5}$$

where $\overline{m}(c)$ is average mass of particles in the volume of the layer. The average particle velocity fluctuations $\overline{V'}$ in the volume of the elementary layer is determined by multiplication of the average values of the particle collision frequency $\overline{F}$ and the distance *s* between them in a hypothetically uniform medium

$$\overline{V'} = \overline{F}\, s\,. \tag{6}$$

The collision frequency $\overline{F}$ is calculated based on the law of conservation of energy, which is generated during shear deformation and dissipated by dissipation effects during particle collision, using the combined oblique impact hypothesis [7].

In accordance with assumption 1 and taking into account dependences (5) and (6), the average amplitude of chaotic displacements of a particle of *i*-type under specific conditions of its contact is determined by the following expression:

$$l_i = s\frac{V_i'}{\overline{V}}\left(\frac{\overline{d}}{d_i}\right)^2 = \frac{\overline{V'}}{\overline{F}}\frac{\overline{m}(c)}{m_i}\left(\frac{\overline{d}}{d_i}\right)^2, \tag{7}$$

where $\overline{d} = cd_1 + (1-c)d_2$ is mean value of particle diameter.

The relative rate of diffusive transport of nonuniform particles, taking into account expressions (4) – (7), can be expressed in the following form

$$q_{\text{rel}} = \frac{\left(\overline{m}(c)\overline{V'}\right)^2}{2\overline{F}}\left(\left(\frac{\overline{d}}{m_1 d_1}\right)^2 - \left(\frac{\overline{d}}{m_2 d_2}\right)^2\right). \tag{8}$$

The change in the concentration of particles of the *i*-th type in the elementary layer of thickness Δy under $c(y) = \text{const}$ will be determined only by the spatial inhomogeneity of the conditions directly affecting the direction and intensity of the transverse quasi-diffusive transport of particles in the shear flow. Since these conditions are fully determined by the nonuniformity of the microstructure of the medium, and according to (4) the most relevant characteristic of the microstructure is the distance between the particles, it is reasonable to express the driving force of quasi-diffusive separation as a relative value of the gradient of the distance between the particles in the *y* direction of quasi-diffusion.

Using an appropriate partial derivative, the driving force of quasi-diffusive separation is formulated as [13]:

$$\frac{\Delta s}{s\Delta y} \cong \frac{1}{s}\frac{\partial s}{\partial y} = \frac{\partial \ln s}{\partial y}. \tag{9}$$

Since the right part of expression (8) has a physical meaning of the quasi-diffusive separation coefficient (migration coefficient [13]) D_m, the value of its flux per unit surface area perpendicular to the separation direction can be expressed in the following form

$$q(m) = \text{c}\rho\frac{\left(\overline{m}(c)\overline{V'}\right)^2}{2\overline{F}}\left(\left(\frac{\overline{d}}{m_1 d_1}\right)^2 - \left(\frac{\overline{d}}{m_2 d_2}\right)^2\right)\frac{\partial \ln \text{s}}{\partial y} =$$

$$= \text{c}\rho D_m \frac{\partial \ln \text{s}}{\partial y}\,. \tag{10}$$

The second assumption concerning the determination of the conditions of quasi-diffusive interaction of particles assumes that the relative velocity of particles in the shear direction essentially exceeds the velocity of their fluctuations $\Delta u >> \overline{V'}$, i.e., under this assumption, the collision of particles occurs with a frequency that depends on their relative velocity, particle properties, and the distance between them. In this case, the dependence of the frequency of collision of particles on the velocity of their fluctuations is negligibly small. As a consequence, the collision frequency is in direct dependence on the relative velocity of particles Δu and is proportional to d^2, and the free path length of particles negligibly little depends on the velocity of their fluctuations. Thus, according to the second variant of the assumption, the free path length is the same for all particles of the mixture and is equal to the average distance between them.

Taking into account the peculiarities of this assumption, the particle fluctuation velocity V_i' of the *i*-th component is determined on the basis of the law of conservation of momentum as a function of the averaged value of the fluctuation velocity of particles of the mixture under constrained conditions of particle collision, in which the total momentum acting on a particle is proportional to its surface and inversely proportional to its mass:

$$V_i' = \overline{m}(c)\overline{V'}m_i^{-1}(d_i/\overline{d})^2\,. \tag{11}$$

According to this assumption, the amplitude of fluctuations is invariant for all particles of the mixture and corresponds to the average value of the distance between them

$$l_i = \overline{l} = s. \tag{12}$$

Taking into account relations (11) and (12), the kinetic coefficient of quasi-diffusive separation caused by mutual quasi-diffusive transfer of nonuniform particles in the shear flow of granular medium under conditions of its structural nonuniformity is expressed [13] in the following form

$$D_m = \frac{\overline{m}(c)(\overline{V}')^2}{2\overline{F}}\left(\frac{d_1^2}{m_1\overline{d}^2} - \frac{d_2^2}{m_2\overline{d}^2}\right). \qquad (13)$$

Obviously, regardless of the version of assumption, the flow intensity of quasi-diffusive separation by size and density in a fast shear flow of particles is determined according to the kinetic dependence (10). The transition from one assumption to another one is carried out by changing the dependence to calculate the process kinetic coefficient. When using the first variant of the assumption, the separation coefficient is calculated according to expression (8), and the second assumption is realized when determining the separation coefficient using the calculation dependence (13).

4.3. Modeling the dynamics of size and density separation under conditions of structural nonuniformity of fast gravitational particle flows

The results of the analysis of the mechanism and kinetics of quasi-diffusive separation were used in mathematical modeling of the dynamics of separation by size and density in a fast gravitational flow of particle mixtures (Table 1) on a rough chute. The modeling was performed using the general mass transfer equation [21], transformed to the specifics of the problem to be solved. In [5, 6, 10, 12, 22], the basic mass transfer equation was adapted to predict the evolution of the particle concentration field of a test component in a gravity flow. In the adapted version, the equation describes the concentration field of particles of the test component with reference to its fluxes of convection, quasi-diffusive mixing and separation in accordance with one of the segregation mechanisms due to the local nonuniformity of the granular medium under gravity flow conditions. According to the results of the analysis, when modeling the separation in gravity flows with high structural nonuniformity, a term is introduced into the equation describing the dynamics of the process, given the kinetics of quasi-diffusive separation (10), which is a consequence of the spatial nonuniformity of the structural characteristics of the flow. After the corresponding addition, the equation of separation dynamics [7, 13, 18] is obtained in the following form

$$\frac{\partial(c\rho)}{\partial t} = -\frac{\partial(uc\rho)}{\partial x} +$$

$$+\frac{\partial}{\partial y}\left[\rho\left(D_{\text{dif}}\frac{\partial c}{\partial y} - cD_m\frac{\partial \ln s}{\partial y} - K_S c\Delta M\right)\right], \qquad (14)$$

where $D_{\text{dif}} = 1/3s\overline{V'}$ is quasi-diffusion mixing coefficient [7, 18].

When modeling the dynamics of the separation process in a gravitational particle flow, equation (14) is integrated numerically using the Crank-Nicholson finite-difference scheme [23]. When solving the equation, the initial condition is set as corresponding to a homogeneous distribution of mixture components in the volume of the bed $c(0,x,y) = c_0$, where c_0 is the average concentration of particles of the test component in the mixture. The boundary conditions are set in the form of relations governing the homogeneous distribution of mixture components on entering the bed ($c(t,0,y) = c_0$) and the absence of particle flows through the free surface ($y = h$) and the bottom of the bed ($y = 0$)

$$D_{\text{dif}}\frac{\partial c}{\partial y} = cD_m\frac{\partial \ln s}{\partial y} = K_s c\Delta M\Big|_{y=0,h} = 0. \qquad (15)$$

A preliminary evaluation of the predictive properties of equation (14) allows us to note that the kinetic coefficients of the quasi-diffusion effects of separation D_m and mixing D_{dif}, as well as the driving force of shear flow segregation ΔM, are analytically determined. The only kinetic parameter in the equation that requires experimental determination is the segregation kinetic coefficient K_S. According to the method described in [19], the segregation coefficient K_S is determined experimentally as the velocity of the test particle during its transverse motion in the shear flow, referred to the driving segregation force ΔM. Approbation of the method has shown that the K_S coefficient obtained using it exhibits the properties of a kinetic constant with respect to a certain mixture of particles in a sufficiently wide range of their properties and structural and kinematic characteristics of the flow [18, 19]. The analysis of equation (14) indicates its sufficiently high predictive capabilities, allowing us to model the dynamics of separation by size and density using only one experimental coefficient.

When modeling the $c(y)$ concentration profiles of test particles in mixtures 1–3 (Table 1) on a rough chute, experimental information on the structural and kinematic characteristics of the flows, obtained as profiles of the void fraction $\varepsilon(y)$ and velocity in the shear direction $u(y)$, was used as input data. The experimental profiles $u(y)$ and $\varepsilon(y)$, as well as the profiles of the concentration of test particles $c(y)$, necessary to evaluate the adequacy of the modeling results, were obtained using the method and experimental unit described in the section "Research methods and model materials".

Figures 5–7 show the results of different variants of mathematical modeling of profiles of concentration distribution profiles of test particles in binary mixtures 1–3 (Table 1) in comparison with experimentally obtained profiles. Mathematical modeling was carried out at different variants of determination of the quasi-diffusion separation coefficient in order to analyze the predictive properties of variants and the significance of the corresponding flux in the separation process.

The analysis of modeling options (Fig. 5) shows that the calculation of the quasi-diffusive separation coefficient using assumption 1 ($\overline{V}' >> \Delta u$) in accordance with dependence (8) does not provide adequate modeling of the concentration distribution profile.

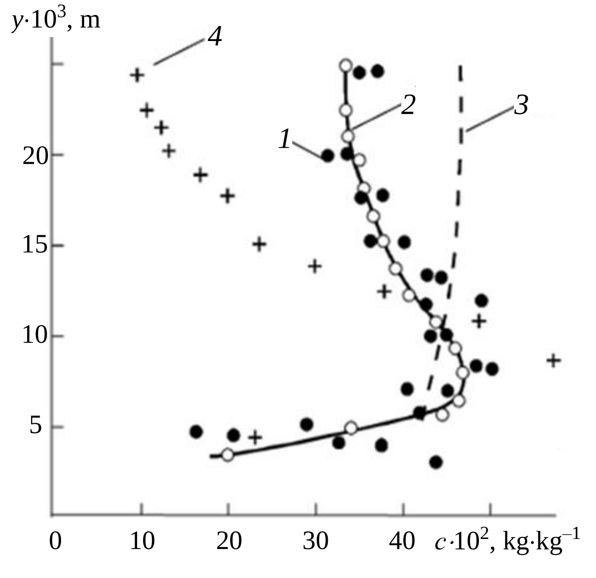

Fig. 5. Concentration profiles of large particles in the flow of mixture *1* (Table 1) on a rough gravity chute, obtained by experimental *1* and analytical *2–4* methods, under different variants of determining the quasi-diffusion separation factor D_m: 2) calculation under assumption (2) in accordance with (13); 3) calculation under $D_m = 0$; 4) calculation under assumption (1) in accordance with (8)

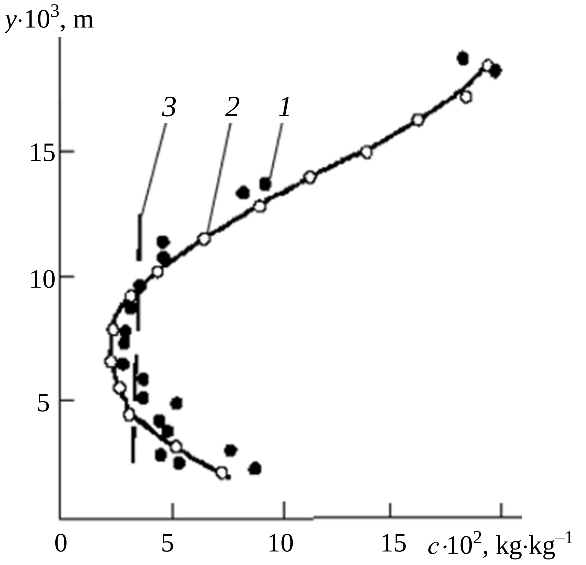

Fig. 6. Experimental *1* and calculated *2* and *3* profiles of concentration distribution of low density particles in the flow of mixture 2 (Table 1) on a rough gravity chute at different variants of determination of quasi-diffusion separation coefficient: 2) calculation under assumption (2) in accordance with (13); 3) calculation under $D_m = 0$

The inadequacy of the modeling option under assumption 1 is also revealed when modeling the separation dynamics in mixtures 2 and 3 in terms of density and complex particle size and density differences.

On the contrary, the use of the second variant of the assumption in modeling, based on the assumption of the dominant role in the process of impact interaction of particles of their relative shear velocity ($\Delta u >> \overline{V}'$), provides adequate results. This is clearly confirmed by comparing the calculated concentration profiles obtained using the second assumption for all types of mixtures (curves *2* in Figs 5–7) with the experimentally obtained concentration distributions of test particles. The adequacy of the calculated results was confirmed at a significance level of 5 % using Fisher's F-criterion to evaluate the ratio of adequacy and reproducibility dispersions.

As a result of analyzing the set of experimental and calculated concentration profiles of cohesionless particles in thin-bed gravity flows (Figs. 5–7), it is possible to conclude that under the influence of structural nonuniformity of flows the effect of quasi-diffusive separation by size and density, which significantly affects the distribution of nonuniform particles, is manifested. This conclusion is confirmed by comparing the calculated concentration profiles obtained considering the quasi-diffusive separation

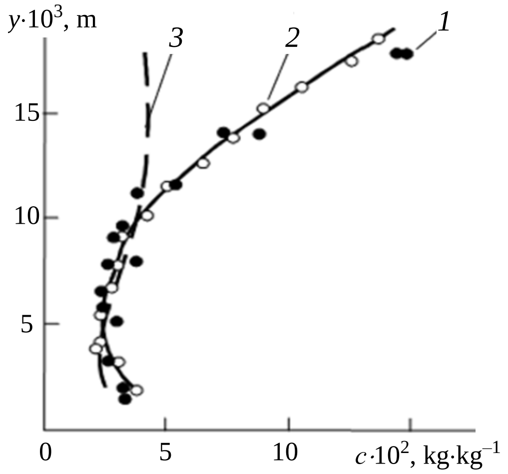

Fig. 7. Experimental *1* and calculated *2* and *3* profiles of concentration distribution of particles with small mass in the flow of mixture 3 (Table 1) on a rough gravity chute at different variants of determination of the quasi-diffusion separation coefficient: 2) calculation under assumption (2) according to (13); 3) calculation at $D_m = 0$

effect (curves *2*) and in the absence of this effect ($D_m = 0$) (curves *3*). In this case, a quasi-diffusive segregation flow is formed due to spatial inhomogeneity of structural and kinematic parameters of the flow, which can dominate over the flow of shear flow segregation, which is a consequence of relaxation of local stress concentrators.

To evaluate the predictive properties of the mathematical model of separation based on equation (14), it is important to note that the concentration profiles of test particles for mixtures 2 and 3, which differ in the disperse composition of components of different densities, are obtained at an invariant value of the kinetic segregation coefficient K_S. Thus, the mathematical model provides the possibility of predicting the distribution of nonuniform in size and density cohesionless spherical particles in gravity flow with high inhomogeneity of structural and kinematic characteristics using a single experimental kinetic parameter.

The determining role of quasi-diffusive separation in accordance with its mechanism under the second variant of the assumption ($\Delta u >> \overline{V}'$) is confirmed by a large number of studies, e.g. [7, 13, 18], performed with mixtures of particles differing in a complex of properties in fast gravity flows in a wide range of flow parameters. However, at the same time, individual cases have been noted, indicating that in special flow conditions of a certain type of granular matter it is reasonable to describe the kinetics of quasi-diffusive separation using the first variant of the assumption.

Figure 8 shows the calculated profiles (curves *2*(1) and *2*(2)) of the concentration distribution of small particles in the mixture of glass bead fractions in a fast gravity flow. When modeling profile *2*(1) in the upper rarefied zone of the flow ($\varepsilon \geq 0.75$), the quasi-diffusive separation coefficient D_m is calculated by (8) (according to the first version of the assumption) and by (13) (according to the second version of the assumption) in the rest of the flow volume. In the modeling of profile 2(2), the quasi-diffusive separation coefficient D_m is calculated by (13) (according to the second version of the assumption) in the whole flow volume. The simulation results (curves *2*(1) and *2*(2)) are presented in comparison with the experimental concentration distribution profile (curve *1*). Comparison of modeling variants (Fig. 8) shows that within the analyzed object adequate modeling of quasi-diffusive separation in a rarefied flow region at the void fraction above 0.75 is provided using the hypothesis of fluctuation velocity ($\overline{V}' >> \Delta u$)dominance in relative particle movements according to the first variant of the assumption. This can be explained by presumably very low effects of dissipation of kinetic energy at collision of glass beads particles (high restitution coefficient and low friction coefficient) in the rarefied region of the shear flow "cloud" at low gradient of particle velocity in the shear direction.

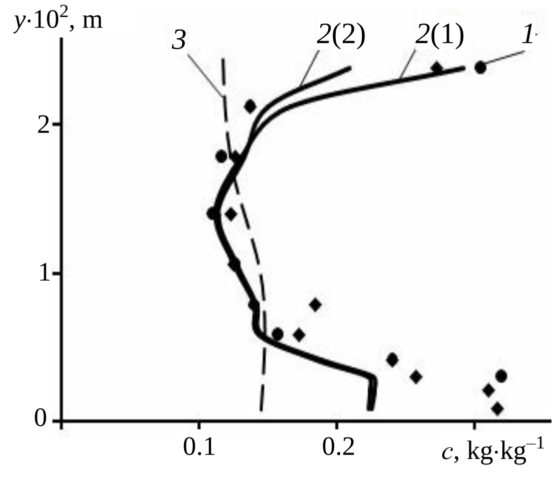

Fig. 8. Concentration profiles of glass beads particles of fine fraction (+2.5–3.0) mm in mixture with coarse fraction (+3.25–3.5) mm under gravitational flow on rough chute: *1* – experimental; *2*, *3* – calculated at different variants of determination of quasi-diffusion separation coefficient D_m : *2*(1) calculation at the first variant of assumption according to (8); *2*(2) calculation at the second variant of assumption according to (13); 3) calculation at $D_m = 0$

Obviously, under the action of turbulent pulsations occurring in the flow core and at low intensity of the effects of dissipation of kinetic energy in binary particle collisions in the flow "cloud", the conditions corresponding to the first variant of the assumption ($\overline{V}' >> \Delta u$)can be fulfilled.

The analyzed mechanism of quasi-diffusion separation enables to explain the physical nature of some paradoxical effects that were found in the experimental study of failure zones formed in the process of shear deformations of mixtures of granular matter in the annular shear cell and can be taken into account when organizing the processes of preparing mixtures of composite materials and their structuring [24, 25]. For example, according to the authors of [12], the mysterious behavior of mustard seeds in the shear flow of their mixture with bead granules is probably explained by the formation of shear flows with large gradients of shear strain rate and, accordingly, the fraction of voids in the flow volume between its core and the cell walls. Under conditions of void fraction gradients, mutual movement of mustard seeds and glass particles will occur under the effect of quasi-diffusive separation. Less massive mustard seeds will move in the direction of the void fraction gradient toward the cell walls while heavy glass particles will move toward the center of the failure zone. Due to the quasi-diffusion effect, mustard seeds are distributed in the near-wall zones of the cell with replacement of the denser glass particles into the core of the shear flow. For a more convincing explanation of the extraordinary separation effects, detailed experimental information on the structural characteristics in the shear flow volume in the annular cell is required.

5. Conclusion

The physical nature and mechanisms of quasi-diffusive separation of cohesionless spherical particles with a complex difference in size and density in fast shear flows with high inhomogeneity of structural and kinematic parameters have been analyzed. It is established that in the conditions of thin-bed fast gravitational flows on a rough chute the determining role in the formation of quasi-diffusive separation flow belongs to the character of structural nonuniformity of the flow. The analysis of kinetic regularities of the quasi-diffusive separation process in alternative conditions of quasi-diffusive interaction of particles in a fast shear flow, which are characterized by the dominance of either the velocity of chaotic fluctuations of particles or their relative velocity in the shear direction.

The results of experimental and analytical study show that the intensity of quasi-diffusive separation flow is in direct dependence on the particle collision frequency. It is established that in the general case of steady fast gravitational flow of granular matter on a rough chute, the collision frequency is determined by the dominant value of the component of the relative shear velocity of particles and depends to a lesser extent on the velocity of their chaotic fluctuations. At the same time, under conditions of fast gravitational flow of smooth elastic spherical particles in the region of the "cloud" of particles near the open surface of the flow, the frequency of particle collisions can be determined at the dominant value of the velocity of their fluctuations. It has been established that in thin-bed fast gravitational flows quasi-diffusive separation due to spatial structural nonuniformity of the flow can dominate over segregation as a manifestation of the effect of local nonuniformity of the shear flow.

6. Funding

The study was supported by the RFBR grant No. 09-08-97521.

7. Conflict of interests

The authors declare no conflict of interests.

References

1. Nagel SR. Experimental soft-matter science. *Reviews of Modern Physics*. 2017;89(2):025002. DOI:10.1103/RevModPhys.89.025002
2. Forterre Y, Pouliquen O. Flows of dense granular media. *Annual Review of Fluid Mechanics*. 2008;40(1):1-24. DOI:10.1146/annurev.fluid.40.111406.102142
3. Shen HH, Ackermann NL. Constitutive relationships for fluid-solid mixtures. *Journal of Engineering Mechanics-ASCE*. 1982;108(5):748-763. DOI:10.1061/JMCEA3.0002868
4. Campbell CS. Granular material flows – an overview. *Powder Technology*. 2006;162(3):208-229. DOI:10.1016/j.powtec.2005.12.008
5. Duan Y, Peckham J, Umbanhowar PB, Ottino JM, et al. Designing minimally segregating granular mixtures for gravity-driven surface flows. *AIChE Journal*. 2023;69(4): e18032. DOI:10.1002/aic.18032
6. Duan Y, Umbanhowar PB, Ottino JM, Lueptow RM. Modelling segregation of bidisperse granular mixtures varying simultaneously in size and density for free surface flows. *Journal of Fluid Mechanics*. 2021;918:A20. DOI:10.1017/jfm.2021.342
7. Dolgunin VN, Kudi AN, Tuev MA. Mechanisms and kinetics of gravity separation of granular materials. *Physics-Uspekhi*. 2020;63(6):545-561. DOI:10.3367/UFNe.2020.01.038729
8. Hill KM, Fan Y. Granular temperature and segregation in dense sheared particulate mixtures. *KONA Powder and Particle Journal*. 2016;33:150-168. DOI:10.14356/kona.2016022

9. Savage SB. Granular flows down rough inclines – review and extension. In: *Studies in Applied Mechanics*. Elsevier; Vol. 7, 1983. p. 261-282.

10. Gray JMNT, Thornton AR. A theory for particle size segregation in shallow granular free-surface flows. *Proceedings of the Royal Society A: Mathematical, Physical and Engineering Sciences*. 2005;461(2057):1447-1473. DOI:10.1098/rspa.2004.1420

11. Goldhirsch I. Rapid granular flows. *Annual Review of Fluid Mechanics*. 2003;35:267-293. DOI:10.1146/annurev.fluid.35.101101.161114

12. Stephens DJ, Bridgwater J. The mixing and segregation of cohesionless particulate materials. Part I. Failure zone formation. *Powder Technology*. 1978;21(1):17-28. DOI:10.1016/0032-5910(78)80104-1

13. Stephens DJ, Bridgwater J. The mixing and segregation of cohesionless particulate materials. Part II. Microscopic mechanisms for particles differing in size. *Powder Technology*. 1978;21(1):29-44. DOI:10.1016/0032-5910(78)80105-3

14. Dolgunin VN, Kudy AN, Ukolov AA. Development of the model of segregation of particles undergoing granular flow down an inclined chute. *Powder Technology*. 1998;96(3):211-218. DOI:10.1016/S0032-5910(97)03376-7

15. Bagnold RA. Experiments on a gravity-free dispersion of large solid spheres in a Newtonian fluid under shear. *Proceedings of the Royal Society of London. Series A. Mathematical and Physical Sciences*. 1954;225(1160):49-63. DOI:10.1098/rspa.1954.0186

16. Khakhar DV, McCarthy JJ, Ottino JM. Radial segregation of granular mixtures in rotating cylinders. *Physics of Fluids*. 1997;9(12):3600-3614. DOI:10.1063/1.869498

17. Hill KM, Tan DS. Segregation in dense sheared flows: gravity, temperature gradients, and stress partitioning. *Journal of Fluid Mechanics*. 2014;756:5488. DOI:10.1017/jfm.2014.271

18. Gray JMNT, Chugunov VA. Particle-size segregation and diffusive remixing in shallow granular avalanches. *Journal of Fluid Mechanics*. 2006;569:365. DOI:10.1017/S0022112006002977

19. Dolgunin VN, Kudi AN, Tarakanov AG. Structural inhomogeneity and effects of separation by size and density in gravity flow of granular materials. *Journal of Engineering Physics and Thermophysics*. 2022;95(2):484-494. DOI:10.1007/s10891-022-02505-y

20. Dolgunin VN, Ukolov AA, Ivanov OO. Segregation kinetics in the rapid gravity flow of granular materials. *Theoretical Foundations of Chemical Engineering*. 2006;40(4):393-404. DOI:10.1134/S0040579506040099

21. Ferziger JH, Kaper HG. *Mathematical theory of transport processes in gases*. Amsterdam: North-Holland Publ. house; 1972. 606 p.

22. Lykov AV. *Heat and mass transfer: reference book*. Moscow: Energy; 1978. 480 p. (In Russ.)

23. Gray JMNT. Particle segregation in dense granular flows. *Annual Review of Fluid Mechanics*. 2018;50(1):407-433. DOI:10.1146/annurev-fluid-122316-045201

24. Marchuk GI. *Methods of numerical mathematics*. New York: Springer; 1975. 510 p.

25. Klyuev AV, Kashapov NF, Klyuev SV, Zolatareva SV, et al. Experimental studies of the processes of structure formation of composite mixtures with technogenic mechanoactivated silica component. *Stroitel'nye Materialy i Izdeliya = Construction Materials and Products*. 2023;6(2):5-18. DOI:10.58224/2618-7183-2023-6-2-5-18 (In Russ.)

26. Klyuev AV, Kashapov NF, Klyuev SV, Lesovik RV, et al. Development of alkali-activated binders based on technogenic fibrous materials. *Stroitel'mye Materialy i Izdeliya = Construction Materials and Products*. 2023;6(1):60-73. DOI:10.58224/2618-7183-2023-6-1-60-73 (In Russ.)

Information about the authors / Информация об авторах

Viktor N. Dolgunin, D. Sc. (Eng.), Professor, Tambov State Technical University (TSTU), Tambov, Russian Federation; ORCID 0000-0002-6227-5224; e-mail: dolgunin-vn@yandex.ru

Andrey N. Kudi, D. Sc. (Eng.), Associate Professor, TSTU, Tambov, Russian Federation; Scopus ID 6504451028; e-mail: andrey.kudi@bk.ru

Andrey A. Zhilo, Postgraduate Student, TSTU, Tambov, Russian Federation; ORCID 0000-0001-5033-8315; e-mail: zhilo97@mail.ru

Konstantin A. Kudi, Line Manager, PJSC “MTS Bank”, Moscow, Russian Federation; ORCID 0009-0009-5068-2234; e-mail: kostya.kudi@mail.com

Vasily A. Pronin, Cand. Sc. (Eng.), Associate Professor, TSTU, Tambov, Russian Federation; ORCID 0000-0002-1507-2969, e-mail: ua3rbs65@mail.ru

Долгунин Виктор Николаевич, доктор технических наук, профессор, Тамбовский государственный технический университет (ТГТУ), Тамбов, Российская Федерация; ORCID 0000-0002-6227-5224; e-mail: dolgunin-vn@yandex.ru

Куди Андрей Николаевич, доктор технических наук, доцент, ТГТУ, Тамбов, Российская Федерация; Scopus ID 6504451028; e-mail: andrey.kudi@bk.ru

Жило Андрей Андреевич, аспирант, ТГТУ, Тамбов, Российская Федерация; ORCID 0000-0001-5033-8315; e-mail: zhilo97@mail.ru

Куди Константин Андреевич, руководитель направления, ПАО «МТС-Банк», Москва, Российская Федерация; ORCID 0009-0009-5068-2234; e-mail: kostya.kudi@mail.com

Пронин Василий Александрович, кандидат технических наук, доцент, ТГТУ, Тамбов, Российская Федерация; ORCID 0000-0002-1507–2969, e-mail: ua3rbs65@mail.ru

Received 25 September 2024; Accepted 31 October 2024; Published 20 December 2024

Journal of Advanced Materials and Technologies. Vol. 9, No. 4. 2024

Review
Advanced structural materials, materials for extreme conditions

УДК 537.533 DOI: 10.17277/jamt.2024.04.pp.312-325

Desorption of gases from cathode materials in electrovacuum devices during the production process

© Anastasia V. Parashchuk[a]✉, Evgeniy P. Sheshin[a], Aleksey V. Shumanov[b]

[a]*Moscow Institute of Physics and Technology, 9, Institutsky Ln., Dolgoprudny, 141701, Russian Federation,*
[b]*Pluton JSC, 11, Nizhnyaya Syromyatnicheskaya St., Moscow, 105120, Russian Federation*

✉ parashchuk.av@mipt.ru

Abstract: Desorption of gases from cathode materials in electrovacuum devices (EVDs) is one of the key problems in the production process, which has a significant impact on the performance and durability of devices such as magnetrons, X-ray tubes and vacuum amplifiers. For example, cleaning the surfaces of EVD parts during production inevitably entails their reactions with air components after extraction from the processing zone, and the process of degassing heating during pumping often contributes to an additional complication of the structure and chemical composition of the surface layer, since impurities diffusing to the surface can cause the appearance of new substances. Therefore, even when choosing cathode materials or parts of internal fittings, EVDs are guided by the ability of the material to quickly remove gases, maintain strength at high temperatures and have high chemical resistance. The present paper is a detailed analysis of modern methods of desorption acceleration, the mechanisms of this process and their computational basis, including known physical laws and models of adsorption and desorption. Promising approaches to improving the quality of cathodes at different stages of their production, with an emphasis on the use of new materials and technologies, are evaluated. Calculations confirming the effectiveness of the proposed solutions are analyzed, as well as the influence of various factors on minimizing the impact of desorption processes and increasing the durability of cathodes in EVDs.

Keywords: desorption; cathode materials; thermal desorption; vacuum technologies; gas release; electro-vacuum devices; pumping; emission properties; ion purification; desorption kinetics.

For citation: Parashchuk AV, Sheshin EP, Shumanov AV. Desorption of gases from cathode materials in electrovacuum devices during the production process. *Journal of Advanced Materials and Technologies*. 2024;9(4):312-325. DOI: 10.17277/jamt.2024.04.pp.312-325

Десорбция газов из материалов катодов в электровакуумных приборах в процессе производства

© А. В. Паращук[a]✉, Е. П. Шешин[a], А. В. Шуманов[b]

[a] *Московский физико-технический институт (национальный исследовательский университет),*
Институтский пер., 9, Долгопрудный, 141701, Российская Федерация,
[b] *АО «Плутон», ул. Нижняя Сыромятническая, 11, Москва, 105120, Российская Федерация*

✉ parashchuk.av@mipt.ru

Аннотация: Десорбция газов из материалов катодов в электровакуумных приборах (ЭВП) является одной из ключевых проблем в процессе производства, оказывающей существенное влияние на производительность и долговечность таких устройств, как магнетроны, рентгеновские трубки и вакуумные усилители. К примеру, очищение поверхностей деталей ЭВП в процессе производства неизбежно влечет за собой их реакции с компонентами воздуха после извлечения из зоны обработки, а процесс обезгаживающего нагрева во время откачки нередко способствует дополнительному усложнению структуры и химического состава поверхностного слоя, поскольку примеси, диффундирующие к поверхности, могут вызвать появление новых веществ. Поэтому даже при выборе материалов катодов, деталей внутренней арматуры ЭВП руководствуются способностью материала быстро удалять газы, сохранять прочность при высоких температурах и обладать высокой химической устойчивостью. Приведен подробный анализ современных методов ускорения десорбции, механизмов этого процесса и их расчетных основ, включая известные физические законы и модели адсорбции и десорбции.

Оценены перспективные подходы к улучшению качества катодов на разных этапах их производства, с акцентом на использование новых материалов и технологий. Проанализированы расчеты, подтверждающие эффективность предложенных решений, а также влияние различных факторов на минимизацию влияния процессов десорбции и повышение долговечности катодов в ЭВП.

Ключевые слова: десорбция; материалы катодов; термодесорбция; вакуумные технологии; газовыделение; электровакуумные приборы; откачка; эмиссионные свойства; ионная очистка; кинетика десорбции.

Для цитирования: Parashchuk AV, Sheshin EP, Shumanov AV. Desorption of gases from cathode materials in electrovacuum devices during the production process. *Journal of Advanced Materials and Technologies*. 2024;9(4):312-325. DOI: 10.17277/jamt.2024.04.pp.312-325

1. Introduction

The production of vacuum tubes is one of the most complex industries. This is due to the fact that the stability of the electrovacuum device (EVD) depends not only on the preservation of the shape and condition of the parts, the choice of materials, the appropriate technology for their processing and compliance with the entire technological process of manufacturing the device. Fulfillment of the conditions of mechanical precision of manufacture and assembly does not guarantee durability and manufacturability due to the processes of material desorption during the technochemical stages of production and further operation or storage of EVDs. In particular, the materials of electrodes, which ensure the correct functioning of the device, are subject to desorption or spraying.

During various stages of production, a layer of the gas phase inevitably forms on the surface of cathodes. During degassing heating during pumping out EVDs, the structure of oxide films and adsorbed impurities becomes more complex, often changing its chemical composition due to diffusing elements from the volume of materials. This can lead to significant changes in the emission properties of the cathode, contamination of the vacuum environment and complete failure of the device. Therefore, one of the main production tasks is to remove chemically adsorbed gases and impurities such as hydrogen, oxygen and hydrocarbons from the cathode surface. The materials used in production are assessed by their ability to quickly remove gases, low vapor pressure, strength at high temperatures, thermal expansion coefficient, thermal conductivity, electrical conductivity, high insulation resistance even at high temperatures and chemical resistance. The purity of the material also plays a decisive role, since even small impurities can significantly affect the performance characteristics and service life of devices. In particular, when the vacuum conditions in instantaneous magnetrons deteriorate from 10^{-8} to 10^{-7} mm Hg, the current density from the field emission cathode decreases from 7.0 to 5.6 $mA\cdot cm^{-2}$ (Fig. 1) [1]. The use of materials with a minimum gas content can be attributed to the mandatory requirements for the materials of EVD parts, since maintaining low pressure in the vacuum

In recent years, research in the field of adsorption and desorption phenomena on EVD cathodes has focused on understanding the physicochemical processes occurring on the surface and inside the cathode material, as well as on developing new methods for controlling these processes in order to improve the efficiency and stability of devices [2–4]. Thus, modern studies emphasize the importance of not only the chemical nature of adsorption, but also its kinetic aspects. For example, experiments using various spectroscopy methods allow observing changes in the surface states of cathodes in real time when exposed to a gas environment [5]. This helps to refine the interaction models and optimize the operating conditions of devices to minimize the negative impact of desorption. Another important aspect of recent research is related to the effect of adsorption on the emission properties of cathodes [6]. Especially it is noticed in the context of high-precision and highly sensitive applications, where even small changes in the emission level can significantly affect the operation of the device. Studies show that adsorbed layers can cause temporary or permanent changes in the function of the cathode, which requires the development of specialized coatings or evacuation methods to eliminate or minimize this effect. At the same time, promising solutions related to the development of new materials and modifications of cathode surfaces by forming protective layers are increasingly being proposed.

The purpose of this review is to comprehensively analyze modern approaches to gas desorption processes from cathode materials used in vacuum tubes with an emphasis on increasing their durability and performance characteristics. The review covers the latest advances in heat treatment, radiation and electron exposure, and the use of nanomaterials, providing an interdisciplinary approach to solving desorption problems. Particular attention is paid to theoretical models based on Fick's

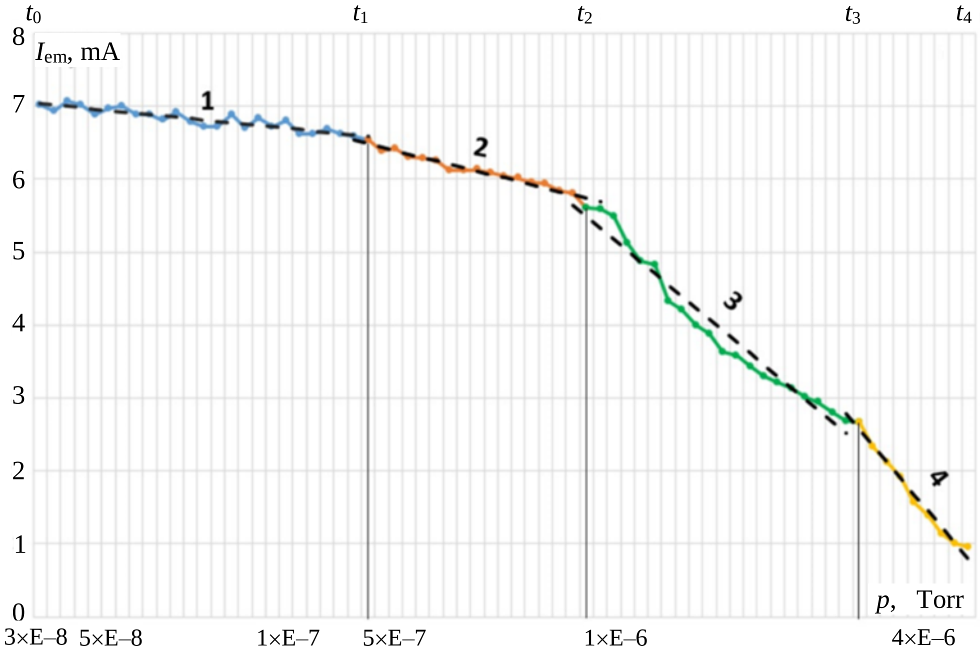

Fig. 1. Dependence of the autoelectronic emission current on the pressure in the chamber [1]

and Arrhenius's laws, as well as practical recommendations for production optimization. The work is aimed at integrating theoretical knowledge and modern technologies to create more efficient and reliable devices.

2. Thermally activated desorption

Thermally activated desorption is widely used in industrial processes to improve the quality of cathodes in EVDs. In most cases, vacuum degassing requires thermal activation of cathodes or additional thermal cleaning. Classical studies of cathode heat treatment [7–9] provided the basis for modern methods of removing impurities through heating. These studies showed that cathode temperature above 1000 °C significantly increases the desorption rate for all materials. Modern studies [10, 11] have confirmed these data and proposed more accurate models to describe the processes of gas diffusion on the cathode surface. For example, the Fick equation for diffusion allowed us to accurately calculate the concentration of impurity gases on the cathode surface and the time required for their complete removal:

$$\frac{\partial C}{\partial t} = D\frac{\partial\ C}{\partial x^2},$$

where C is the impurity concentration, D is the diffusion coefficient. If we assume that the activation energy of capture is identical to the activation energy of diffusion in the lattice the activation of desorption will be equal to the sum of the diffusion energy and the energy barrier, which is in good agreement with the experimental spectrum of pure iron with careful surface treatment [12].

At the same time, more often, modern studies of basic EVD designs give hope for the creation of computer methods for calculating and modeling surface processes for their further generalization to technological units with a more complex elemental composition [13].

Detailed studies of thermal desorption are presented in [14]. An extensive analysis of the temperature and pressure effect on the desorption characteristics of various cathode materials was carried out. In the process of thermal vacuum treatment of cathodes, an incorrectly selected pressure can lead to insufficient or excessive desorption. Thus, a pressure of 10^{-3} mbar leads to an increase in the desorption flux for scandate-based cathodes by 25 % compared to a pressure of 10^{-2} mbar. With regard to thermal treatment, scandium oxides are preferable in production, since they reduce the work function to 1.6–1.8 eV compared to traditional cathodes, for which this figure is 2.0–3.0 eV. The addition of scandium oxides to cathodes made of other materials helps to improve the thermal stability of cathodes at high temperatures (up to 1500 K). In particular, Sc_2O_3-based cathodes demonstrate stable emission characteristics for 1000 hours of continuous operation at temperatures up to 1200 K, which is superior to most similar materials [15]. Tungsten and thorium-based cathodes also demonstrate the efficiency of thermal desorption under high-temperature conditions. For them, a characteristic increase in desorption begins at a temperature of 1200 K, contributing to an increase in gas evolution by 40 % compared to a temperature of 1000 K [16].

From a physical point of view, the activation of desorption and diffusion processes during pumping out EVDs through long-term thermal vacuum treatment can effectively remove a significant amount of gas components from the internal surfaces and from the volume of the device parts. However, long-term thermal vacuum treatment can entail a decrease in the emission characteristics of the cathodes due to additional chemical transformations on the surface or destruction of the surface layer. Improvement in the work function of tungsten, molybdenum and barium oxide cathodes was noted only when heated in a certain temperature range [17]. Samples made of nickel, after preliminary long-term 12-hour thermal degassing at a temperature of 800 °C in a vacuum, released CO at each bombardment pulse with energy of 270 eV at room temperature. Further investigation revealed that the surface of the nickel samples was covered with a thin but strong insulating film of carbon-containing nickel oxides [18]. In addition, the possibility of mass transfer of metals inside and outside the finished devices should be separately highlighted. Quite a few cases of the manifestation of the volatile properties of metal oxides have been described in the literature [19–21]. Some volatile properties of molybdenum MoO_3 and copper CuO oxides have been considered in detail. The partial pressures of these oxides when heated to 600 °C are approximately 10^{-3} and 10^{-2} Torr, respectively. It is also noted that BaO molecules evaporate without decomposition at low temperatures, despite the high boiling point of this compound. At approximately 800 K, dissociation of BaO_2 molecules begins, which leads to further evaporation of metallic barium [20].

It is known theoretically that the cathode temperature can be affected by several factors simultaneously: the heating model and the temperature coefficient of heater resistance. To solve the problem of excessive desorption during heating, they resort to optimizing temperature conditions [22] and monitoring the current cathode temperature during thermionic emission [23] or using a synergistic effect with new approaches to stimulating desorption and diffusion processes [24–26]. The paper [26] shows that the cathode temperature decreases as the current collected by the anode increases. When the emission current was 180 mA, which corresponded to a current density of 2.92 $A{\cdot}cm^{-2}$ the cathode temperature decreased by 29 °C in the constant voltage heating mode and by 35 °C in the constant current heating mode.

3. Ultraviolet radiation and ion cleaning

At certain stages of vacuum tube production, methods such as ultraviolet irradiation or ion cleaning are used to accelerate desorption processes. Compared to traditional heat treatment, calculated data indicate an increase in the rate of desorption processes during UV treatment by several times [27]. The threshold energy for neutral desorption can be quite low, down to 5 eV (far ultraviolet radiation). At higher energies (15 eV), ion desorption can be expected [28]. The promise of this method lies in its effectiveness when used at the final stages of cathode production, when it is necessary to remove remaining impurities before installing the cathodes in devices. In addition to removing contaminants at the atomic level, UV radiation, due to its local effect of high energy density, made it possible to carry out controlled nanostructuring [29].

Research in this area over the past 10 years has been aimed at finding modes and criteria for cleaning electrodes. The optimal ratio between the ignition voltage, working gas pressure, DC glow discharge current and the distances between the EVD components made it possible to reduce the pumping time by 2.0–2.5 times with lower energy costs about 15 years ago [30]. However, with the advent of new cathode materials and more stringent operational requirements for devices, it became necessary to improve the classical methods. Cathodic plasma electrolytic treatment is a new technology for preparing a surface for further processing or creating surfaces with specified properties [31]. Using a plasma discharge caused by electrolysis and the cooling effect of the electrolyte, metal cleaning and subsequent deposition of a thin metal film are effectively achieved. The most common methods of film creation in production are physical or chemical vapor deposition [32, 33]. These methods require separate preliminary treatment of materials, while the spraying process itself is quite lengthy. The plasma electrolytic processing process, having four simultaneous effects from a strong electric field, oxidizing free radicals, ultraviolet light and a shock wave, turns out to be cost-effective and environmentally friendly [34].

However, its application in the field of electronics still needs to be adjusted in relation to the modes and conditions of the process. The most practically oriented developments are pumping technologies for EVDs with secondary-emission cold (non-heating) cathodes [35]. The main feature of the method is a combination of ion cleaning with sequential degassing of the device components, which includes the use of high-energy ions to remove adsorbed gas molecules. In the process of ion cleaning, ion flows are created directed at the surface being cleaned. This helps remove contaminants at the molecular level, including residual molecules such as hydrogen and oxygen, and reduces the preparation time of devices by 40 %. Other studies show the same results [29], which reinforces the prospects of the method in its application for mass production. The most successful examples of combined technologies to date include the processing of cathodes in instantaneous devices such as magnetrons. In these devices, the use of combined methods ensures low levels of desorption in the vacuum cavity and stability of thermionic emission.

The disadvantages of the method include the possibility of initiating a chemical reaction with impurity gas molecules on the cathode surface or an uneven temperature distribution, which becomes especially noticeable in nanoscale areas. Nanosecond pulses of UV radiation are capable of transferring energy so quickly that the material does not have time to transfer heat to deeper layers. Due to this, it is possible, if necessary, to controllably limit the surface effects of evaporation and desorption [36–38]. This ability additionally opens up possibilities for using these effects in microelectronics and nanotechnology, especially for the creation of thin films or controlled modification of surfaces [39, 40].

4. Electron desorption and radiation effects

Electron desorption was actively studied back in the 1960s, which made it possible to establish the mechanisms of this process [41]. It was found that even low-energy electrons can effectively desorb gases adsorbed on the metal surface, and the desorption rate increases with increasing electron energy and increasing irradiation time. Thus, when exposed to electrons in the range from 1 to 30 eV on tungsten, copper and platinum under conditions of maintaining a pressure of 10^{-9} Torr, desorption of oxygen and carbon dioxide occurs. Cold cathodes made of nickel and cobalt when exposed to electrons with energies from 1 to 50 eV demonstrate acceleration of hydrogen and argon desorption.

Among modern studies, there are works that examine in detail the effect of all types of radiation on the desorption capacity of the surface [42, 43]. Experimental data show that radiation can significantly change the desorption mechanisms, accelerating or slowing down this process depending on the type and intensity of radiation. In addition, it has been shown that an applied electric field can change the distribution of charged particles and increase the repulsive force between the adsorbed molecules and the cathode surface. This is especially noticeable at high voltages, where electric fields promote acceleration of desorption. For example, when molybdenum cathodes were exposed to intense ionizing radiation, a significant activation of desorption was recorded, increasing by 30 %. Moreover, this method not only increases the quantum efficiency of the cathodes, but also does not affect the surface roughness, which is especially important for the operation of cathodes under high vacuum conditions [44].

Later, a model of gas and radiation desorption during initial high-voltage conditioning in vacuum was created [45]. The applied voltages varied from 20 to 100 kV for stainless steel electrodes, as a result of which intense desorption of impurity gases (mainly hydrogen and oxygen) began at voltages above 60 kV. According to the author, the increase in the desorption rate before reaching the threshold voltage of 80 kV is associated with the accumulation of energy in the surface layers of the metal. For example, at a voltage of 80 kV, the measured desorption rate reached 10^{16} molecules$\cdot$cm$^{-2}\cdot$s^{-1}, while at 40 kV it was about 10^{14} molecules$\cdot$cm$^{-2}\cdot$s^{-1}. It was also noted that desorption reaches a peak in the first few minutes of processing, after which the desorption rate decreases, indicating saturation of the process. A feature of this model is that it takes into account the radiation effect caused by accelerated electrons and ions, which additionally contribute to desorption. This radiation effect increases the local surface temperature to values about 200 °C, which stimulates thermally activated desorption of molecules. It is confirmed that under such conditions, radiation desorption can account for up to 20 % of the total number of released molecules in the early stages of high-voltage processing.

Thus, high radiation load leads to significant improvement of vacuum conditions in EVDs, due to active desorption of ions and molecules from the cathode surface. Desorption intensity increases sharply under radiation exposure, especially in the case of hydrogen molecules, which is associated with their high mobility and penetration into materials. At the same time, vacuum recovery after irradiation occurs slowly, which indicates prolonged activation of desorption processes in the material after exposure.

5. Cathode materials

With the increase in frequency ranges and power of modern devices, more stringent requirements arise for heat resistance, durability and stability of cathodes to external factors, such as high temperatures and intense electric fields. The manufacture of cathodes from traditional materials such as nickel, tungsten, alkaline earth metal oxides requires precise control over the conditions of all stages of their manufacture, operation and storage [46, 47]. Moreover, the structure of the cathode surface or the morphology of its coatings due to the presence of microroughness, defects or variable resistance to external influences relative to the chemical composition can also have an accelerating or decelerating effect on the desorption of the material [48]. In this case, it is necessary to take into account not only the stability of cathode emission, but also degradation processes [49]. The latest developments in this area suggest the use of new materials for cathodes, such as oxides of rare earth metals (e.g. scandate) and nanostructured coatings.

However, depending on the required operating modes, the state of all technological units of the devices should still be constantly monitored [50]. Being the most popular for high-temperature applications, scandate cathodes during long-term operation promote active accumulation of desorbed particles on the inner surfaces of EVDs [51]. Therefore, it is proposed to use more stable coatings on the cathode surface or to create multilayer structures that prevent the interaction of active elements of the cathode with the environment. The most widely used are the deposition of thin layers of atoms of alkali, alkaline earth elements and polar molecules of barium oxide [52].

The dependence of the work function on the thickness of the deposited layer is characterized by a curve in which a minimum is observed at a layer thickness of 0.6–0.7 monolayers, which is typical for various materials. The exact reason for the appearance of this minimum continues to cause controversy: it may be due not only to a decrease in the positive moment on the surface due to the bond between adatoms, but also to the presence of traces of electronegative contaminants in the device. These atoms, binding with electropositive adatoms, can enhance the emission. For example, films containing Cs–O–W or Ba–O–W demonstrate a lower work function (1.6–1.9 eV) compared to Ba–W and Cs–W films (2–2.5 eV). According to [53], the mechanism of this phenomenon is that a group of metallic adatoms is formed around the oxygen ions on the surface. Their effect compensates for the increase in the work function caused by oxygen adsorption, thereby reducing it.

The valence state of the deposited atoms can significantly affect the work function, especially if the covalent component plays a role in their interaction with the substrate. Studies described in [54] showed that when barium is deposited on a clean iridium surface (Ir(111)) the barium atoms are uniformly distributed over the surface until a monolayer is formed. However, in the presence of a small amount of carbon, the adsorbed Ba atoms tend to form island structures. This is due to the weakening of the electron interaction of adatoms with the carbon substrate, which in turn strengthens the bonds between the adatoms themselves. The opposite effect was recorded during the adsorption of barium on a tungsten surface coated with a germanium film [55]. In this case, the deposition of barium on the W surface coated with germanium led to a greater decrease in the work function compared to pure tungsten.

As noted earlier, the introduction of scandium into the tungsten base of cathodes significantly improves their thermionic characteristics. This allows for a decrease in operating temperatures, improved emission efficiency and increased durability of cathodes under operating conditions. After a more detailed analysis of the physicochemical processes on the cathode surface, it was found that the introduction of scandium helps to reduce thermal desorption, due to which the cathodes demonstrate high stability even when exposed to radiation and mechanical loads, which confirms their high reliability under harsh operating conditions.

Currently, many industrial enterprises, including JSC Pluton, manufacture microwave vacuum tubes using dosing cathodes based on tungsten sponge impregnated with barium-calcium aluminate $2.5BaO \cdot 0.4CaO \cdot Al_2O_3$. The thermionic current density of such a cathode at a temperature of 1050–1100 °C is 10–15 $A{\cdot}cm^{-2}$ [56]. Studies of the chemical composition using electron spectroscopy methods confirmed the solubility of calcium, aluminum, tungsten, and scandium in cathode materials. It was shown that the emission properties of dispersing and scandate cathodes are determined by the properties of barium oxide crystallites formed in the cathode material at the stage of its manufacture and activation, as well as the type and concentration of point defects in barium oxide. Thus, the use of thin-film coatings based on oxides and nitrides effectively blocks the penetration of gases to the active centers of the cathodes and reduces the likelihood of desorption [56].

The use of plasma technologies, such as plasma etching or ion plating, for the purpose of modifying the surface of cathodes additionally contributes to increasing the resistance of cathodes to thermal and mechanical destruction [57, 58]. Due to the precise control of the process of ion flow formation by heating the cathode to high temperatures, thermionic emission of electrons is initialized and a dense plasma discharge is created. These discharges play a key role in ion plating processes, providing a high degree of control over the parameters of thin films, such as thickness, composition and structure [40]. And plasma etching of cathodes is useful for creating specific microstructures [59, 60].

The paper [61] is a significant study devoted to the development of tungsten-based thermionic cathodes activated with nanothorium (ThO_2). The cathode fabrication involved a sintering method, which resulted in a uniform distribution of nanothorium over the surface. Such cathodes provide a lower work function and improved thermionic emission compared to traditional cathodes. For example, after activation and sintering, the operating temperature of cathodes was reduced by 200 K. An additional sintering or high-temperature annealing step to achieve better thermal stability and electrical properties of the coatings has proven useful for other materials as well [62, 63].

Palladium-barium based cathodes have also demonstrated superiority over traditional materials. Metal-alloy cathodes of this type are a dense form-forming matrix based on palladium containing the intermetallic compound Pd_5Ba distributed in the volume [64]. Their high emissivity is explained by the fact that when heated, a thin layer of the active element or its oxide is formed on the cathode surface, which helps to reduce the work function. Also, the presence of active elements in the volume of the material helps to maintain an emission layer on the working surface of the cathode, which provides secondary electron emission. However, the emission properties of such cathodes strongly depend on the surface structure. It is known that dispenser hot cathodes made of tungsten sponge impregnated with barium-calcium aluminate when heated to temperatures in the range of 1100–1400 K due to decomposition and thermal diffusion form a submonolayer film of Ba and BaO, which reduces the work function. The application of a thin layer of such elements as rhenium, osmium, iridium or their alloys with tungsten enhances the effect, acting as activators. It is known that the emission properties of pure BaO crystallites are determined by oxygen vacancies, which form acceptor-type surface states on the oxide surface. This leads to a significant curvature of the energy bands [65]. In this case, the electronic structure of barium oxide changes according to the synergistic effect of all the impurities present at once [66, 67]. To study the arrangement of atoms surrounding the Ba atom on the surface, a method for determining the extended fine structure of X-ray absorption by the surface was used in [68]. This method makes it possible to obtain information on the distances to the nearest neighboring atoms along the oscillating part of the absorption coefficient beyond the main band. The spectra of such absorption by three types of dispenser thermionic cathode (without coating, with Os–W and Pt – W coatings) were studied using a synchronous radiation source. The results showed that in the first two types of cathodes, barium atoms form clearly defined short-range bonds with oxygen with the Ba–O distance equal to 2.62 Å. However, in thermionic cathodes with the Os–W coating, the barium atom is bonded to two oxygen atoms, which leads to an increase in the surface dipole moment and a more significant decrease in the work function. In the case of cathodes with the Pt–W coating, the Ba–O distance turned out to be greater, and the bond between the atoms was less pronounced. In [69], the classical dipole theory of thermionic emission from dispenser cathodes was challenged by spectroscopic data obtained at a later time. The role of oxygen in providing the increased emission activity of the cathode was noted. However, in [70], when studying the secondary emission properties of impregnated tungsten cathodes using the same spectroscopy methods, as well as thermionic microscopy and high-resolution contact potential difference, a violation of the correlation of the secondary emission and thermionic properties of individual “active” surface areas was discovered. In particular, with increasing temperature corresponding to the process of heat treatment of the cathode, the secondary emission properties eventually worsen, and the thermionic properties improve, which the authors associate with a decrease in the amount of oxygen on the surface and with a change in the nature of the chemical bond of Ba with the substrate for this reason. The effect of carbon impurities on the secondary electron emission coefficient is noted. The effect of various methods of preliminary surface treatment on the emission properties of the cathode is studied. The greatest effect is achieved with sandblasting. It is shown that an increase in the pore size in the tungsten matrix reduces the secondary electron emission coefficient due to the effects of surface charging. At the same time, it should be noted that the secondary emission and thermionic properties of emitters based on metals and metal-oxide film systems depend significantly on the heating temperature, which limits the range of their use in electronic devices.

At temperatures in the range from 1000 to 1300 K, the efficiency of thermionic emission increased significantly due to the reduced work function of the barium coating (2.1–2.4 eV compared to 4.5 eV for tungsten). It was also found that secondary electron emission has a maximum quantum yield of electron emission at primary electron energies from 100 to 500 eV, which improves the performance of cathodes in microwave devices where it is important to maintain a stable electron flow. According to the proposed model of the surface structure of the palladium-barium cathode, it was calculated that the emission properties of the palladium-barium cathode significantly depend on the emission properties of the barium oxide crystallites and on the relative surface area of the cathode they occupy [71]. Quite often, various versions of the design of metal-alloy palladium-barium cathodes, which are a Pd matrix in which the intermetallic phase Pd_5Ba is distributed [72, 73], exhibit a decrease in the secondary electron emission coefficient due to the uneven distribution of the Pd_5Ba phase in the Pd matrix [74]. For the same reason, the greatest number of alloy defects and diffusion welding defects (lack of fusion, “swelling”, “delamination” of the alloy foil from the core) occur [75]. In order to eliminate the above-mentioned shortcomings, a pressed metal-alloy cathode was proposed for the industrial production of magnetrons with non-heater start-up. Activation of the surface of the working edges of field-electron cathodes (FEC) during the activation of secondary emission cathodes (SEC). After pressing and additional sintering of the cathodes in a vacuum furnace, a homogeneous and uniform distribution of barium on the working surface of the palladium-barium cathode was achieved, as shown in Fig. 2 [76, 77].

In order to increase the stability and reproducibility of generation initiation, a structurally similar cathode based on palladium with barium (Fig. 3) was subjected to special activation in the temperature range T~970–1370 K, observing the condition $T \cdot t \sim 1.0 \cdot 10^6 – 1.5 \cdot 10^7$ (K s) [78]. In this case, filiform crystals of palladium with a length of ~50–100 nm and a cross-sectional size of ~5–20 nm, partially or completely covered with barium, are grown on the end surface of the FEC.

The presence of filamentary crystals on the FEC surface significantly increases the value of the field emission current, thereby ensuring the failure-free operation of the magnetron (Fig. 4). In such a cathode design, various metals and alloys with stable secondary emission properties and resistant to the effects of ion and reverse electron bombardment can be used as SECs, along with palladium-barium emitters, for example, impregnated or oxide cathodes, iridium, platinum, osmium, intermetallic compounds, platinum with barium, iridium with lanthanum, iridium with cerium, osmium with lanthanum, etc.

The search for solutions to ensure stable electron emission has led researchers to develop alloys and composite materials. The most suitable materials for the matrix of composite cathodes are palladium, platinum, silver, copper, nickel, molybdenum and tungsten, while cesium, magnesium, lithium, barium, aluminum and their oxides are used as additives.

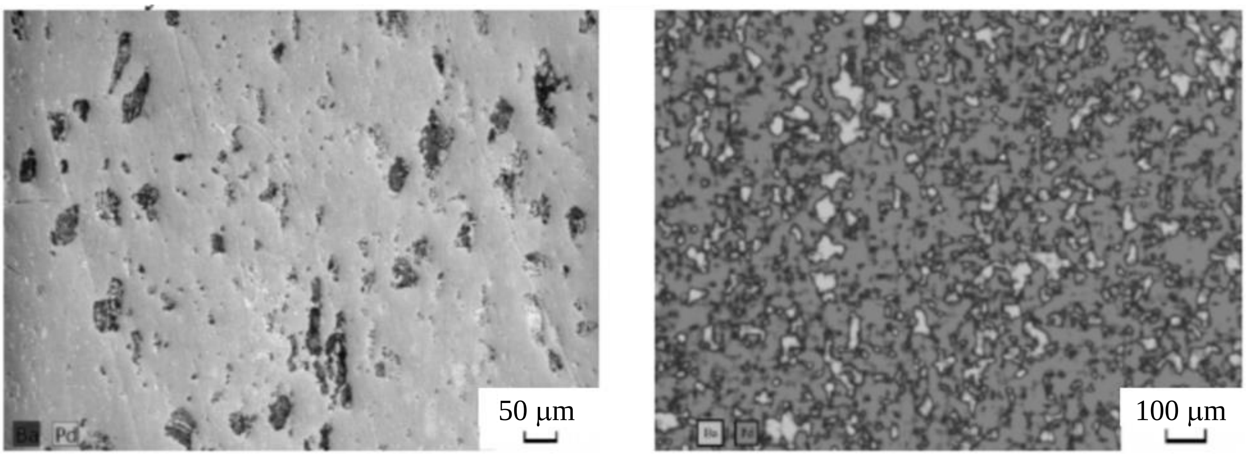

(a) *(b)*

Fig. 2. Samples of palladium-barium emitters with fractional compositions of the initial powder *a*) 20–45 μm, *b*) 45–63 μm [76]

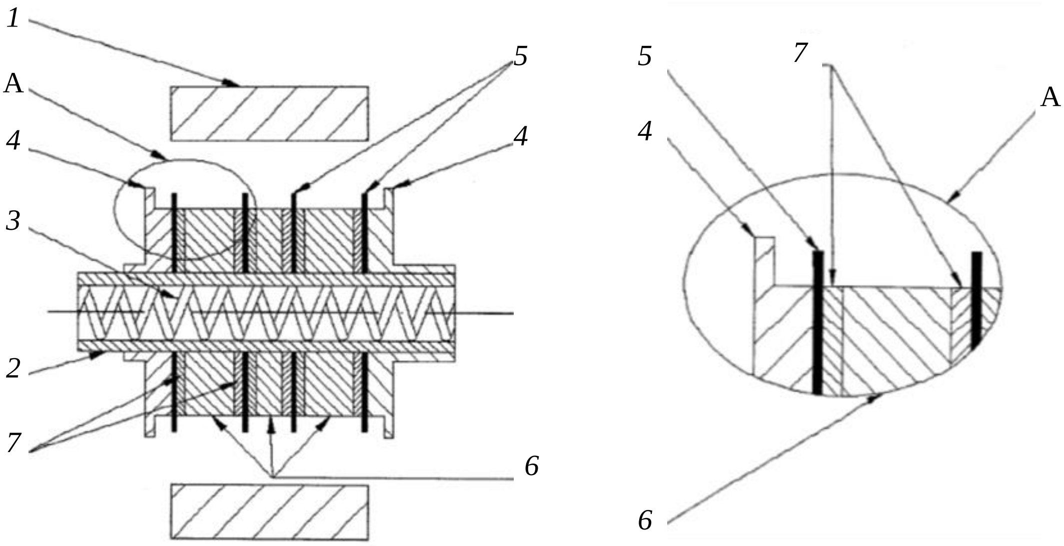

Fig. 3. Schematic representation of the magnetron structure: *1* – anode; *2* – cathode core; *3* – heater; *4* – screens; *5* – autoelectronic cathodes; *6* – secondary emission emitters; *7* – AEC activator washers [78]

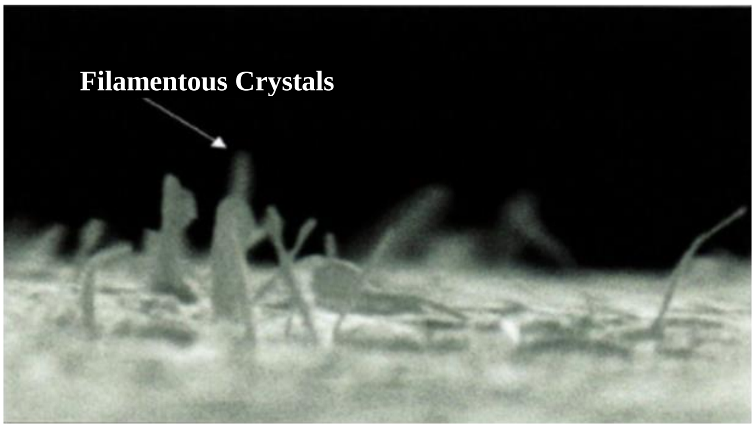

Fig. 4. Micrographs of fragments of the FEC end surface at magnification of M ~ 50000×
(inside the image: filamentous crystals) [78]

Of particular interest are alloys that can demonstrate high emission properties after activation due to the adsorption of a surface-active component located in the volume of the alloy. For example, alloys of platinum and palladium with metals of group II of the Periodic Table demonstrate good emission characteristics. In these experiments, the content of low-melting components in the alloys ranged from 0.5 to 2 weight percent. Activation of platinum alloys was carried out at temperatures of 1350–1480 K, while palladium-based alloys were activated at 1200–1300 K [79].

However, in some vacuum tubes it is impossible to achieve such high temperatures, or they may be undesirable. Low-temperature treatment of cathode assemblies does not allow for the complete removal of gas impurities and activation of the Pd–Ba alloy, so in this case activation can be carried out at lower temperatures, but in the environment of certain gases (usually H_2, N_2 or their mixtures) [80,81].

In addition to surface and structural modifications, attention has recently shifted to the latest nanomaterials that demonstrate a high density of active centers, a large specific surface area and increased catalytic activity. For example, cathodes based on nanostructured carbon nanotubes (CNTs) have improved gas desorption characteristics due to high surface activity and the presence of multiple active centers for adsorption of impurities [82, 83]. This allows for a significant reduction in desorption time and an increase in the vacuum quality in EVDs. In addition, nanostructured cathodes improve the thermal stability of materials, which is especially important at high operating temperatures of cathodes in vacuum tubes. Nanomaterials demonstrate resistance to thermal destruction and have higher durability compared to traditional metal-based cathodes.

Table 1. Summary characteristics of modern cathode processing methods

Method	Reduced pumping time (compared to basic vacuum degassing), %	Rationaluse inproduction	Disadvantages
Heat treatment	10–20	Suitable for mass production, especially when processing traditional materials (tungsten, nickel)	Risk of surface damage due to overheating; activation of chemical transformations on the surface of the material; long process; high energy consumption
Ion cleaning	30–40	Effective for removing deep contaminants. Ideal for high-precision devices	May damage the cathode surface; requires complex equipment settings; not suitable for delicate materials
Ultraviolet irradiation	20–30	Recommended for processing delicate materials and nanostructured cathodes	Less effective for heavy contamination; requires strict control of wavelength and intensity
Laser treatment	20–50	Useful for limited quantities or complex cathodes such as carbon nanotubes	High equipment cost; risk of local damage to the material due to improper settings
Plasma treatment	40–60	Ideal for processing cathodes with high thermal and mechanical loads	High energy consumption; difficulty maintaining stable plasma parameters; possible damage to the structure
Use of nanostructured materials	10–30	Rational for use in high-precision and unique devices	High production cost; difficulty in applying nanostructures

In order to improve the characteristics of CNT cathodes for their use in vacuum tubes, laser irradiation is used to treat the surface [84]. This method is used to modify the surface structure, improve electron emission and remove contaminants that may arise during the production stage. At the same time, the correct choice of gas environment during laser processing significantly affects electron emission. It was found that the presence of oxygen in the gas atmosphere during laser processing helps remove carbon impurities and improves the structural and emission properties of the cathodes. At the same time, the vacuum atmosphere preserves the structure of the nanotubes without causing significant destruction. Such treatment in an oxygen atmosphere resulted in an increase in the emission current density by 30–40 % compared to cathodes treated in a nitrogen atmosphere or vacuum.

Various carbon nanoclusters [85–87], recently used to modify metal-porous cathodes [88], seem promising from the point of view of obtaining high emission characteristics. The results of the studies indicate that nanocarbon materials improve the structural stability of cathodes and contribute to an increase in the emission current density due to an increase in the active surface area. Along with this, the durability and resistance to degradation of the cathode under thermal influence are improved [89].

Thus, in this work, a review of existing methods for controlling desorption of impurity gases necessary to increase the durability of cathodes and the stability of their operation under high vacuum conditions was conducted. Table 1 provides a summary of the characteristics of modern cathode treatment methods.

An evaluation of the literature data has demonstrated that synergy between traditional physical and chemical models and the latest scientific developments and experimental data is necessary to increase the productivity, durability and reliability of vacuum devices.

6. Conclusion

Desorption of cathode materials remains one of the main problems in the production and operation of vacuum tubes. Over the past 15 years, many methods have been proposed to improve these processes, including heat treatment, electron and radiation exposure, ion cleaning, and ultraviolet irradiation.

The importance of controlling desorption of impurity gases to ensure the durability of cathodes and the stability of their operation under high vacuum conditions has been confirmed by both experimental and calculated data. Today, depending on the practical focus and the requested requirements for the design details of various vacuum tubes, many promising approaches are available for upgrading production technologies. Studies have shown that the combined use of classical physicochemical models and modern experimental data opens up new opportunities for improving the emission characteristics of cathodes. This, in turn, helps to increase the productivity and reliability of vacuum tubes, which is especially important for high-tech applications such as microelectronics, medical equipment, and telecommunications.

7. Funding

This study received no external funding.

8. Conflict of interest

The authors declare no conflict of interests.

References

1. Li IP, Kapustin VI, Shumanov AV, Bychkov DV, et al. Influence of the vacuum state on the field emission properties of the cathode-heating unit of magnetrons with instant readiness. *XXVIII Scientific and Technical Conference with the participation of foreign specialists "Vacuum science and technology"*. Moscow: Nanoindustry; 2021. p. 278-282. (In Russ.)

2. Li IP, Kapustin VI, Ledentsova NE, Shumanov AV. Design features of three-module cathode heating units of magnetrons with instant readiness. *XXVIII Scientific and Technical Conference with the participation of foreign specialists "Vacuum science and technology"*. Moscow: Nanoindustry; 2021. p. 283-288. (In Russ.)

3. Khanbekov IF, Mikhailov VP. Research of the ultrasonic activation processes of diffusion and desorption in electrovacuum devices. *XXVIII Scientific and Technical Conference with the participation of foreign specialists "Vacuum science and technology"*. Moscow: Nanoindustry; 2021. p. 306-310. (In Russ.)

4. Gaertner G. History of vacuum electronics and vacuum electron sources and future development trends. *Modern Developments in Vacuum Electron Sources. 135*. Cham: Springer; 2020. p. 1-31.

5. Ogura S, Fukutani K. Thermal desorption spectroscopy. *Compendium of Surface and Interface Analysis*. Singapore: Springer; 2018. p. 719-724.

6. Umirzakov BE, Sadikzhanov Zh, Tashmukhamedova DA, Abduvaitov A, Rabbimov EA. The effect of adsorption of Ba atoms on the composition, emission and optical properties of CdS single crystals. *Pis'ma v zhurnal tekhnicheskoy fiziki = Letters to the Journal of Technical Physics*. 2021;47(12):3. DOI:10.21883/PJTF.2021.12.51057.18632 (In Russ.)

7. Ubbelohde ARJP, Alfred CE. The kinetics of adsorption processes. *Proceedings of the Royal Society of London. Series A, Containing Papers of a Mathematical and Physical Character*. 1931;134(824):512-523. DOI:10.1098/rspa.1931.0211

8. Langmuir I. The effect of space charge and residual gases on thermionic currents in high vacuum. *Physical Review*. 1913;2(6):450-486. DOI:10.1103/PhysRev.2.450

9. Nottingham WB. Thermionic emission. *Electron-Emission Gas Discharges I / Elektronen-Emission Gasentladungen I*. Berlin: Springer; 1956. V. 4(12). p. 1-175.

10. Wei FG, Hara T, Tsuzaki K. Precise determination of the activation energy for desorption of hydrogen in two Ti-added steels by a single thermal-desorption spectrum. *Metallurgical and Materials Transactions B*. 2004;35(3):587-597. DOI:10.1007/s11663-004-0057-x

11. Gao J-Y, Yang Y-F, Zhang X-K, Li S-L, et al. A review on recent progress of thermionic cathode. *Tungsten*. 2020;2(3):289-300. DOI:10.1007/s42864-020-00059-1

12. Ono K, Meshii M. Hydrogen detrapping from grain boundaries and dislocations in high purity iron. *Acta Metallurgica et Materialia*. 1992;40(6):1357-1364. DOI:10.1016/0956-7151(92)90436-I

13. Sveshnikov VK, Bazarkin AF. Physical model and computer calculation of the diffusion coefficient of sodium into the oxide coating of the cathode. *Fundamental'nye Issledovaniya = Fundamental research*. 2014;(5-5):990-993. (In Russ.)

14. Seif MN, Balk TJ, Beck MJ. Temperature effects on desorption behavior and characteristic Wulff shapes of scandate cathodes. *2020 IEEE 21st International Conference on Vacuum Electronics (IVEC) 20-23 April 2020*. Monterey: IEEE; 2020. p. 83-84. DOI:10.1109/IVEC45766.2020.9520596

15. Kapustin VI, Li IP, Shumanov AV. Electronic structure of variants of scandate cathodes. *XXVIII Scientific and Technical Conference with the participation of foreign specialists "Vacuum science and technology"*. Moscow: Nanoindustry; 2021. p. 272-277.

16. Dai C, Saidi P, Topping M, Béland LK, et al. A mechanism for basal vacancy loop formation in zirconium. *Scripta Materialia*. 2019;172:72-76. DOI:10.1016/j.scriptamat.2019.07.006

17. Bouwknegt A, Kooi AG van der. Calorimetric measurements of the emission properties of oxide cathodes in a low-pressure gas discharge. *Journal of Physics D: Applied Physics*. 1975;8(8):952-963. DOI:10.1088/0022-3727/8/8/009

18. Cherepnin NV. *Sorption phenomena in vacuum technology*. Moscow: Soviet radio; 1973. p. 383. (In Russ.)

19. Cherepnin NV. *The basics of cleaning, decontamination and pumping in vacuum technology*. Moscow: Soviet radio; 1967. p. 408. (In Russ.)

20. Kazenas EK, Tsvetkov YuV. *Thermodynamics of oxide evaporation*. Moscow: URSS; 2008. p. 474. (In Russ.)

21. Chernyak EN, Zakurdaev IV, Shuppe GN, Yakovlev VK. Asymmetric change of the thermoemission current and surface structure in crystals of refractory metals during oriented transfer processes. *Bulletin of the Academy of Sciences of the USSR. Physical Series.* 1973. (In Russ.)

22. Dyke WP, Charbonnier FM, Strayer RW, Floyd RL, et al. Electrical stability and life of the heated field emission cathode. *Journal of Applied Physics*. 1960;31(5):790-805. DOI:10.1063/1.1735700

23. Kuchina IYu, Polushin NI, Zakharova ES, Li IP, et al. Experimental support of magnetron nickel oxide cathode fabrication process. *Izvestiya Vysshikh Uchebnykh Zavedenii. Materialy Elektronnoi Tekhniki = Materials of Electronics Engineering*. 2015;18(4):285-290. DOI:10.17073/1609-3577-2015-4-285-290

24. Khanbekov IF, Li IP, Petrov VS, Mikhaylov VP, et al. Research of acoustically stimulated thermal desorption in electrovacuum microwave devices. *IOP Conference Series: Materials Science and Engineering*. 2018;387:012032. DOI:10.1088/1757-899X/387/1/012032

25. Khanbekov IF, Mikhailov VP. Research of the ultrasonic activation processes of diffusion and desorption in electrovacuum devices. *Nanoindustriya*. 2022;15(1):20-27. DOI:10.22184/1993-8578.2022.15.1.20.27 (In Russ.)

26. Liu Y, Tian H, Han Y, Xu Z, et al. Temperature variation of a thermionic cathode during electron emission. *Science in China Series E: Technological Sciences*. 2008;51(9):1497-1501. DOI:10.1007/s11431-008-0161-2

27. Hara T, Ishiguro T, Shinozaki K. Ultraviolet-light-induced desorption of oxygen from $SrTiO_3$ surfaces. *Japanese Journal of Applied Physics*. 2011;50(4R): 041502. DOI:10.1143/JJAP.50.041502

28. Yates JT, Madey TE. *Vibrational spectroscopy of molecules on surfaces.* Boston: Springer US; 1987. p. 468.

29. Kolacek K, Schmidt J, Straus J, Frolov O, et al. Interaction of extreme ultraviolet laser radiation with solid surface: ablation, desorption, nanostructuring. *SPIE Proceedings XX International Symposium on High-Power Laser Systems and Applications 2014*. China: SPIE; 2015. p. 92553U. DOI:10.1117/12.2071273

30. Voronin VI, Lemyakin AA, Zorkina OA. Nest pumping of electrovacuum devices with ion-plasma electrode cleaning. V*estnik Saratovskogo gosudarstvennogo tekhnicheskogo universiteta*. 2008;2(1(32)):119-126. (In Russ.)

31. Lu S, Sun X, Zhang B, Wu J. Review of cathode plasma electrolysis treatment: progress, applications, and advancements in metal coating preparation. *Materials*. 2024;17(16):3929. DOI:10.3390/ma17163929

32. Ramezani M, Mohd RZ, Pasang T, Jiang C-P. Surface engineering of metals: techniques, characterizations and applications. *Metals*. 2023;13(7): 1299. DOI:10.3390/met13071299

33. Pshyk AV, Petrov I, Bakhit B, Lu J, et al. Energy-efficient physical vapor deposition of dense and hard Ti–Al–W–N coatings deposited under industrial conditions. *Materials & Design*. 2023;227:111753. DOI:10.1016/j.matdes.2023.111753

34. Yang L, Zhang P, Shi J, Liang J, et al. Dual electrolytic plasma processing for steel surface cleaning and passivation. *Journal of Materials Engineering and Performance*. 2017;26(10):5009-5015. DOI:10.1007/s11665-017-2826-0

35. Zorkin AYa, Semenov AS, Konyushkov GV. *Method of pumping electric vacuum devices*. Russian Federation patent 2,185,676. 20 September 2021. (In Russ.)

36. Besozzi E, Maffini A, Dellasega D, Russo V, et al. Nanosecond laser pulses for mimicking thermal effects on nanostructured tungsten-based materials. *Nuclear Fusion*. 2018;58(3):036019. DOI:10.1088/1741-4326/aaa5d5

37. Lukin VG, Khvostenko OG. Desorption processes in the measurement of weak currents. *Physics-Uspekhi*. 2020;63(5):487-499. DOI:10.3367/UFNe.2019.07.038615

38. Nikolaev AG, Oks EM, Frolova VP, Yushkov GYu, et al. Effect of the discharge parameters on the generation of deuterium ions in the plasma of a high-current pulsed vacuum arc with a composite zirconium deuteride cathode. *Zhurnal tekhnicheskoy fiziki = Technical Physics*. 2017; 87(5):681-687. DOI:10.21883/JTF.2017.05.44439.1912 (In Russ.)

39. Santecchia E, Hamouda AMS, Musharavati F, Zalnezhad E, et al. Wear resistance investigation of titanium nitride-based coatings. *Ceramics International*. 2015;41(9):10349-10379. DOI:10.1016/j.ceramint.2015.04.152

40. Mustata I, Lungu C, Jepu I, Porosnicu C. Thermionic vacuum discharges for thin film depositions. *Coatings*. 2023;13(9):1500. DOI:10.3390/coatings13091500

41. Menzel D, Gomer R. Desorption from metal surfaces by low-energy electrons. *The Journal of Chemical Physics*. 1964;41(11):3311-3328. DOI:10.1063/1.1725730

42. Li N, Li X, Zeng B. Field emission and emission-stimulated desorption of ZnO nanomaterials. *Applied Sciences*. 2018;8(3):382. DOI:10.3390/app8030382

43. Tyurin YuI, Nikitenkov NN, Larionov VV. Ionizing radiation-stimulated diffusion and desorption of hydrogen from metals. *Russian Journal of Physical Chemistry A*. 2011;85(6):1047-1053. DOI:10.1134/S0036024411060318

44. Dowell DH, King FK, Kirby RE, Schmerge JF, et al. In situ cleaning of metal cathodes using a hydrogen ion beam. *Physical Review Special Topics – Accelerators and Beams*. 2006;9(6):063502. DOI:10.1103/PhysRevSTAB.9.063502

45. Diamond WT. A model of gas desorption and radiation during initial high voltage conditioning in vacuum. *Journal of Applied Physics*. 2019;126(19):193303. DOI:10.1063/1.5124105

46. Yakunin AN, Aban'shin NP, Akchurin GG, Akchurin GG, et al. On the problems of stability and durability of field-emission current sources for electrovacuum devices. *Proceedings SPIE 976, Ultrafast Phenomena and Nanophotonics XX.* San Francisco: SPIE; 2016. p. 974620. DOI:10.1117/12.2213218

47. Yafarov RK, Storublev AV. Stability of the emission characteristics of thermal and cold-field cathodes operating in a vacuum. *Russian Microelectronics*. 2021;50(2):102-107. DOI:10.1134/S1063739721020104

48. Semenov SV, Konyushkov GV, Zorkin AYa. Comprehensive research and analysis of the problems of palladium-barium metal alloy cathodes of high-power vacuum devices. *Vakuumnaya tekhnika i tekhnologiya = Vacuum engineering and technology*. 2012;45-52. (In Russ.)

49. Bhattacharya R, Turchetti M, Keithley PD, Berggren KK, Browning J. Long term stability study of planar, two-terminal field emitters. *2021 22nd International Vacuum Electronics Conference (IVEC)*. Rotterdam: IEEE; 2021. p. 1-2. DOI:10.1109/IVEC51707.2021.9722417

50. Khanbekov I, Petrov V, Kopytov D. Determination of vacuum properties of materials in the production of vacuum electronics devices. *XXX Scientific and technical conference with the participation of foreign experts 'Vacuum science and technology' 2023, 10-14 October*. Makhachkala: NOK "Zhuravli"; 2023. p. 49-50.

51. Seif MN, Balk TJ, Beck MJ. Desorption from hot scandate cathodes: effects on vacuum device interior surfaces after long-term operation. *Materials*. 2020;13(22):5149. DOI:10.3390/ma13225149

52. Pratton M. *An introduction to surface physics*. Izhevsk: SIC 'Regular and chaotic dynamics'; 2000. p. 256. (In Russ.)

53. Korzhavy AP, Zvonetsky VI, Mirzoeva SD, Shishkov AV, Alexandrova GN. *Method of manufacturing a secondary emission cathode*. Russian Federation patent 2,069,915. 25 July 2024. (In Russ.)

54. Ageev VN, Zandberg ÉY, Ionov NI, Tontegode AY. Adsorption-desorption processes on solid surfaces. *Soviet Physics Uspekhi*. 1983;26(4):382-383. DOI:10.1070/PU1983v026n04ABEH004394

55. Zubenko YuV, Ishmukhamedov MB. The effect of germanium on the adsorption bond of barium with tungsten. *Fizika tverdogo tela = Physics of the Solid State*. 1983;25(1):180-183. (In Russ.)

56. Kapustin VI, Li IP, Shumanov AV, Lebedinskii YuYu, et al. Physical operating principles of scandate cathodes for microwave devices. *Technical Physics*. 2017;62(1):116-126. DOI:10.1134/S1063784217010108

57. Santecchia E, Hamouda AMS, Musharavati F, Zalnezhad E, et al. Wear resistance investigation of titanium nitride-based coatings. *Ceramics International*. 2015;41(9):10349-10379. DOI:10.1016/j.ceramint.2015.04.152

58. Niemelä J-P, Marin G, Karppinen M. Titanium dioxide thin films by atomic layer deposition: a review. *Semiconductor Science and Technology*. 2017;32(9): 093005. DOI:10.1088/1361-6641/aa78ce

59. Rakhadilov BK, Miniyazov AZh, Skakov MK, Sagdoldina ZhB, et al. Structural modification and erosion of plasma-irradiated tungsten and molybdenum surfaces. *Technical Physics*. 2020;65(3):382-391. DOI:10.1134/S1063784220030202

60. Lee W-J, Hon M-H. Space-limited crystal growth mechanism of TiO_2 films by atomic layer deposition. *The Journal of Physical Chemistry C*. 2010;114(15):6917-6921. DOI:10.1021/jp911210q

61. Wang F-Z, Zhang H, Ding B-J, Zhu R-H. A thermionic tungsten cathode activated with nanothoria and prepared by swaging method. *Materials Science and Engineering: A*. 2002;336(1-2):59-63. DOI:10.1016/S0921-5093(01)01969-4

62. Chao-Long L, Xin Z, Jiu-Xing Z, Fan-Xing Z, et al. Preparation and property of $La_{1-x}Nd_xB_6$ cathode material. *Journal of Inorganic Materials*. 2015;30(4):363. DOI:10.15541/jim20140471

63. Chang S-C, Hung S-C, Lin T-C, Yu T-A, et al. Thermal stability of hydrogen annealed aluminum doped zinc oxide films investigated by thermal desorption spectroscopy. *2013 8th International Microsystems, Packaging, Assembly and Circuits Technology Conference (IMPACT)*. Taipei: IEEE; 2013. p. 279-282. DOI:10.1109/IMPACT.2013.6706639

64. Li I. Nanostructures in palladium-barium cathodes of microwave devices. *Electronics: Science, Technology, Business*. 2018;(5):144-151. DOI:10.22184/1992-4178.2018.176.5.144.151

65. Kapustin VI. Physicochemical foundations of creation of the multicomponent oxide-containing cathode materials. *Perspektivnye materialy = Inorganic Materials: Applied Research*. 2000;(2):5-17. (In Russ.)

66. Kapustin VI, Li IP, Petrov VS, Ledentsova NE, Turbina AV. Electronic structure and physical-chemical peculiarities of nickel oxide cathode materials. *Elektronnaya Tekhnika. Seriya 1: SVCH-Tekhnika*. 2016; 1(528):8-18. (In Russ.)

67. Kapustin VI, Li IP, Kozhevnikova NE. Trace impurities have synergistic effects on electronic structure of oxide-nickel cathodes. *XXVIII Scientific and Technical Conference with the participation of foreign specialists "Vacuum science and technology"*. Sudak: Nanoindustry; 2021. p. 267-271. (In Russ.)

68. Norman D, Tuck RA, Skinner HB, Wadsworth PJ, et al. Surface structure of thermionic-emission cathodes. *Physical Review Letters*. 1987;58(5):519-522. DOI:10.1103/PhysRevLett.58.519

69. Djubua BCh, Koultashev OK, Polivnikova OV. Emission electronics, nanotechnology, synergetics (to the history of ideas in cathode technology). *Elektronnaya tekhnika. Seriya 1: SVCH-Tekhnika*. 2008;4(497):3-22. (In Russ.)

70. Thomas RE, Morrill CD. Secondary emission properties of impregnated tungsten cathodes. *Applications of Surface Science*. 1983;16(1-2):292-311. DOI:10.1016/0378-5963(83)90075-2

71. Kapustin VI, Li IP, Moskalenko SO, Shumanov AV. Theory of thermionic and secondary emission properties of palladium–barium cathodes of microwave electrovacuum devices. *Technical Physics*. 2020;65(2):317-323. DOI:10.1134/S1063784220020073

72. Pashkov AN, Romanova YuV, Popov RN, Dubinina OV, Khabachev MN. The development of production technology for cathode alloys based on platinum group metals for high-power electrovacuum microwave devices. *Elektronnaya Tekhnika. Seriya 1: SVCH-Tekhnika*. 2014;4(523):73-77. (In Russ.)

73. Gaidar AI, Bondarenko GG, Petrov VS, Kashirina NV. Surface processes at the first stage of magnetron cathode $Pd–Pd_5Ba$ activation. *Vacuum*. 2018;154:333-339. DOI:10.1016/j.vacuum.2018.05.024

74. Kostishyn VG, Kaloshkin SD, Adantsov AYu, Ursulyak ND, et al. Stusy of the phase and impurity composition of Pd–Ba and Pt–Ba cathode alloys. *Izvestiya Vysshikh Uchebnykh Zavedenii. Materialy Elektronnoi Tekhniki = Materials of Electronics Engineering*. 2015;18(3):212-220. DOI:10.17073/1609-3577-2015-3-212-220 (In Russ.)

75. Zorkin AYa, Myasnikova S. Technology of manufacturing metal-alloy cathodes for millimeter-wave magnetrons. *Materials of the XVI scientific and technical conference "Vacuum science and Technology"*. Moscow: MIEM; 2009. p. 210-212. (In Russ.)

76. Khabachev MN, Makarov AP, Drovnenkova GV, Zhukov YuA, et al. The industrial technology for the production of barium cathode alloys based on platinum and palladium for high-power microwave devices. *Elektronnaya Tekhnika. Seriya 1: SVCH-Tekhnika*. 2021;(4(551)):49-66. (In Russ.)

77. Li IP, Petrov VS, Polyakov VS, Silaev AD, et al. Simultaneous activation of the autoelectronic and secondary emission cathode of the magnetron with initial start. *Izvestiya vysshikh uchebnykh zavedeniy. Elektronika = Semiconductors*. 2014;3(107):30-37. (In Russ.)

78. Li IP, Komissarchik SV, Lifanov ND. *Magnetron with initial start with special activation of autoelectronic cathodes*. Russian Federation patent 2,494,489. 27 September 2013. (In Russ.)

79. Alekseev YuV, Kanicheva IR. Comparison of the emission properties and auger spectrum of an alloy emitter. *Bulletin of the Academy of Sciences of the USSR. Physical Series*. 1976;40:2587-2590. (In Russ.)

80. Sytnik AYa, Overcooked CH. The change in the emission properties of a cathode based on a palladium-barium alloy under the influence of ion bombardment under gas discharge conditions. *Elektronnaya Tekhnika. Seriya 1: SVCH-Tekhnika*. 1977;(12):98-102. (In Russ.)

81. Li IP, Bondarenko GG. The use of hydrogen-vacuum treatment of palladium powders to obtain effective metal-alloy cathodes of a steel magnetron. *Perspektivnyye materialy = Inorganic Materials: Applied Research*. 2012;(1);30-34. (In Russ.)

82. Swanwick ME, Keathley PD, Kartner FX, Velasquez-Garcia LF. Ultrafast photo-triggered field emission cathodes using massive, uniform arrays of nano-sharp high-aspect-ratio silicon structures. *2013 Transducers & Eurosensors XXVII: The 17th International Conference on Solid-State Sensors, Actuators and Microsystems (Transducers & Eurosensors XXVII)*. Barcelona: IEEE; 2013. p. 2680-2683. DOI:10.1109/ Transducers.2013.6627358

83. Nechaev YS, Denisov EA, Cheretaeva AO, Shurygina NA, et al. Method of thermal desorption study of hydrogen states in carbon materials and nanomaterials. *Physics-Uspekhi*. 2023;66(09):936-942. DOI:10.3367/ UFNe.2022.11.039274

84. Rochanachirapar W, Murakami K, Yamasaki N, Abo S, et al. Influence of gas atmosphere during laser surface treatment of CNT cathode. *Technical Digest of the 17th International Vacuum Nanoelectronics Conference (IEEE Cat. No.04TH8737)*. Cambridge: IEEE; 2004. p. 144-145. DOI:10.1109/IVNC.2004.1354941

85. Arkhipov AV, Gabdullin PG, Gnuchev NM, Davydov SN, et al. Field-induced electron emission from nanoporous carbon of various types. *St. Petersburg Polytechnical University Journal: Physics and Mathematics*. 2015;1(1):47-55. DOI:10.1016/j.spjpm.2015.03.011

86. Fursey GN, Polyakov MA, Kantonistov A, Yafyasova M, et al. Autoelectronic and explosive emission from graphene-like structures. *Zhurnal tekhnicheskoy fiziki = Technical Physics*. 2013;83(6):71-77. (In Russ.)

87. Bernatsky DP, Pavlov V. Field electron microscopy of carbonized rhenium. *Pis'ma v zhurnal tekhnicheskoy fiziki = Technical Physics Letters*. 2017; 43(12):104. DOI:10.21883/PJTF.2017.12.44715.16748. (In Russ.)

88. Krachkovskaya TM, Storublev AV, Sahaji GV, Yemelyanov AS. Investigation of the characteristics of a metal-porous cathode modified with nanocarbon. *Collection of articles VII of the All-Russian Conference. ”Microwave Electronics and Microelectronics"*. St. Petersburg: St. Petersburg State Technical University ”LETI“; 2018. p. 155-159. (In Russ.)

89. Krachkovskaya TM, Melnikov LA. Emission properties of metal-porous cathodes modified with nanocarbon. *Pis'ma v zhurnal tekhnicheskoy fiziki = Technical Physics Letters*. 2018;44(22):11-18. (In Russ.)

Information about the authors / Информация об авторах

Anastasia V. Parashchuk, Postgraduate Student, Moscow Institute of Physics and Technology (MIPT), Dolgoprudny, Russian Federation; ORCID 0009-0009-4173-9227; e-mail: parashchuk.av@mipt.ru

Evgeniy P. Sheshin, D. Sc. (Phys. and Math.), Professor, Deputy Head of the Department, MIPT, Moscow, Russian Federation; ORCID 0000-0003-2750-4797; e-mail: sheshin.ep@mipt.ru.

Aleksey V. Shumanov, Head of the Department of Cathode-vacuum systems, JSC "Pluton"; Moscow, Russian Federation; e-mail: a.shumanov@pluton.msk.ru

Паращук Анастасия Владиславовна, аспирант, Московский физико-технический институт (МФТИ), Долгопрудный, Российская Федерация; ORCID 0009-0009-4173-9227; e-mail: parashchuk.av@mipt.ru

Шешин Евгений Павлович, доктор физико-математических наук, профессор, заместитель заведующего кафедрой, МФТИ, Москва, Российская Федерация; ORCID: 0000-0003-2750-4797; e-mail: sheshin.ep@mipt.ru

Шуманов Алексей Владимирович, начальник отделения катодно-вакуумных систем, АО «Плутон»; Москва, Российская Федерация; e-mail: a.shumanov@pluton.msk.ru

Received 27 September 2024; Accepted 06 November 2024; Published 20 December 2024

Территория распространения – Российская Федерация, зарубежные страны
Distributed is the Russian Federation and foreign countries

Computer layout: Olga V. Mochalina, TSTU, Tambov, Russian Federation
Компьютерный дизайн и верстка: Мочалина О. В., ТГТУ, Тамбов, Россия

Оригинал-макет подготовлен в Издательском центре ФГБОУ ВО «ТГТУ»,
392032, Тамбовская обл., г. Тамбов, ул. Мичуринская, д. 112А

Подписано в печать 05.12.2024. Дата выхода в свет 20.12.2024.
Формат 60×90/8. Усл. печ. л. 11,25. Уч.-изд. л. 11,75. Тираж 100 экз. Цена свободная. Заказ № 038.
СМИ журнал “Journal of Advanced Materials and Technologies”
(Журнал современных материалов и технологий). Том 9, № 4. 2024